

UNIVERSITÄTSKLINIKUM HAMBURG-EPPENDORF

Klinik für Pädiatrische Hämatologie und Onkologie

Prof. Dr. med. Stefan Rutkowski

Brg1 in neural development and disease

Dissertation

zur Erlangung des Doktorgrades Dr. rer. biol. hum. / PhD
an der Medizinischen Fakultät der Universität Hamburg.

vorgelegt von:

Dörthe Holdhof
aus Kiel

Hamburg 2020

Angenommen von der Medizinischen Fakultät am: 14.05.2020
Veröffentlicht mit der Genehmigung der Medizinischen Fakultät der Universität Hamburg

Prüfungsausschuss, der/die Vorsitzende: Prof. Dr. med. Ulrich Schüller

Prüfungsausschuss, zweite/r Gutachter/in: Prof. Dr. rer. nat. Matthias Kneussel

Prüfungsausschuss, dritte/r Gutachter/in: Prof. Dr. med. Udo Schumacher

Part of this work has been published as:

hGFAP-Positive Stem Cells Depend on Brg1 for Proper Formation of Cerebral and Cerebellar Structures

Holdhof, D., Schoof, M., Hellwig, M., Holdhof, N. H., Niesen, J., Schüller, U.

Cereb Cortex. 2019 Sep 3. pii: bhz173. doi: 10.1093/cercor/bhz173. [Epub ahead of print]

Table of contents

Table of contents	I
1 Introduction	1
1.1 Brain and eye development	1
1.1.1 Brain development	1
1.1.2 Eye development	3
1.2 Atypical Teratoid/Rhabdoid Tumors	5
1.2.1 Epidemiology	5
1.2.2 Clinical features, diagnosis and therapy	5
1.2.3 Genetics and epigenetics	7
1.2.4 Attempts to model human AT/RTs in mice	8
1.3 The SWI/SNF chromatin remodeling complex	9
1.3.1 The ATPase Brg1	10
2 Aim of the study	14
3 Materials and methods	16
3.1 Materials	16
3.1.1 Chemicals, reagents and solutions	16
3.1.2 Primer	18
3.1.3 Antibodies	18
3.1.4 Kit systems	20
3.2 Mouse experiments	20
3.2.1 Genotyping	20
3.2.2 Conditional and inducible knockout mice	21
3.2.3 Tamoxifen induction and BrdU pulse	22
3.2.4 Body and brain weights	22
3.2.5 Fluorescence-activated cell sorting for fate mapping experiments	22
3.3 Primary cell culture	23
3.3.1 Neurosphere generation	23

3.3.2 Cerebellar explant cultures	23
3.4 Immunohistochemistry and immunocytochemistry	24
3.4.1 Cytospin.....	24
3.4.2 Tissue embedding.....	24
3.4.3 IHC	25
3.4.4 H&E stains	26
3.4.5 IF staining	26
3.4.6 Golgi-Cox staining.....	26
3.5 RNA isolation	26
3.6 RNA sequencing.....	27
3.6.1 Bioinformatics	27
3.7 Image analysis and quantification	28
3.8 Statistical analyses	28
4 Results	29
4.1 Multipotent NSCs depend on Brg1 for proper formation of cerebral and cerebellar structures.....	29
4.1.1 <i>hGFAP-cre::Brg1^{fl/fl}</i> mice die early and have severe abnormalities in all major brain structures.....	29
4.1.2 Proper expression of <i>Brg1</i> is essential for cerebellar development	31
4.1.3 Stem cells in the SVZ survive less in the absence of Brg1	35
4.1.4 The upper layers of the cerebral cortex are thinner, and neurons display pathological dendrites.....	37
4.1.5 Brg1 deficiency causes a severely underdeveloped hippocampus.....	39
4.2 A postnatal knockout of Brg1 in GNPCs results in a transient increase in proliferation	41
4.2.1 An acute Brg1 loss in <i>Math1</i> expressing cells at P3 enhances proliferation at P8	41
4.2.2 Brg1 deprivation at P3 in <i>Math1</i> expressing cells does not obstruct cerebellar development	42
4.3 Brg1 has time point specific roles in Sox2 positive NSCs and is essential for brain and eye development.....	45

4.3.1 A Brg1 loss between E7.5 and E12.5 causes morphological abnormalities in the embryonic brain	45
4.3.2 Morphological altered regions in <i>Sox2-creER^{T2}::Brg1^{f/f}</i> embryos are formed primarily by Brg1 positive cells and show no increase in proliferation.....	48
4.3.3 Brg1 deprivation decreases cell survival and causes distinct changes in gene expression	50
4.3.4 Early loss of Brg1 in Sox2 positive NSCs does not result in tumor formation in young mice.....	59
5 Discussion.....	61
5.1 <i>hGFAP</i> mediated Brg1 loss causes multiple brain alterations and causes death during adolescence.....	61
5.2 A Brg1 deficiency in GNPC increases proliferation but is not enough to drive tumor formation.....	64
5.3 Brg1 has time point dependent functions in Sox2 expressing NSCs	65
6 Outlook.....	71
7 Summary.....	74
8 Zusammenfassung.....	75
9 Abbreviations.....	76
10 References.....	79
11 Appendix	i
11.1 Supplementary Figures.....	i
11.2 Supplementary Tables	ii
12 List of all figures and tables	xii
13 Danksagung	xiv
14 Curriculum Vitae.....	xv
15 List of publications	xvi
16 Eidesstattliche Versicherung	xvii

1 Introduction

1.1 Brain and eye development

Neural tissues derive from the ectoderm, which first forms the neural tube and then develops into three primary vesicles: prosencephalon (forebrain), mesencephalon (midbrain) and rhombencephalon (hindbrain). The spinal cord derives from the caudal part of the neural tube. The three primary vesicles then turn into five secondary vesicles, which give rise to all specified brain structures and neural cell types [1]. For instance, the prosencephalon develops into telencephalon and diencephalon. Afterwards, brain structures such as the cerebral cortex, the presumptive eye or the hypothalamus originate from these two regions [2]. During the entire process of neural development, *Sex determining region Y-box 2 (Sox2)* is an important gene for maintaining self-renewal and proliferation capacities of neural stem cells (NSCs) [3].

1.1.1 Brain development

The neocortex is a complex structure in the brain, which harbors 19-23 billion neurons in humans and is essential for our cognitive abilities including learning, language and creativity [4, 5]. It develops from the telencephalic vesicle by a process of neuronal migration [6, 7]. Postmitotic neuroblasts originate from the ventricular zone (VZ) and migrate along radial glia cells towards the pial surface, where they settle in distinct laminae [8-10]. A second germinal zone is the subventricular zone (SVZ), which becomes recognizable as soon as the first cells leave the VZ. The cells in the neocortex emerge from both, the VZ and the SVZ [10]. In the VZ, radial glia cells reside and proliferate asymmetrically. One daughter cell serves self-renewal, whereas the other (intermediate precursor cell) migrates into the overlying SVZ and proliferates symmetrically yielding in two neurons [11]. Already in the early 1960s, it was elucidated that the neocortical layers are formed by migrating cells in an inside-out-fashion: By labelling cells radioactively during different stages of embryonic development, it was shown that early born cells form the deeper layers and late born neurons the upper layers of the cerebral cortex [12]. Only Cajal-Retzius cells are born early and are found in the most superficial layer of the neocortex (layer I) [13]. As a result, from embryonic day 15.5 (E15.5) in mice onwards, the neocortex consists of six layers [14]. At around E18, neurogenesis in the cerebral cortex is finalized, while gliogenesis is initiated and the first astrocytes appear, a process called "neurogenic-to-gliogenic switch". The first oligodendrocytes are generated after birth [15]. The general organization of the neocortex is conserved between mice and men. Still, the human cerebral cortex is gyrencephalic, i.e. highly folded, whereas the structure in mice is lissencephalic (non-folded) [16].

Another eminent brain structure is the cerebellum, which is important for motor, cognitive and emotional functions [17]. The mature cerebellum consists of two hemispheres divided by a

vermis and is organized into ten lobules. Like the cerebral cortex, the cerebellar cortex is laminated. It consists of three distinct layers, which are arranged above an inner core of white matter. Within the white matter, deep cerebellar nuclei are located in clusters. The inner granule cell layer (IGL) is the innermost layer and made up of primarily excitatory granule neurons that are the most abundant neurons in the mature brain. Still, the IGL also harbors Golgi cells, Lugaro cell interneurons as well as unipolar brush cells. Located on top of the IGL is a monolayer of inhibitory Purkinje cells (PCs), the PC layer (PCL), which also contains the somata of Bergmann glia cells (BGs). Lastly, above the PCL resides the molecular layer (ML), harboring PC dendrites, the axons of the granule neurons, BG fibers and stellate as well as basket interneurons (reviewed in [18]). Cerebellar development initiates during embryogenesis, starting around E9 in mice in the rhombomere 1 of the rhombencephalon, and proceeds after birth [19]. There are two distinct germinal zones, where cerebellar cells originate from: the cerebellar VZ (cVZ) and the cerebellar rhombic lip, specified by the basic helix-loop helix (bHLH) transcription factors *Pancreas transcription factor 1a (Ptf1a)* and *Atonal Homolog 1 (Atoh1, Math1)*, respectively [20-24]. Granule neuron precursor cells (GNPCs) for instance are generated in the rhombic limb [25]. Formation of GNPCs is highly dependent on *Math1* expression [26]. They migrate independent from glia cells over the dorsal surface and form the external granular layer (EGL) at around E15.5 in mice [20]. From this time point onwards, the EGL is mitotically active until the first two weeks of life. Proliferation of GNPCs is dependent on Sonic Hedgehog (SHH), which is secreted by PCs, and peaks around postnatal day 8 (P8) [27, 28]. At birth, the first GNPCs differentiate into granule cells (GCs) and migrate radially along the BG fibers to form the IGL. At P20, maturation and migration of the granule neurons is finalized (Figure 1) [18]. Like GCs, the neurons of the deep cerebellar nuclei also descend from progenitors of the rhombic limb [21]. However, all gamma-Aminobutyric acid (GABA)ergic neurons including PCs, Golgi, basket, and stellate cells, are descendants from the cVZ [23]. PCs are generated between E10.5 and E12.5 and their final mitosis occurs prior to E13.5 before they migrate to their final destination [29, 30].

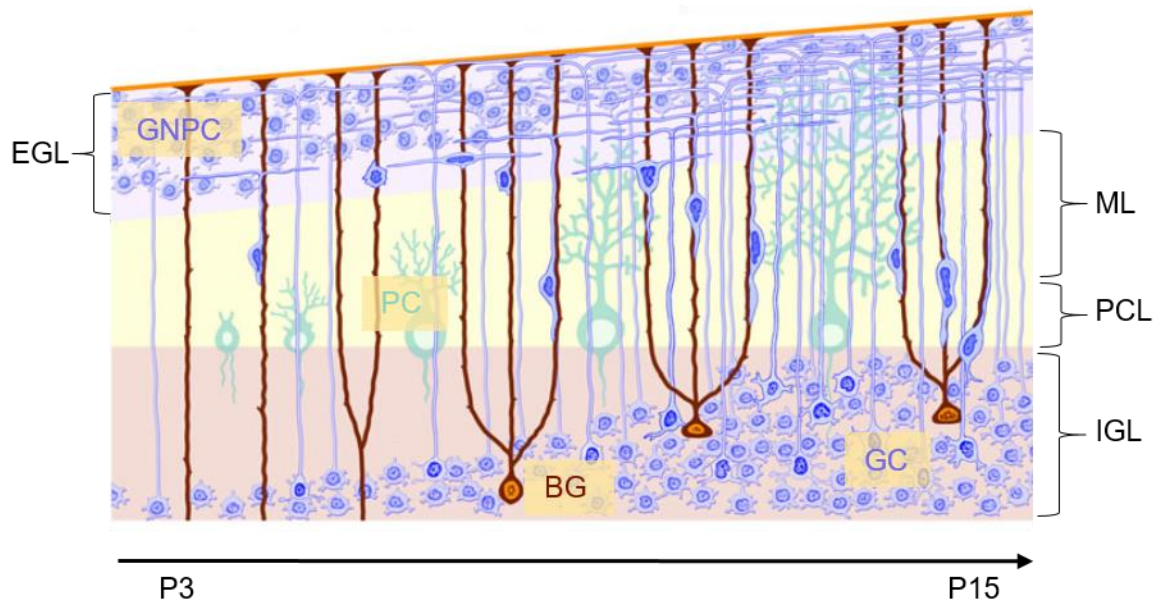


Figure 1 Overview of postnatal cerebellar development. Shortly after birth (P3) the EGL is present and harbors proliferating GNPCs (blue). In the course of postnatal development, these cells leave the cell cycle, start to differentiate into GCs and migrate inwards along the fibers of the BGs through the ML and PCL to form the IGL. While the IGL becomes more prominent, the EGL starts to disappear. Simultaneously, PCs (turquoise), which are located in the PCL, differentiate and develop their characteristic dendritic branches. The somata of BGs (brown) are found in the IGL, but their glial endfeet are located at the pial surface (orange). EGL: external granular layer, ML: molecular layer, PCL: Purkinje cell layer, IGL: inner granule layer, GNPC: granule neuron precursor cell, PC: Purkinje cell, BG: Bergmann glia cells, GC: granule cell. Modified after [31].

1.1.2 Eye development

Development of the eye originates in the anterior neural plate [32]. Here, the eye field is established by the expression of certain genes, including *Retinal homeobox protein (Rax, Rx)*, *Paired box protein (Pax6)*, *sine oculis-related homeobox 3 (Six3)* and *Six6* as well as *LIM Homeobox 2 (Lhx2)* [33-37]. The correct expression of these so called eye field transcription factors (EFTFs) is facilitated by the upregulation of *Orthodenticle homeobox 2 (Otx2)*, *Sox2* and non-canonical Wingless (WNT) signaling, whereas the Bone morphogenic protein (BMP) pathway is inhibited [32, 33, 38-42]. At around E7.5 in mice, the eye field starts to evaginate bilaterally at the ventral part of the prosencephalon and forms two optic vesicles [43-45]. Shortly afterwards, the optic vesicle contacts the surface ectoderm and starts invaginating into the optic cup (Figure 2). Concurrently, the surface ectoderm first thickens, becomes a vesicle and finally develops into the lens [46]. Other cell lineages and structures of the eye including the corneal endothelium and stroma, iris stroma, ciliary body muscles, trabecular mesh work, Schlemm's canal, sclera, ocular blood vessels, and extraocular muscles derive from the periocular mesenchyme [47]. During optic cup formation, the optic neuroepithelium is divided into three regions: the distal/ventral region giving rise to the future neural retina, the dorsal region developing into the retinal pigment epithelium (RPE) and the proximal region from

which the optic stalk emerges [45, 46, 48]. The RPE can be recognized in mice from E11.5 onwards as a cuboidal monolayer of pigmented epithelium expressing *Microphthalmia-associated transcription factor (Mitf)*. In contrast, the neural retina has a thickened morphology, consists of multiple layers, expresses *Visual system homeobox 2 (Vsx2, Chx10)* and is the tissue responsible for the light-sensing properties of the eye [32, 49]. However, several studies have shown that all anatomical sites of the optic neuroepithelium can give rise to both neural retina and RPE during this early developmental phase [36, 50].

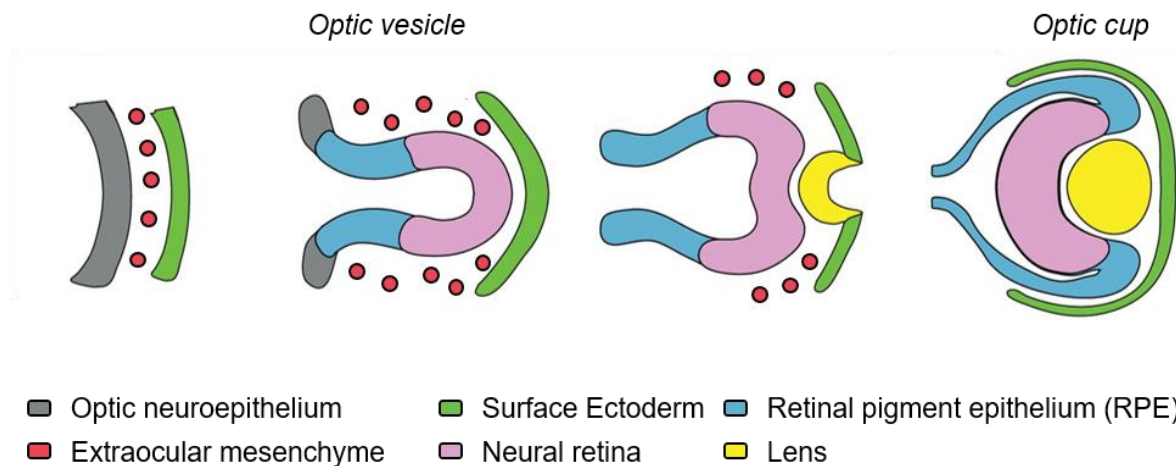


Figure 2 Schematic overview of the embryonic eye development. The optic vesicle develops from the optic neuroepithelium (grey), which evaginates from the diencephalon and grows through the mesenchyme (red) towards the surface ectoderm (green). Upon contact with the surface ectoderm, the optic vesicle consisting of presumptive neural retina (pink) and RPE (blue) invaginates and forms the optic cup. Simultaneously, the surface ectoderm invaginates as well and gives rise to the lens vesicle (yellow). Modified after [51].

The regionalization process of the optic neuroepithelium is mediated by extrinsic factors that are secreted by the surrounding tissues (i.e. surface ectoderm or periocular mesenchyme) or by the optic neuroepithelium itself [46]. One example of extracellular molecules involved are members of the fibroblast growth factor (FGF) family. FGF is able to downregulate *Mitf*, which is expressed in the entire optic vesicle prior to regionalization, resulting in neural retina formation and an increase in *Vsx2* expression [50]. Other secreted proteins involved in the structuring are members of the transforming growth factor β (TGF β) family including the BMPs, WNT or the hedgehog (HH) family [52-56]. They all contribute to the spatial and temporal specific gene expression pattern needed for the correct development of the eye. The importance of the right interplay of extrinsic as well as intrinsic factors became obvious, when certain genes like *Pax6*, *Mitf* or *Fgf receptor (Fgfr)* were knocked out in various mouse models [57-62]. Loss of *Mitf* expression, for example, causes hyperproliferation of the RPE, which does not become pigmented but develops into an ectopic neural retina. This process is often termed “RPE to retina transdifferentiation” [61]. An additional *Pax6* deficiency results in an even more pronounced phenotype, since *Pax6* together with *Mitf* inhibits the expression of

Fgf15 and *Dkk3*. They, in turn, are pro-retinogenic by suppressing WNT signaling, which activates gene expression of retina promoting genes like *Vsx2* [62].

1.2 Atypical Teratoid/Rhabdoid Tumors

Rhabdoid tumors (RTs) are rare, highly malignant embryonal tumors which can arise in almost any part of the body but are usually found in the central nervous system (CNS (atypical teratoid/rhabdoid tumor (AT/RT)), in the kidney (rhabdoid tumor of the kidney (RTK)) or in the soft tissues (malignant rhabdoid tumor (MRT)) [63]. Before they were recognized as a distinct tumor entity at the end of the last century, AT/RTs were often misdiagnosed as medulloblastoma or primitive neuroectodermal tumors [64-66]. Histologically, the tumors are World Health Organization (WHO) grade IV tumors and defined by the absence of either Integrase interactor 1 (*Ini1*, *SmarcB1*, *hSnf5*, *Baf47*) or Brahma homolog 1 (*Brg1*, *SmarcA4*, *Baf190A*) protein [67].

1.2.1 Epidemiology

Despite its rarity, AT/RT is the most common embryonal CNS tumor in infants below the age of 12 months: Up to 50 % of all embryonal CNS tumors in the first year of life are AT/RTs [68]. The majority of patients are younger than 3 years with a peak incidence in infants younger than 2 years. In adults AT/RTs are seldomly diagnosed [69, 70]. The tumor occurs slightly more often in boys than in girls (male/female ratio: 1.3). The incidence is 1.4 per million in Germany with a 5-year survival probability of 32 % [64, 71]. Patients with AT/RTs have a very poor prognosis with a median overall survival of 6-18 months [72-76].

1.2.2 Clinical features, diagnosis and therapy

Patients present with signs and symptoms like vomiting, headache, lethargy, cranial nerves palsies, ataxia, macrocephaly, head tilt or hemiplegia/paraplegia depending on the patient's age as well as tumor location and size [64, 77-79]. Usually, computed tomography (CT) or magnetic resonance imaging (MRI) is performed, but these radiological findings are often similar to those of medulloblastoma or other embryonal tumors. The majority of cases show cystic components and hydrocephaly. Calcification is found in 40 % and leptomeningeal dissemination in 24 % of AT/RTs [80, 81]. AT/RTs arise in almost any part of the CNS but usually occur intracranially and are only occasionally found in the spinal cord. Within the brain, AT/RTs are found in both infra- and supratentorial regions [72, 82, 83]. Twenty percent of patients present with metastasis [84]. On a microscopic level, AT/RTs are very heterogeneous and can be composed of nests or sheets of rhabdoid cells as well as mesenchymal, epithelial and primitive neuroectodermal elements. Mitotic cells, necrotic areas and hemorrhages are often found in Hematoxylin and Eosin (H&E) stains. The eponymous rhabdoid cells are characterized by eccentric nuclei with vesicular chromatin, prominent eosinophilic nucleoli,

abundant cytoplasm, eosinophilic cytoplasmic inclusions and clear cell borders [67, 85]. Still, the majority of AT/RTs cannot be diagnosed solely based on the presence of the rhabdoid features. Therefore, the absence of *Ini1* or, in rare cases, *Brg1* needs to be verified by immunohistochemistry (IHC) in order to ensure the diagnosis (Figure 3) [86, 87].

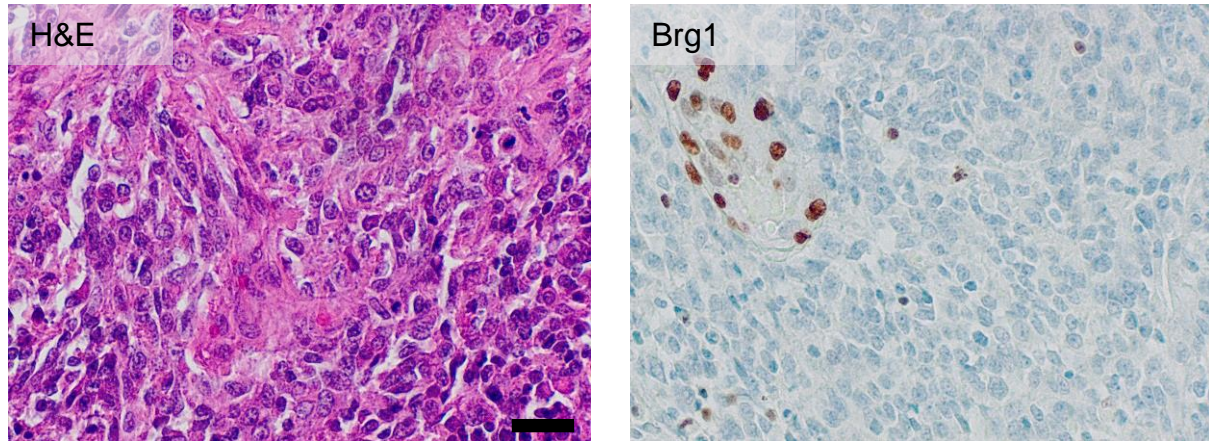


Figure 3 Histopathology of a *Brg1* deficient AT/RT. H&E stain of a tumor shows the typical heterogeneous image of an AT/RT. It displays rhabdoid features, including eosinophilic inclusions as well as large nuclei with prominent nucleoli. IHC reveals that the *Brg1* protein is lost as the majority of cells appear blue. The brown nuclei belong to blood vessels and serve as an internal positive control of the *Brg1* staining. Scale bar is representative for both images and corresponds to 30 μm .

Other IHC features of AT/RTs are positivity for epithelial membrane antigen (EMA), α smooth muscle actin (SMA), vimentin and sometimes neurofilament protein (NFP), glial fibrillary acidic protein (GFAP), synaptophysin and cytokeratins. Concordant with the high abundance of mitotic figures in H&E stains, the Ki67 proliferation index is often higher than 50 % [67]. A new diagnostic tool utilizes the DNA methylation profile of 450,000 or 850,000 CpG islands across the tumor genome to classify the cancer. This method is based on a random forest machine learning algorithm and compares the methylation profile of the sample to the profiles of a reference cohort [88]. Even though the tool is currently still in development, it is already often applied to diagnose brain tumors in toddlers who are younger than 3 years.

Treatment of AT/RTs includes surgery, chemotherapy and, if the patient is older than 18 months, radiotherapy according to protocols provided by the European Rhabdoid Registry (EU-RHAB). The chemotherapy consists of a sequential administration of DOX (doxorubicin, intra-ventricular methotrexate), ICE (ifosfamide, carboplatinum, etoposide, intra-ventricular methotrexate) and VCA (vincristine, cyclophosphamide, actinomycin-D, intra-ventricular methotrexate). Afterwards, a high dose chemotherapy of carboplatinum and thiotepa may be added to the treatment scheme, but survival benefits are currently under investigation [63, 89].

1.2.3 Genetics and epigenetics

On deoxyribonucleic acid (DNA) level, RTs are characterized by a simple genome with biallelic inactivating mutations in *INI1* and, in rare cases, *BRG1* as the only recurrent alterations known so far [90, 91]. The mutation rate is the lowest among all sequenced cancer types and in some tumor samples, no other mutation besides the one in *INI1* was detected in exome sequencing [92]. Heterozygous germline mutations in either *INI1* or *BRG1* increase the risk to develop an AT/RT (Rhabdoid Tumor Predisposition Syndrome type 1 (OMIM # 609322) and Rhabdoid Tumor Predisposition Syndrome type 2 (OMIM # 613325), respectively) [87, 93, 94]. Hasselblatt *et al.* demonstrated that 6 of 7 patients with *BRG1* mutated AT/RTs were carriers of a germline mutation, which is significantly more frequent than in patients suffering from *INI1* mutated AT/RTs (9/33). Additionally, the overall survival is shorter, indicating that Brg1 deficient AT/RTs might be even more aggressive than those with absence of the Ini1 protein (Figure 4) [91].

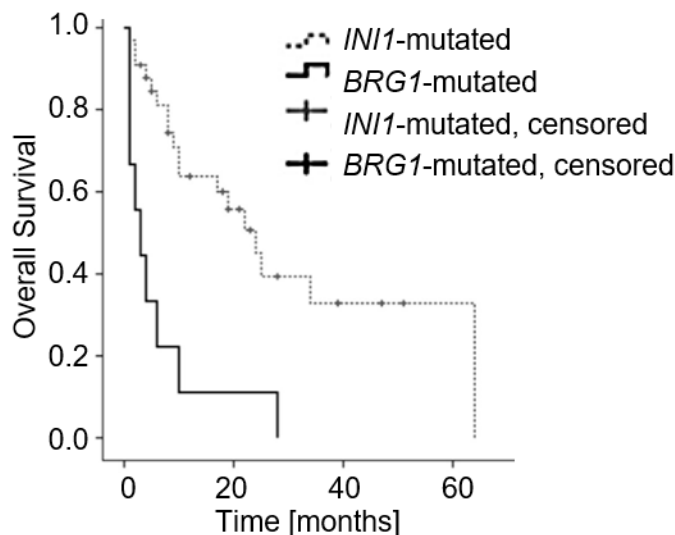


Figure 4 Survival of AT/RT patients is reduced in case of a *BRG1* mutation. Kaplan-Meier curve of *INI1* (n=33, dotted line) and *BRG1* (n=9, solid line) mutated AT/RTs reveals significantly reduced survival in case of a *BRG1* mutation (log-rank test, $p < 0.001$). Modified after [91]

Although on the genetic level AT/RTs appear as a homogenous tumor entity, two independent research groups identified three distinct subgroups based on methylation and gene expression data [95, 96]. Later, both groups published a consensus paper and agreed to name the subgroups AT/RT-TYR, AT/RT-SHH and AT/RT-MYC according to the terminology proposed by Johann and colleagues (Figure 5). Furthermore, they unraveled that the AT/RT-SHH subgroup is in fact subdivided into two groups (AT/RT-SHH-1, AT/RT-SHH-2) [97]. The three main subgroups differ in terms of tumor location, type of *INI1* mutation and overexpression of certain genes and pathways [95]. Additionally, the AT/RT-TYR subgroup has been proposed to correlate with the best overall survival, especially if the patient is older than one year [98].

Furthermore, based on DNA methylation, ChIP sequencing and transcriptome data, the AT/RT-MYC subgroup shows similarities to extra-cranial RTs [99]. Since the vast majority of AT/RTs are caused by *INI1* mutations, the subgroup classification is based mainly on *Ini1* deficient tumors. How *BRG1* mutated AT/RTs fit into this scheme remains elusive and is currently under investigation.

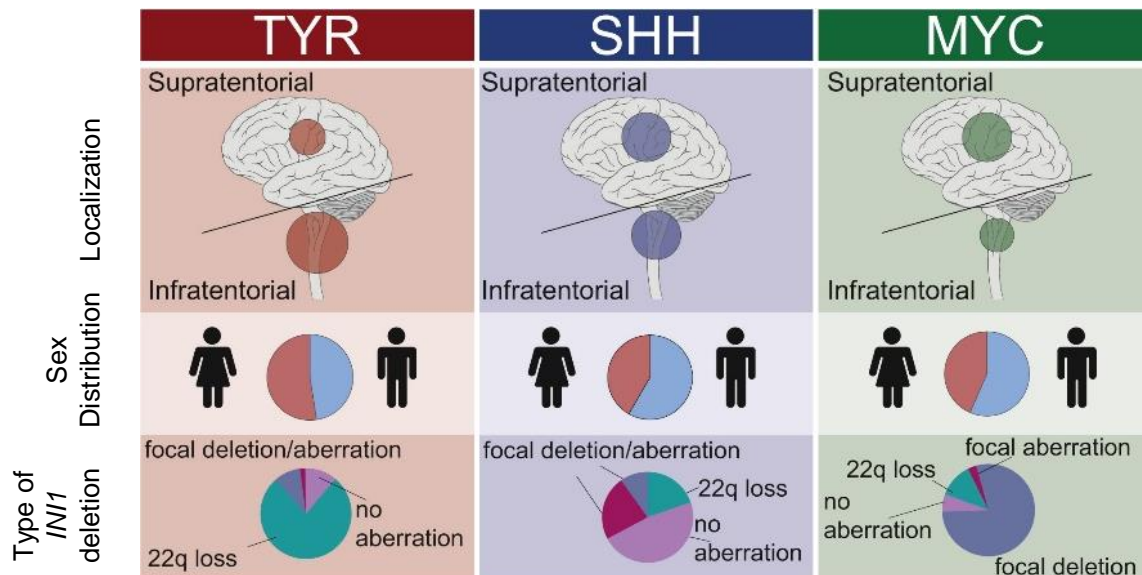


Figure 5 Characteristics of AT/RT subgroups. Three main AT/RT subgroups have been identified based on methylation and gene expression data so far: AT/RT-TYR (red), AT/RT-SHH (blue), AT/RT-MYC (green). They differ, for example, in terms of tumor location, sex distribution and type of *INI1* deletion. Modified after [95]

1.2.4 Attempts to model human AT/RTs in mice

In order to understand the molecular mechanisms behind a disease like cancer, patient-derived xenografts (PDX) or genetically engineered mouse models (GEMM) are often used. So far, only a handful of mouse models recapitulating *INI1* mutated AT/RTs and no model resembling *BRG1* deficient AT/RTs have been developed. In a first approach to develop GEMM for RTs, conventional *Ini1* knockout mice were generated. A homozygous knockout of *Ini1* is embryonically lethal, but a heterozygous *Ini1* loss causes tumor development resembling human MRT, though not human AT/RT [100, 101]. Ng and colleagues published the first AT/RT GEMM in 2015. They used the cyclization recombinase/ locus of crossing [xing]- over bacteriophage P1 (*cre/loxP*) system to investigate *Ini1* loss specifically in human *glial fibrillary acidic protein (hGFAP)* expressing cells. In detail, they bred *hGFAP-cre::Ini1^{fl/fl}::p53^{fl/fl}* mice, which developed aggressive brain tumors resembling human AT/RTs in terms of histology and gene expression [102]. Nevertheless, a drawback of this model is the absence of inactivating *P53* mutations in the vast majority of AT/RT patients. Another mouse model revealed that the development of murine brain tumors caused by an *Ini1* deficiency is highly dependent on the time point, at which *Ini1* is inactivated.

Rosa26-creER^{T2}::Ini1^{fl/fl} mice developed AT/RT-like tumors with a 100 % penetrance when the loss of *Ini1* was introduced between E6 and E7. Inactivation of the gene between E8 and E10 caused tumor formation in only 36 % of the animals, whereas a deficiency introduced at E11 or E12 resulted in a tumor-free survival. Based on this timespan (E6-E10) and transcriptome analyses, the authors suggested neural progenitors and ectomesenchyme as possible cells of origin for AT/RT development [103].

1.3 The SWI/SNF chromatin remodeling complex

Human DNA encodes for about 20,000 genes and without further modifications it would result in a two-meter-long chain of nucleotides [104-106]. Since a molecule of this size is unable to fit into the nucleus of cells, it is condensed into nucleosomes, which consist of 147 bp DNA wrapped around an octamer of histones [107]. Nucleosomes are further condensed into chromatin. In addition to solving the issue of fitting into the nucleus, packaging of DNA also contributes to transcriptional regulation, since genes need to be accessible for proteins like transcription factors in order to be expressed [106, 108]. Therefore, chromatin structure is dynamic and can be altered by either posttranslational histone modifications or by ATP-dependent chromatin remodelers [109, 110]. ATP-dependent chromatin remodeling complexes control nucleosome repositioning, editing as well as ejecting and are therefore able to activate or repress transcription [110]. So far, four subfamilies of ATP-dependent chromatin remodeling complexes have been described based on their catalytic Snf2-like ATPase subunits: chromodomain helicase DNA-binding (CHD), Inositol Requiring 80 (INO80), imitation switch (ISWI) and switch/sucrose non-fermentable (SWI/SNF, Brahma (BRM, SMARCA2)/BRG1-associated factor (BAF)) complexes [111-117]. The latter was discovered first and is the best described one so far. The SWI/SNF complex was identified in 1984 in yeast when studies were performed to find genes involved in mating type switching and sucrose fermentation [116, 117]. Ten years later, it was discovered that the complex increases DNA accessibility by the hydrolysis of ATP and that homologous complexes are also present in mammals [118-121]. The SWI/SNF complex has a size of about 2 MDa and is an assembly of up to 15 subunits [122]. In total, about 29 genes encode for components that can be combined in a modular manner to form cell type specific SWI/SNF complexes [123, 124]. For instance, different SWI/SNF complex compositions have been described for embryonic stem cells (esBAF), neural progenitors (npBAF) and post-mitotic neurons (nBAF) [125, 126]. Some SWI/SNF subunits are exchanged during the transition of neural progenitors into mature neurons (PHD finger protein 10 (PHD10), BAF53a), whereas others like *Ini1* and *Brg1* are retained [126]. As a result, distinct gene expression patterns of the SWI/SNF subunits can be found for all cell types [127]. The SWI/SNF complex regulates transcription of genes involved in the differentiation of diverse cell types and tissues, including cardiac and muscle

development, hematopoiesis or neurogenesis [126, 128-135]. However, the complex is also involved in other processes such as DNA damage repair, cellular senescence and cell cycle control [136-144]. The SWI/SNF complex has gained great attention, since sequencing studies detected that 20 % of all human tumors contain mutations in one or more subunits [145]. If these mutations result in loss of the respective subunit, it can lead to the expression of an altered SWI/SNF complex with aberrant functions that contribute to cancer development [146, 147]. Furthermore, mutations have also been found in the germline of patients suffering from intellectual disability or autism spectrum disorders (ASDs) [148-152]. So far, three distinct subtypes of SWI/SNF complexes have been described: the canonical BAF (cBAF), the polybromo-associated BAF (pBAF) and the non-canonical BAF (ncBAF). They all consist of subunits, which are either specific for one SWI/SNF complex class (cBAF, pBAF or ncBAF), or can be found in at least two subtypes [123, 153]. The exact functional distinctions of the different SWI/SNF complexes are not fully understood. However, it is known that cBAF and pBAF subunits are frequently mutated in cancer, whereas the mutation rates of ncBAF components are rather low [123, 154].

1.3.1 The ATPase Brg1

Each SWI/SNF chromatin remodeling complex contains one ATPase subunit, i.e. either Brg1 or Brm [124]. Even though Brg1 and Brm share 75 % sequence identity, they can have different, context-dependent functions [155]. In pBAF complexes, only Brg1 is found. Additionally, it has been shown that the two ATPases can interact with different proteins [156, 157]. Furthermore, Brg1 containing complexes have been identified to be preferentially found at chromatin epigenetically marked as active, whereas Brm containing complexes are rather located at repressively marked chromatin [158]. Another study revealed that at some genomic sites, Brg1 and Brm have cooperative interactions, whereas at other sites, they antagonize each other [159]. *BRG1* encodes for a 1647 amino acid long protein consisting of different evolutionarily conserved domains and motifs [160]. At the N-terminal region of the protein, a glutamine-leucin-glutamine (QLQ), a helicase/SANT-associated (HSA) and a BRM and KIS (BRK) motif is located. The ATPase domain consists of the SNF2_N motif containing a DEAD-like helicase superfamily domain (DEXHc) and a helicase domain (HELICc). Located at the C-terminus, there is a bromodomain, which interacts with acetylated lysine residues (Figure 6) [161-163]. Although the role of some domains regarding the function of Brg1 is still unknown, it has been proposed that the ATPase domain is the most important one [164].

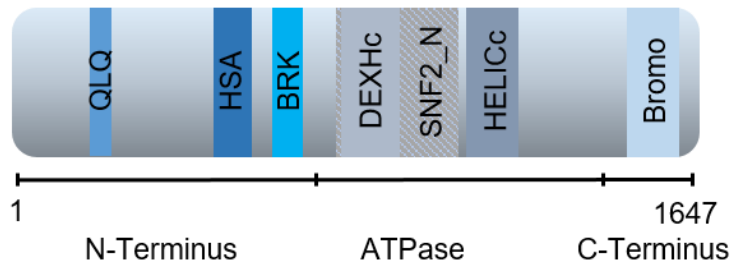


Figure 6 Structure of Brg1. The protein has a size of 1647 amino acids and harbors a QLQ, an HSA and a BRK domain at its N-Terminus. The catalytic ATPase domain is composed of a DEXHc as part of the SNF2_N motif and a HELICc domain. At the C-Terminus, a bromodomain is found. Designed after [161]

1.3.1.1 Role of Brg1 in development

Brg1 has been proposed to be essential for the development and homeostasis of many cell types, tissues and organs. Already very early in embryonic development, the protein is indispensable, as homozygous knockout mice die during peri-implantation stage. In contrast to that, a heterozygous Brg1 loss results in a predisposition to mammary tumors and exencephaly [165, 166]. Singh and colleagues further demonstrated that the gene is also important during gastrulation as *Rosa26-creER^{T2}::Brg1^{fl/fl}* embryos die due to increased apoptosis when Brg1 deficiency is induced by tamoxifen injections at E6.5 [167]. Other mouse models indicated that Brg1 is also essential for erythropoiesis, early vascular development, heart development, limb patterning, cardiac and duodenal homeostasis, spermatogenesis, development of the lymphatic system and many other processes [168-173]. Neural development also seems to be heavily dependent on *Brg1* expression [135, 174]. In *Nestin-cre::Brg1^{fl/fl}* mice, Brg1 is lost around E10.5 in NSCs, which differentiate prematurely into neurons and generate less astrocytes and oligodendrocytes. Their brains are smaller compared to controls, accompanied by a thinner neocortex and a hypoplastic cerebellum. Furthermore, these animals are unable to breathe and die during birth. Studying *Nestin-cre::Brg1^{fl/fl}* mice indicated that NSCs depend on Brg1 for self-renewal and that Brg1 represses neuronal differentiation in order to facilitate production of glia cells [126, 175]. In another study, Moreno *et al.* demonstrated that a Brg1 loss in cerebellar GNPCs results in a hypoplastic cerebellum [176]. At least in parts, this phenotype is caused by the inability of Brg1 deficient GNPCs to respond to SHH in order to proliferate [177]. In adult neurogenesis proper *Brg1* expression is also of high importance as demonstrated by the use of *Glast-creER^{T2}::Brg1^{fl/fl}* and *Nestin-creER^{T2}::Brg1^{fl/fl}* mice. In these models, Brg1 loss was induced in adult mice, which caused neuroblasts in the rostral migratory stream to switch towards the glial lineage and reduced numbers of adult NSCs in the hippocampus, respectively [178, 179]. Moreover, other mouse models suggested a role of Brg1 in neural crest development, oligodendrogenesis, differentiation and myelination of Schwann cells as well as retinogenesis [180-183]. In

agreement with these findings in mice, *BRG1* also seems to be essential for human development, as mutations in the gene have been associated with Coffin Siris Syndrome (CSS, OMIM # 135900) [148, 184-187]. CSS is a rare congenital disease characterized by a broad spectrum of clinical abnormalities such as intellectual disability, distinctive facial features, growth deficiencies and malformations in several organs including the brain [184, 188, 189]. Germline mutations in components of the SWI/SNF complex, including *BRG1* missense mutations, have been proposed to be the underlying genetic cause of the disease [148]. Furthermore, a genetic network analysis by De Rubeis and colleagues suggests that *BRG1* might be a key node in the pathogenesis of ASDs [190]. In another study, *BRG1* mutations in ASD patients have been identified and proposed to lead to misexpression of ASD risk genes like *GRIN2B* [191, 192].

1.3.1.2 Role of Brg1 in tumorigenesis

Even though many of the SWI/SNF complex subunits have been reported to be mutated in human cancers, mutations in the *BRG1* subunit are the second most common. Only *ARID1A* mutations are more frequent [145]. The first indication that Brg1 might be a tumor suppressor came from *in vitro* studies. Several cancer cell lines showed a loss of the Brg1 protein and reintroduction of Brg1 caused growth arrest [193-196]. In the meantime, Brg1 deficiency, often in combination with Brm loss, has also been reported in primary tumors, including lung cancer, thoracic sarcomas, clear cell renal carcinoma and several other cancer types [197-199]. Especially in small cell carcinoma of the ovary hypercalcemic type (SCCOHT) and *BRG1* mutated AT/RTs, loss of the Brg1 protein has been proposed as the main driver event in tumor formation [77, 87, 161, 200, 201]. About 5 % of AT/RTs linked to germline mutations in either *INI1* or *BRG1* are diagnosed with loss of Brg1 positivity in IHC [202]. Since this tumor is very rare, only little is known about the role of Brg1 in this entity. Additionally, suitable *in vitro* and *in vivo* models are lacking to investigate the molecular mechanisms behind *BRG1* mutated AT/RTs. One general mechanism how loss of Brg1 contributes to malignancy has recently been proposed by Stanton and colleagues. They claim that the SWI/SNF complex controls binding and release of the Polycomb complexes from chromatin in an ATP-dependent manner. In case of a Brg1 deficiency, Polycomb complexes are maintained at promoters across the genome causing aberrant silencing of gene expression [203]. Noteworthy, the majority of *BRG1* mutations collected in the Catalogue Of Somatic Mutations In Cancer (COSMIC) database are not nonsense mutations or large deletions resulting in protein loss but missense mutations scattered over the entire gene sequence [204, 205]. For instance, in Burkitt lymphoma *BRG1* missense mutations in the helicase domain are often found. They have been proposed to obstruct helicase function, causing a decreased transcription of target genes without affecting Brg1 protein expression [206, 207]. Some of the mutations found in Burkitt

lymphoma have also been found in medulloblastoma, the most common malignant brain tumor during childhood. As for Burkitt lymphoma, all mutations in medulloblastoma described so far are located in the catalytic ATPase domain of Brg1 indicating that they might have a similar effect [208-212].

Even though Brg1 is usually described as a tumor suppressor, a tumor promoting role has also been described for some cancer types. Hepatocellular carcinoma, glioma and neuroblastoma cell lines proliferated less in case of Brg1 silencing [213-215]. Furthermore, high *BRG1* expression correlated with reduced survival in advanced-staged neuroblastoma and prostate cancer [214, 216]. Also, in mice both, tumor suppressive and oncogenic roles of Brg1 have been described. As mentioned earlier, heterozygous *Brg1* knockout mice are prone to develop mammary tumors [165, 166]. Furthermore, using the cre/loxP to investigate Brg1 loss in specific cell types, it was shown that Brg1 knockdown can promote retinoblastoma development, lung carcinogenesis and the formation of uterine tumors [217-219]. However, in melanoma and pancreatic ductal adenocarcinoma mouse models, loss of the Brg1 protein delayed tumor formation [220, 221]. Furthermore, in a mouse model for SHH driven medulloblastoma, Brg1 loss inhibited tumorigenesis completely [222]. The diversity of *BRG1* mutations and the impact of the presence or absence of the Brg1 protein on accelerating or preventing tumor formation in mice or men further highlight the cell type and time point specific role of this protein.

2 Aim of the study

BRG1 mutations have been associated with a variety of cancer types but also with congenital neurodevelopmental disorders [148, 184-187, 204]. The gene is essential for early embryonic development and for diverse processes during organogenesis [167-170, 172, 173, 175]. Using different mouse models, it has been shown that *Brg1* is also important for several steps of CNS development. However, these studies either focused on the consequences of *Brg1* deficiency in NSCs for prenatal development or investigated adult neurogenesis [126, 175, 179, 223]. Therefore, the first aim of this study was developing a mouse model, in which the impact of an embryonal *Brg1* loss on postnatal brain development could be examined. We used the *cre/loxP* system to generate mice, in which *Brg1* expression was lost in *hGFAP* positive multipotent NSCs and investigated survival and the development of all major brain structures.

It has already been published that a chronic *Brg1* deficiency in *Math1* positive cells causes hypoplasia in the cerebellum [176]. Since chromatin modifying proteins can have temporal specific roles, we were interested if an acute postnatal *Brg1* loss in *Math1* expressing cells might have a different effect on cerebellar development [224]. Hence, in a second part of this project we generated *Math1-creER^{T2}::Brg1^{fl/fl}* mice and induced the *Brg1* deficiency by injecting tamoxifen at P3. We examined the mice for overall survival and investigated the impact of the *Brg1* loss on cerebellar development und tumor formation.

For different tumor entities, including a subset of AT/RTs which are characterized by negativity of the *Brg1* and positivity for the *Ini1* protein in IHC, *Brg1* has been described as a tumor suppressor [91]. However, little is known about this subset of AT/RTs, since AT/RT cell lines with *BRG1* mutations as well as mouse models are currently missing. GEMM of *INI1* mutated AT/RTs revealed that the *Ini1* deficiency only drives AT/RT formation in mice when the gene is lost in a specific period of time during embryonic development. Han *et al.* speculated that NSCs during their differentiation into neuronal progenitors might be susceptible for oncogenic transformation in case of *Ini1* deprivation. Additionally, it was shown that *Sox2* is overexpressed in murine and human AT/RTs, suggesting that *Sox2* positive cells might be the cells of origin for this tumor entity [103]. Thus, in the third part of this study, we investigated if *Sox2* positive cells might be the cell of origin for *Brg1* deficient AT/RTs in mice. Further, we examined whether the time point of *Brg1* loss had different consequences for brain and AT/RT development. We generated *Sox2-creER^{T2}::Brg1^{fl/fl}* mice and induced *Brg1* deficiency between E6.5 and E14.5 via tamoxifen injections into the pregnant mothers. The alterations in the brains of the mutant offspring were characterized by different staining methods. Additionally, neurospheres were cultured *in vitro* to investigate functional consequences of the *Brg1* deficiency. *Brg1* is part of the SWI/SNF chromatin remodeling complex, which regulates

global gene expression. Thus, we investigated the changes in the transcriptome after Brg1 knockdown by RNA sequencing analysis.

In conclusion, the aim of this study was to elucidate temporal and spatial roles of Brg1 in brain development and tumorigenesis in mice.

3 Materials and methods

3.1 Materials

3.1.1 Chemicals, reagents and solutions

Table 1 List of all chemicals, reagents and solutions

Chemicals, reagents, solutions	Manufacturer
2-Deoxy-D-glucose	Sigma-Aldrich, Munich, DE
4'6'-diamidino-2-phenylindole (DAPI)	Sigma-Aldrich, Munich, DE
5-bromo-2'-deoxyuridine (BrdU)	Sigma-Aldrich, Munich, DE
5X Green GoTaq Reaction Buffer	Promega, Mannheim, DE
Acetic Acid	Carl Roth GmbH, Karlsruhe, DE
Agarose	Life Technologies, Carlsbad, USA
bFGF	PeproTech, Rocky Hill, USA
Borax Anhydrous	Sigma-Aldrich, Munich, DE
Chloroform	Merck Millipore, Darmstadt, DE
Corn oil	UKE Apotheke, Hamburg, DE
Diethyl pyrocarbonate (DEPC)	Sigma-Aldrich, Munich, DE
DMEM/F12	Gibco/ Life Technologies, Carlsbad, USA
Dnase I from bovine pancreas	Sigma-Aldrich, Munich, DE
dNTPs	Promega, Mannheim, DE
DPX mountant	Sigma-Aldrich, Munich, DE
Eosin	Merck Millipore, Darmstadt, DE
Ethanol	Merck Millipore, Darmstadt, DE
Ethylenediaminetetraacetic acid (EDTA)	Sigma-Aldrich, Munich, DE
Fetal bovine serum (FBS)	Life Technologies, Carlsbad, USA
Formaldehyde (4 %, buffered solution)	Chemsolute/ Th. Geyer GmbH, Renningen, DE
GoTaq® G2 DNA Polymerase	Promega, Mannheim, DE
Hank's balanced salt solution (HBSS)	Gibco/ Life Technologies, Carlsbad, USA
Hematoxylin	Carl Roth GmbH, Karlsruhe, DE
HEPES buffer	Life Technologies, Carlsbad, USA
Hydrochlorid acid (HCl, 25 %)	Merck Millipore, Darmstadt, DE
Hydrogen peroxide (H ₂ O ₂)	Merck Millipore, Darmstadt, DE

Isopropanol	Chemsolute/ Th. Geyer GmbH, Renningen, DE
Laminin	Sigma-Aldrich, Munich, DE
L-Glutamin	Life Technologies, Carlsbad, USA
Low-melting plaque agarose	Biozym Scientific GmbH, Hessisch Oldendorf, DE
Magnesium chloride (MgCl ₂)	Promega, Mannheim, DE
mEGF	PeproTech, Rocky Hill, USA
Methanol	Carl Roth GmbH, Karlsruhe, DE
Mowiol	Carl Roth GmbH, Karlsruhe, DE
N2 supplement	Gibco/ Life Technologies, Carlsbad, USA
Non essential amino acids (NEM)	Sigma-Aldrich, Munich, DE
Normal goat serum (NGS)	Merck Millipore, Darmstadt, DE
Papain	Worthington Biochemical Corporation, Lakewood, USA
Paraffin	Sakura, Alphen aan den Rijn, NL
Penicillin/Strepomyocin	Life Technologies, Carlsbad, USA
Phloxine B	Sigma-Aldrich, Munich, DE
Phosphate-buffered saline (PBS)	
Phosphate-buffered saline (PBS, 10x)	Biochrom/ Merck, Darmstadt, DE
poly-L-ornithine	Sigma-Aldrich, Munich, DE
Potassium chloride (KCl)	Thermo Scientific, Schwerte, DE
Potassium dihydrogenphosphate (KH ₂ PO ₄)	Merck Millipore, Darmstadt, DE
Proteinase K	Carl Roth GmbH, Karlsruhe, DE
Sodium dodecyl sulfate (SDS)	Carl Roth GmbH, Karlsruhe, DE
Sodium chloride (NaCl)	Carl Roth GmbH, Karlsruhe, DE
Sodium phosphate monobasic monohydrate (NaH ₂ PO ₄ x2H ₂ O)	Carl Roth GmbH, Karlsruhe, DE
TAE buffer (50X)	PanReac Applichem, Darmstadt, DE
Tamoxifen	Sigma-Aldrich, Munich, DE
Tri-Na-Citrat-Dihydrat (10 mM)	Carl Roth GmbH, Karlsruhe, DE
Tris (1 M)	Carl Roth GmbH, Karlsruhe, DE
Triton X100	Sigma-Aldrich, Munich, DE
TRIzol reagent	Life Technologies, Carlsbad, USA

Trypsin inhibitor	Carl Roth GmbH, Karlsruhe, DE
Trypsin/EDTA	Life Technologies, Carlsbad, USA
Xylol	Chemsolute/ Th. Geyer GmbH, Renningen, DE

3.1.2 Primer

Table 2 List of all primers used for genotyping

Gene	Direction	Sequence (5'→3')	Fragment length [bp]
<i>Cre</i>	forward	TCCGGGCTGCCACGACCAA	448
	reverse	GGCGCGGCAACACCATTTT	
<i>Brg1</i>	forward	GTCATACTTATGTCATAGCC	241 (wildtype), 387 (floxed), 313 (recombined)
	reverse	GCCTTGTCTCAAACCTGATAAG	
	forward (recombined DNA)	GATCAGCTCATGCCCTAAGG	
<i>Rosa*</i>	forward	AAAGTCGCTCTGAGTTGTTAT	600 (wildtype), 250 (mutant)
	reverse (mutant)	GCGAAGAGTTTGTCTCAACC	
	reverse (wildtype)	GGAGCGGGAGAAATGGATATG	

* detection of *IsIR26tdRFP* transgene

3.1.3 Antibodies

3.1.3.1 Primary antibodies

Table 3 Table of primary antibodies

Antigen	Provider	Catalog #	Source	Dilution (IHC)	Dilution (IF)
BrdU (clone MoBU-1)	Invitrogen/ Thermo Scientific, Schwerte, DE	B35128	Mouse	1:100	1:100
Brg1 [EPNCIR111A]	Abcam, Cambridge, UK	ab110641	Rabbit	1:500	1:25
Calbindin	Merck Millipore, Darmstadt, DE	AB1778	Rabbit	1:100	-
Caspase-3 (Asp175) (cleaved Caspase 3)	Cell Signaling, Frankfurt, DE	9664	Rabbit	1:100	-
Ctip2	Abcam, Cambridge, UK	ab18465	Rat	1:100	1:100

Cux1	Proteintech, Rosemont, USA	11733-1-AP	Rabbit	1:200	1:200
GFAP	Thermo Scientific, Schwerte, DE	#149892	Mouse	-	1:500
Ki67	Abcam, Cambridge, UK	ab15580	Rabbit	1:100	-
NeuN	Merck Millipore, Darmstadt, DE	MAB377	Mouse	1:50	1:25
Olig2	Merck Millipore, Darmstadt, DE	AB9610	Rabbit	1:200	-
Otx2	Thermo Scientific, Schwerte, DE	1H12C4B5	Mouse	1:2000	-
Pax2	Zymed/ invitrogen/ Thermo Scientific, Schwerte, DE	71-6000	Rabbit	1:500	-
Pax6 (clone Poly19013)	biolegend, Fell, DE	901301	Rabbit	1:1000	-
Prox1	Abcam, Cambridge, UK	ab199359	Rabbit	1:500	-
Reelin	Merck Millipore, Darmstadt, DE	MAB5364	Mouse	1:200	-
Sox2	Abcam, Cambridge, UK	ab97959	Rabbit	1:200	-
TuJ1 (beta III tubulin)	biolegend, Fell, DE	801201	Mouse	1:200	-
Vimentin	Abcam, Cambridge, UK	ab92547	Rabbit	1:1000	-
Zbtb20	Sigma-Aldrich, Munich, DE	HPA016815	Rabbit	1:200	-

3.1.3.2 Secondary antibodies

Table 4 List of all secondary antibodies used in this study

Antigen	Vendor/Provider	Catalog #	Source	Dilution
anti-mouse Alexa555	Cell Signaling, Frankfurt, DE	CST4409	Goat	1:500
anti-rabbit Alexa488	Cell Signaling, Frankfurt, DE	CST4412S	Goat	1:500
anti-rat Alexa594	Abcam, Cambridge, UK	ab150160	Goat	1:500

3.1.4 Kit systems

Table 5 List of all kit systems used in this study

Kit	Manufacturer
DCS Supervision 2	DCS Innovative Diagnostik-Systeme, Hamburg, DE
Ventana Benchmark xt	Roche, Basel, CH
FD Rapid GolgiStain Kit	FD Neurotechnologies, Inc., Columbia, USA
NEBNext® Poly(A) mRNA Magnetic Isolation Module	New England Biolabs, Ipswich, USA
NEXTflex® Rapid Directional qRNA-Seq™ Kit	Bioo Scientific Corp., Täby, SE

3.2 Mouse experiments

All experimental procedures were approved by the Government of Hamburg, Germany (113/16) and performed according to national regulations. Mice were kept on a 12 h dark/light cycle and food and water was available *ad libitum*. Animals of both sexes were used for all experiments. Mice younger than 13 days were sacrificed by decapitation. Older mice were first anesthetized by floating the cage with CO₂ (30-50 % of cage volume/min) and then sacrificed by cervical dislocation. Embryos were isolated via Caesarean Section: Pregnant mothers were sacrificed and the uterus removed. Then, the embryos were collected and sacrificed by decapitation.

3.2.1 Genotyping

3.2.1.1 DNA isolation

Tail tips or ear biopsies were used for genotyping. They were transferred into 500 µL lysis buffer (5 M NaCl, 20 % SDS, 1 M Tris-HCl, 0.5 M EDTA, 200 µg/µL Proteinase K in ddH₂O) and incubated at 56 °C and 1200 rpm for 2 h. Afterwards, each sample was centrifuged at 4 °C and 14000 rpm for 5 min. The supernatant containing the genomic DNA (gDNA) was transferred into a new 1.5 mL eppendorf tube containing 500 µL isopropanol. Then, the tube was centrifuged at 4 °C and 14000 rpm for 5 min and the isopropanol was discarded. The gDNA pellet was air-dried and resuspended in 100 µL TE Buffer (1 M Tris, 0.5 mM EDTA in ddH₂O). Afterwards, the solution was incubated at 37 °C and 1200 rpm for 1 h. The isolated gDNA was kept at 4 °C.

3.2.1.2 PCR

The genotype-specific regions were amplified by PCR using the previously isolated gDNA. The formulation of the master mixes were as follows:

Table 6 Formula for PCR mastermixes

Reagent	Concentration	Volume [μ L]
gDNA		1.0
fw Primer	0.25 M	0.25
rv Primer	0.25 M	0.25
dNTPs	10 mM	0.15
5x PCR Buffer	1x	2.0
MgCl ₂	25 mM	0.5
ddH ₂ O		5.75
Taq Polymerase		0.1

The following PCR programs were used:

Table 7 Overview of the PCR programs used for genotyping

No.	Step	<i>Cre</i>	<i>RFP</i>	<i>Brg1</i> , <i>Brg1 R</i>
1	Initial denaturation	94 °C, 3 min	94 °C, 3 min	94 °C, 3 min
2	Denaturation	94 °C, 20 sec	94 °C, 30 sec	94 °C, 20 sec
3	Annealing	65 °C, 30 sec	55 °C, 60 sec	55 °C/ 50 °C, 30 sec
4	Elongation	72 °C, 60 sec	72 °C, 60 sec	72 °C, 60 sec
5	Steps 1-4	32 cycles	35 cycles	35 cycles
6	Final elongation	72 °C, 2 min	72 °C, 2 min	72 °C, min
7	Cooling	4 °C, ∞	4 °C, ∞	4 °C, ∞

Afterwards, an electrophoresis in an agarose gel (2 % TAE buffer) at 150 mA for 30 min was performed to analyze the fragment sizes of the PCR products.

3.2.2 Conditional and inducible knockout mice

In order to investigate a Brg1 loss in a cell type- and time point-specific manner, the cre/loxP system was used. The cre enzyme recognizes 34 bp long DNA sequences (loxP sites) and catalyzes the recombination between these sites. LoxP sites flank (“flox”) essential exons of a target gene, leading to a knockout when a cre expressing mouse strain is crossed with a mouse strain harboring the floxed gene of interest. In order to control the time point of the cre mediated knockout, cre-ER^{T2}- driver mouse strains were used. The creER^{T2} recombinase is

fused to a mutated estrogen receptor and is therefore inactive. Upon administration of tamoxifen, the creER^{T2} recombinase becomes active and mediates knockout of the target gene [225]. To track cells after successful recombination, fate-mapping mice were generated. They carry a *loxP STOP loxP* (Isl) sequence in front of the *Red fluorescent protein (RFP)* gene (*IslR26tdRFP^{fl/fl}*, short *IslRFP^{fl/fl}*). After excision of the STOP sequence by the creER^{T2} recombinase, the cells and their progeny are marked by RFP expression.

The following mouse strains were used: *Brg1^{fl/fl}* [170, 226], *hGFAP-cre* (JAX #4600), *IslR26tdRFP^{fl/fl}* [227], *Math1-creER^{T2}* (JAX #7684), and *Sox2-creER^{T2}* (JAX #17593).

3.2.3 Tamoxifen induction and BrdU pulse

Pregnant mice (*Brg1^{fl/fl}*, *IslR26tdRFP^{fl/fl}* or *Brg1^{fl/fl}::IslR26tdRFP^{fl/fl}*) were injected intraperitoneally (i.p.) with a single dose tamoxifen dissolved in 50 µL corn oil at 6.5, 7.5, 8.5, 9.5, 12.5 or 14.5 days *post coitum*. The presence of a post-coital plug defined E0.5. If the embryos were isolated by caesarean section and sacrificed for further analyses, 1 mg tamoxifen was injected. If they were born naturally, the dose was reduced to 0.75 mg and foster mothers placed in the cages for support during birth and raising of the neonates. Pups (*Brg1^{fl/fl}* or *Math1-creER^{T2}::Brg1^{fl/fl}*) received a single dose of 0.6 mg tamoxifen dissolved in 30 µL corn oil at P3. Two hours before sacrificing the animals, 25 µg/g body weight bromodeoxyuridine (5-bromo-2'-deoxyuridine, BrdU) was administered i.p. to analyze proliferation rates of different cell types.

3.2.4 Body and brain weights

Body weights of *hGFAP-cre::Brg1^{fl/fl}* mice were measured daily and brain weights determined at P0, P7 and P13. Body and brain weights of *Math1-creER^{T2}::Brg1^{fl/fl}* mice were determined right before and after sacrifice, respectively. Controls were handled accordingly.

3.2.5 Fluorescence-activated cell sorting for fate mapping experiments

Fate-mapping experiments were performed to track all cells and their progeny in which the loxP sites of the *Brg1* gene were recombined, after the creER^{T2} recombinase was activated. For this purpose, *Sox2-creER^{T2}::IslRFP^{fl/fl}* and *Sox2 creER^{T2}::Brg1^{fl/fl}::IslRFP^{fl/fl}* embryos were treated with tamoxifen at E7.5 or E9.5. The first served as controls as upon tamoxifen treatment only *RFP* expression was induced in *Sox2* expressing cells, whereas the latter were used as mutants since the *RFP* expression was accompanied by loss of *Brg1* expression. The embryos were isolated via caesarean section at E14.5 and brains were prepared under a dissecting microscope (Leica M165 FC, Leica, Wetzlar, DE). After removal of the meninges, each brain was transferred into a 2 mL eppendorf tube containing 1 mL Hanks' balanced salt solution (HBSS) supplemented with 6 g/L glucose. The tube was centrifuged at 100 x g for 10 min and the tissue resuspended in Papain (20 U/mL) and Dnase (400 µg/mL) in

DMEM/F12. It was incubated for 30 min at 37 °C, 5 % CO₂ and 86 % humidity for 30 min. The tube was inverted every 10 min manually. The suspension without solid tissue parts was transferred into a new 1.5 mL eppendorf tube and centrifuged at 100 x g for 10 min. The cells were resuspended in 1 mL DMEM/F12. RFP expressing cells were sorted with a *BD FACSAria Fusion* flow cytometer using the software *Diva 8.0.1* (both BD Biosciences, Heidelberg, DE). Later, the results were analyzed using the software *FlowJo 10.6.1* (BD Biosciences, Heidelberg, DE).

3.3 Primary cell culture

3.3.1 Neurosphere generation

RFP positive cells derived from *Sox2-creER^{T2}::lsIR26tdRFP^{fl/fl}* and *Sox2-creER^{T2}::Brg1^{fl/fl}::lsIR26tdRFP^{fl/fl}* after tamoxifen administration at either E7.5 or E9.5 were isolated as described in 3.2.5. They were seeded at a concentration of 100 cells/μL in a 24 well plate in DMEM/F12 supplemented with 1x N2 supplement, 1 % penicillin/streptomycin, 1 % L-Glutamin, 1 % Non-essential amino acids, 20 ng/mL mEGF and 10 ng/mL bFGF and cultured at 37 °C, 5 % CO₂ and 86 % humidity. Fresh growth factors were added every three days. After 7 days in culture, number and size of primary neurospheres were determined using the Nikon Ti2 microscope (Nikon, Tokyo, JP) and quantified using the *ImageJ* software (Wayne Rasband, National Institute of Health, USA). As soon as the neurospheres reached a diameter of 100 μm they were passaged. For this, the cell suspension was centrifuged at 300 x g for 5 min. The supernatant was discarded and the cells resuspended in trypsin/EDTA. The cells were incubated at 37 °C in the waterbath. After 2-3 min the reaction was stopped using a trypsin inhibitor and the cells were reseeded. Five days after passaging number and size of the secondary neurospheres were determined.

3.3.2 Cerebellar explant cultures

Cerebellar explant cultures were performed as previously described [228]. Coverslips in a 24 well plate were coated with poly-L-ornithin (15 μg/mL) overnight and with laminin (20 μg/mL) 2 h before the start of the experiment. Three-day old pups were sacrificed and their cerebella were isolated. After removal of the meninges and the choroid plexus, the tissue was passed through a 400 μm nylon mesh. The cerebella explants were cultured on the previously coated coverslips in DMEM/F12 supplemented with 1x N2 supplement, 1x penicillin/streptomycin, 0.25 mM KCl and 10 % FBS for 7 days at 37 °C, 5 % CO₂ and 86 % humidity. The medium was exchanged every 2 days and the explants were fixed using 4 % formaldehyde solution for 20 min. They were kept in PBS at 4 °C until they were used for IF.

3.4 Immunohistochemistry and immunocytochemistry

3.4.1 Cytospin

Cytospins were performed in order to fix cells in suspension onto glass slides for immunocytochemistry. For each cytospin, $5-8 \times 10^5$ cells in 100 μ L PBS were pipetted into the cytofunnel. After centrifugation at 500 rpm and low acceleration for 5 min using the *Cytospin 4* (Thermo Scientific, Schwerte, DE), the cells were fixed using 4 % formaldehyde solution for 15 min at RT and afterwards dried overnight.

3.4.2 Tissue embedding

For IHC, IF-P analysis and H&E stains, tissue was fixed in 4 % formaldehyde solution for at least 24 h. In order to analyze brains of mice, which were P0 or younger, the brain was left inside the head. The skin was removed and holes were pricked into the skull at bregma and lambda to ensure proper fixation of the brain. The tissue was dehydrated using the *automatic modular tissue processor ASP300S* (Leica, Wetzler, DE) as follows:

Table 8 Programs used for automated tissue dehydration

Reagent	Time (standard program) [min]	Time (extended program) [h]
3.5 % Formaldehyde	60	1
ddH ₂ O	15	0.5
70 % Ethanol	30	2
80 % Ethanol	45	4
96 % Ethanol	75	5
96 % Ethanol	75	5
100 % Ethanol	90	8
100 % Ethanol	120	8
Xylol	45	4
Xylol	120	6
Paraffin	60	6
Paraffin	90	6
Paraffin	90	6

The standard program was used for brains and the extended program for whole embryonic heads. The tissue was embedded in paraffin and cut into 2 μ m thick sections.

3.4.3 IHC

3,3'-Diaminobenzidine stainings were performed using the *DCS SuperVision 2* Kit or using the *Ventana Benchmark xt* system according to manufacturer's instructions. First, the tissue was deparaffinized as follows:

Table 9 Deparaffinization procedure for IHC or IF

Reagent	Time [min]
Xylol	10
Xylol	10
100 % Ethanol	5
100 % Ethanol	5
95 % Ethanol	5
90 % Ethanol	5
80 % Ethanol	5
70 % Ethanol	5
50 % Ethanol	5
ddH ₂ O	1
ddH ₂ O	1

Afterwards, the antigen retrieval was executed by cooking the slides in citrate-phosphate buffer (pH 6.0) for 20 min. After cooldown, the slides were washed three times in PBS-T followed by three washes in PBS for 5 min each. Then, the endogenous peroxidases were saturated by incubating the slides in 5 % H₂O₂ in methanol for 20 min. In case of BrdU stainings, the slides were now incubated in 4 N HCl for 10 min in order to denature the DNA and afterwards put into 0.1 M Borax buffer to neutralize the acid. Next, the samples were incubated in blocking buffer (PBS-T supplemented with 10 % NGS) for 1 h at RT. Finally, the primary antibody in the respective dilution (Table 3) was added and the slides were kept in a wet chamber at 4 °C overnight. On the next day, the samples were washed three times in PBS, incubated with the antibody enhancer for 20 min and washed again twice. Afterwards, the horseradish peroxidase (HRP) polymer was added for 20 min. Then, the slides were washed twice. Now, 3 % DAB Quanto chromogen was diluted in DAB Quanto substrate and added onto the slides for 5-10 min. The slides were washed in ddH₂O for 2 min and then the nuclei were counterstained with hemalaun (1 min hemalaun, 5 min tab water). The slides were dehydrated by incubating them in 95 % ethanol for 20 sec, twice in 100 % ethanol for 20 sec and finally in xylol for 10 min. They were mounted with DPX mountant.

3.4.4 H&E stains

For H&E stains, the tissue slides were deparaffinized the same way as for IHC analysis. Afterwards, they were incubated in freshly filtered hematoxylin for 5 min, washed in ddH₂O for 5 sec and then transferred into a HCl solution (4 mL 25 % HCl, 496 mL ddH₂O) for a few seconds. Then, the slides were incubated in running tap water for 5 min, which resulted into blue stained nuclei. Subsequently, the slides were put into 70 % ethanol for 1 min followed by an eosin solution (0.5 g eosin, 0.05 g phloxine B, 2 mL of 2.1 % acidic acid in ethanol, 100 mL ddH₂O) for 1 min. Next, they were transferred thrice into 100 % ethanol for 20 sec each and finally into xylol for 2 min. The slides were mounted with DPX mountant.

The hematoxylin stains nuclei blue and the eosin step causes the cytoplasm to appear pink.

3.4.5 IF staining

For IF-P stainings, the deparaffinization and the antigen retrieval of the tissue slides was performed the same way as for IHC analysis. Both steps were skipped for fixed cells on cytopins or fixed cerebellar explant cultures. The samples were washed in tap water followed by ddH₂O and PBS for 5 min each. They were incubated in blocking buffer (PBS-T, 5 % NGS) for 60 min at RT. Afterwards, the primary antibody diluted appropriately in blocking buffer (Table 3) was added and the cells or tissues were kept in a wet chamber at 4 °C overnight. Then, they were washed thrice in PBS and the secondary antibody in its respective dilution in PBS (Table 4) was added. To counterstain nuclei 4'6'-diamidino-2-phenylindole (DAPI, 1 µg/mL) was added to the secondary antibody solution and the samples incubated for 1 h at RT. Finally, they were washed three times in PBS and mounted using mowiol.

3.4.6 Golgi-Cox staining

Golgi-Cox staining is used to visualize neuronal morphology. With this method, a random set of neurons is stained as mercury precipitates in these cells. Here, the *FD Rapid GolgiStain Kit* (FD NeuroTechnologies, INC.) was used according to manufacturer's instructions. Freshly dissected brains of P7 animals were impregnated with a solution of mercuric chloride, potassium dichromate and potassium chromate for 1 week at RT in the dark. Afterwards, they were cut into 200 µm thick slices using a vibratome (Leica, Wetzlar, DE). Then, the stains were visualized with another solution provided in the Kit and the slices were placed on a microscope slide. The tissue was mounted using mowiol.

3.5 RNA isolation

RNA was isolated as previously described [229]. FACSed cells (described in 3.2.5) were homogenized in 750 µL TRIzol reagent and incubated at RT for 5 min. Then, 150 µL chloroform were added, each sample was mixed for 15 s and then incubated at RT for 3 min.

Afterwards, each sample was centrifuged at 4 °C and 14 000 rpm for 20 min. Three layers became visible: a red phenol-chloroform organic layer at the bottom, an interphase and an upper aqueous phase containing proteins, DNA and RNA, respectively. The upper phase was transferred into a new 1.5 mL eppendorf tube and an equal volume of isopropanol was added to precipitate the RNA. The sample was mixed and incubated at RT for 10 min. Afterwards, it was centrifuged at 4 °C and 14 000 rpm for 5 min. The supernatant was discarded, the pellet was resuspended in 750 µL of 75 % ethanol and centrifuged at 4 °C and 8000 rpm for 10 min. After the supernatant had been removed, the pellet was air-dried and finally resuspended in 10 µL DEPC H₂O.

3.6 RNA sequencing

RNA sequencing was performed in collaboration with Dr. Daniela Indenbriken (Heinrich Pette Institute, Hamburg, Germany). Prior to RNA sequencing, the RNA integrity number (RIN) was determined with the *RNA 6000 Nano Chip* on the *Agilent 2100 Bioanalyzer* (Agilent Technologies). Only RNA with a RIN of over 6.0 was used. The mRNA was extracted from the total RNA using the *NEBNext Poly(A) mRNA Magnetic Isolation module* (New England Biolabs) according to manufacturer's instructions. In order to generate RNA sequencing libraries, the *NEXTFLEX Rapid Directional qRNA-Seq Kit* (Bioo Scientific) was executed as suggested by the supplier. RNA concentrations were measured with a *Qubit 2.0 Fluorometer* (Thermo Fisher Scientific). The fragment lengths distribution of the RNA sequencing libraries were determined using the *DNA High Sensitivity Chip* on the *Agilent 2100 Bioanalyzer*. For sequencing, all samples were adjusted to a concentration of 2 nM and then pooled equimolarly. The pooled RNA sequencing libraries were sequenced on the *NextSeq500* (Illumina) with 1x75 bp and 14.2- 19.7 x10⁶ reads per sample.

3.6.1 Bioinformatics

Bioinformatic analyses were performed in collaboration with Michael Spohn. The quality of the raw reads was confirmed by using the *FastQC* tool from the Babraham Bioinformatics Institute [230]. Afterwards, the reads were aligned to the mouse reference genome GRCm38 employing the *Spliced Transcripts Alignment to a Reference (STAR)* software (v.2.6.1c) [231]. Concurrently, counts (reads/gene) were determined by the *quantmode Gene-Counts* option. They are based on the *Ensembl* annotation release 95 [105]. The *DESeq2* package (v.1.22.2) was used to estimate differentially expressed genes (DEGs) between Brg1 deficient samples and their Brg1 competent controls [232]. The package calculated log₂ fold changes, p-values and false discovery rates (FDRs). Genes were defined as DEGs, if they had a log₂ fold change > +/-0.6 and a FDR <0.1. Heatmaps were created with the *pheatmap* R package, based on the DEseq2 normalized counts. Enriched gene ontology (GO) terms were

estimated with the *GAGE* R package. To visualize GO terms and their related DEGs, GOchords were created by using the *GOChord* plotting function of the R package *GOplot*.

3.7 Image analysis and quantification

DAB, H&E and Golgi-Cox stainings were analyzed using the *Olympus BX43* microscope and the *Olympus cellSens* software (both Olympus Corporation, Tokyo, JP). In order to take pictures of an entire organ, the *Nikon Ti2* microscope and the camera DS-Fi3 as well as the software *NIS elements* was used (both (Nikon, Tokyo, JP). The same microscope and software were also used for analyzing IF stainings, but pictures were taken with the *DS Qi2* camera. For all quantifications the *ImageJ* software (Wayne Rasband, National Institute of Health, USA) was used. To determine the percentage of labeled cells (chromogenic or fluorescent signal), they were counted and divided by the total number of cells in the respective region. Cell fractions in the cerebellum were ascertained in lobule IX or in a corresponding region if no lobules were present. In cerebellar explant cultures, the migrated distance of cells was determined by counting all GFAP negative cells outside the explant. The thickness, fractions of stained cells as well as cell density in the cerebral cortex was ascertained in the region of the secondary visual cortex using frontal brain sections of P7 animals. The thickness was measured three times in serial sections. To quantify the numbers of neurospheres all spheres per well were counted. For all quantifications at least 3 animals per group were used.

3.8 Statistical analyses

All statistical tests were performed using the *Prism Software Version 7* (GraphPad Software, Inc., San Diego, USA) except for the bioinformatics analyses (described in 3.6.1). In all mouse models, survival curves were compared using a Log-rank (Mantel-Cox) test. To compare *hGFAP-cre::Brg1^{fl/fl}* mice with respective controls or *hGFAP-cre::Brg1^{fl/wt}* mice, the following statistical analyses were executed: A Sidak's multiple comparison test was performed for body weight analyses and neuronal migration in cerebellar explant cultures. A Tukey's multiple comparison test was executed for brain weight analyses. In order to quantify IHC marker expression or to compare cortical thickness and cell densities as well as apical dendrite lengths, an unpaired two-tailed t-test was performed. A chi-square test was executed to determine, whether mice with specific genotypes were born with the expected Mendelian ratio.

In order to study differences between *Math1-creER^{T2}::Brg1^{fl/fl}* and *Brg1^{fl/fl}* mice, we used an unpaired t-test with Welch's correction to determine the Brg1 knockout. Further we performed an unpaired two-tailed t-test to compare the abundance of BrdU positive cells as well as body and brain weights. The yield of RFP positive cells after FACS as well as the numbers of neurospheres per well in *Sox2-creER^{T2}::Brg1^{fl/fl}* mice and their respective controls was compared by unpaired two-tailed t-tests.

4 Results

4.1 Multipotent NSCs depend on Brg1 for proper formation of cerebral and cerebellar structures

Some studies on the role of Brg1 in NSCs have already been published [126, 175, 178, 179]. However, they either investigated how a loss changes prenatal brain development or the impact of a Brg1 deficiency on adult neurogenesis. Examining the role of Brg1 in embryonic NSCs in regard to postnatal brain development was limited by the perinatal death of the mutant mice [126]. Still, this knowledge is of interest because *BRG1* mutations are found in patients suffering from neurodevelopmental disorders. Therefore, we established a new mouse model, in which Brg1 is deleted around E13.5 in multipotent NSCs. In *hGFAP-cre::Brg1^{fl/fl}* mice, the cre recombinase drives excision of loxP sites in the majority of CNS neurons, astrocytes and many oligodendrocytes [233]. *Brg1^{fl/fl}*, *Brg1^{fl/wt}* and *hGFAP-cre* mice served as controls for this part of the study.

4.1.1 *hGFAP-cre::Brg1^{fl/fl}* mice die early and have severe abnormalities in all major brain structures

In a first approach to investigate a homo- and a heterozygous loss of Brg1, birth rates, body and brain weights as well as overall survival of *hGFAP-cre::Brg1^{fl/fl}* and *hGFAP-cre::Brg1^{fl/wt}* mice were determined (Table 10; Figure 7 A-C). Pups of both genotypes were born with the expected Mendelian ratio.

Table 10 *hGFAP-cre::Brg1^{fl/fl}* mice are born with the expected Mendelian ratio (p=0.85).

Outcome	Expected #	Observed #	Expected [%]	Observed [%]
<i>Brg1^{fl/wt}</i>	18.75	21	25.00	28.00
<i>Brg1^{fl/fl}</i>	18.75	18	25.00	24.00
<i>hGFAP-cre::Brg1^{fl/fl}</i>	18.75	20	25.00	26.67
<i>hGFAP-cre::Brg1^{fl/wt}</i>	18.75	16	25.00	21.33
TOTAL	75.00	75	100.00	100.00

hGFAP-cre::Brg1^{fl/fl} mice were indistinguishable from their control littermates until around P7, when they started to appear smaller, did not develop any fur, showed ataxic movements and an increased head circumference. In contrast, *hGFAP-cre::Brg1^{fl/wt}* pups developed normally. From P11 onwards, body weights were significantly lower in *hGFAP-cre::Brg1^{fl/fl}* mice and instead of gaining weight, they became thinner with each day (Figure 7 A). At P13, the mean body weights were 8.3 g, 7.8 g and 5.2 g for controls, *hGFAP-cre::Brg1^{fl/wt}* and *hGFAP-cre::Brg1^{fl/fl}* pups, respectively. A homozygous Brg1 loss decreased the overall survival significantly as *hGFAP-cre::Brg1^{fl/fl}* mice died at about two weeks of age (Figure 7 B).

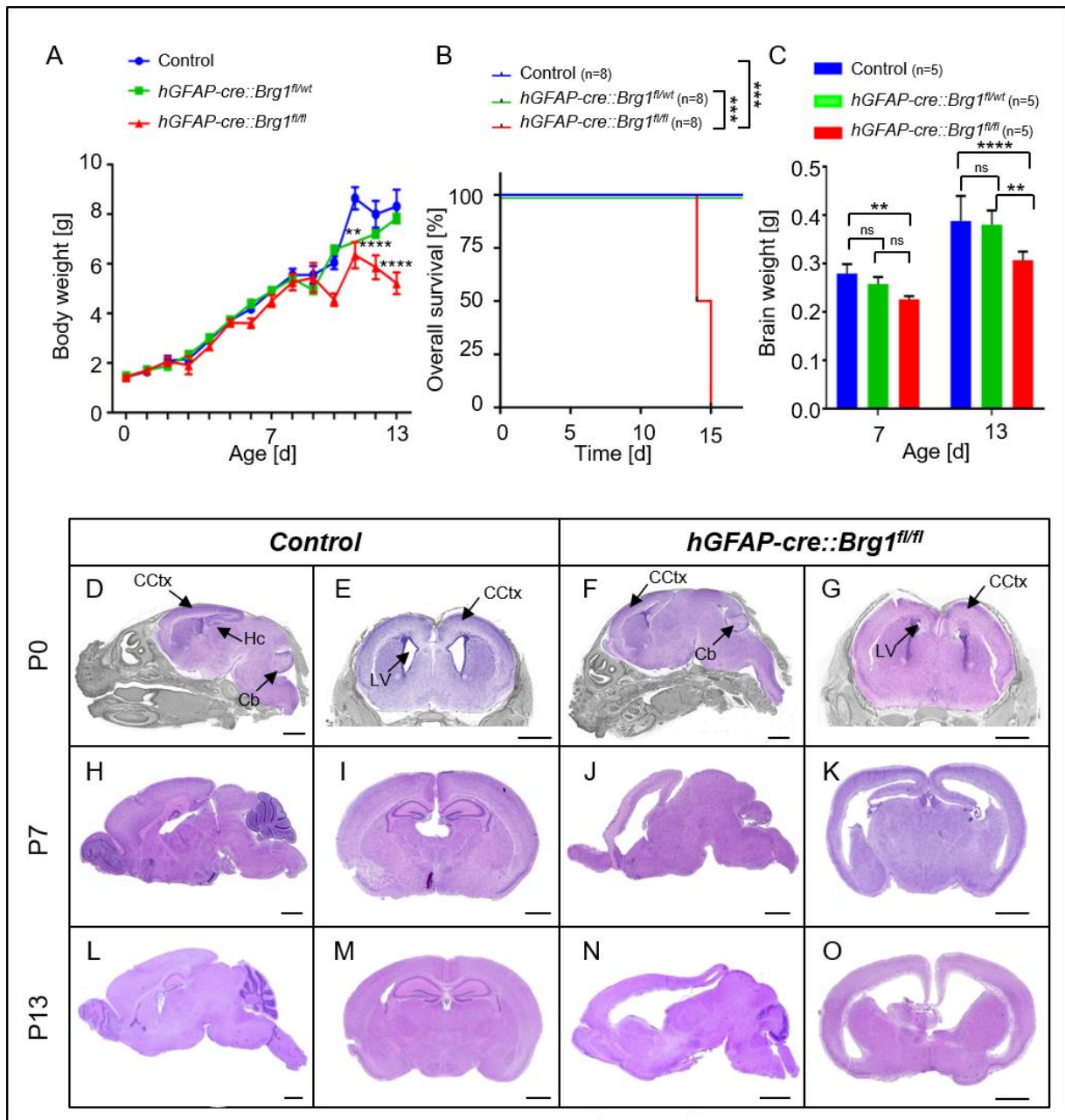


Figure 7 Postnatal development is impaired in *hGFAP-cre::Brg1^{fl/fl}* mice. *hGFAP-cre::Brg1^{fl/fl}* mice (red) present with significantly decreased body weights, survival and brain weights, whereas *hGFAP-cre::Brg1^{fl/wt}* mice (green) develop normally (A-C). Additionally, H&E stains reveal several abnormalities in the brains of *hGFAP-cre::Brg1^{fl/fl}* mice (D-O). All controls (green) include *hGFAP*, *Brg1^{fl/wt}* and *Brg1^{fl/fl}* mice. Scale bars correspond to 1 mm. D, H, L, F, J, N show representative sagittal H&E stained sections and E, I, M, G, K, O display frontal H&E stained sections at P0, P7, and P13. P0 sections show the entire head and all non-CNS parts are greyed out. Graphs show mean +/- standard deviation. ns: not significant/ $p \geq 0.05$, ** $p < 0.01$, *** $p < 0.001$, **** $p < 0.0001$, Cb: cerebellum, CCtx: cerebral cortex, Hc: Hippocampus, LV: lateral ventricle.

Brain weight was analyzed at P7 and P13 and showed a significant decrease in homozygous knockout mice compared to both, controls and *hGFAP-cre::Brg1^{fl/wt}* mice. At P7, the average brain weights were 0.279 g, 0.258 g and 0.226 g and at P13, 0.388 g, 0.381 g and 0.307 g in controls, *hGFAP-cre::Brg1^{fl/wt}* and *hGFAP-cre::Brg1^{fl/fl}* mice, respectively (Figure 7 C).

Next, we examined the brains at P0, P7 and P13 using H&E stains for morphological abnormalities (Figure 7 D-O). Even though at P0, *hGFAP-cre::Brg1^{fl/fl}* brains did not appear massively altered, at P7 and P13, it was obvious that they had multiple abnormalities as shown in frontal and sagittal sections. The cerebellum was hypoplastic with absent lobuli and layering, the cerebral cortex seemed thinner, the lateral ventricles were enlarged, the corpus callosum was absent and the hippocampus was severely underdeveloped. For all three time points, the brains of *hGFAP-cre::Brg1^{fl/wt}* presented like the ones of control animals and are therefore not shown. These mice were monitored for at least 6 months and did not develop any disease-related symptoms (n=15). Furthermore, there were no histological abnormalities found in the adult mice either (n=13, Supplementary Figure 1). Based on these results, we concluded that a homozygous loss of *Brg1* in multipotent NSCs has massive consequences for proper brain development, whereas a heterozygous *Brg1* deficiency does not interfere with normal ontogenesis in this model. Therefore, further analyses were only performed using *hGFAP-cre::Brg1^{fl/fl}* mice.

4.1.2 Proper expression of *Brg1* is essential for cerebellar development

One striking phenotype in *hGFAP-cre::Brg1^{fl/fl}* mice was the hypoplastic cerebellum. Normally, cerebellar foliation initiates around P0 in mice and the entire cerebellar development is completed at P20 [19]. Lobuli with four distinct cortical layers (EGL, ML, PCL and IGL) become recognizable at P7. At P13, the cells of the EGL have almost completely migrated inwards resulting in three distinct layers (ML, PCL, IGL) in the adult cerebellum [31, 234]. This physiological development can be seen in H&E stains of control mice at P0, P7 and P13 (Figure 8 A, G, H, Y). At P0, H&E stains of *hGFAP-cre::Brg1^{fl/fl}* mice as opposed to control cerebella revealed no striking differences, but at P7 and P13, the absence of foliation and distinct layers in *Brg1* knockout mice became visible (Figure 8 D, J, K, BB).

In order to investigate the extent of *Brg1* negative cells in the mutant cerebellum, we performed IHC and stained for *Brg1*. In control cerebella all cells expressed *Brg1*, whereas in *hGFAP-cre::Brg1^{fl/fl}* brains *Brg1* negative cells were found in a subset of cells at all three time points (Figure 8 B, E, I, L, Z, CC). Besides PCs and choroid plexus epithelium, most cerebellar cell types originate from *hGFAP* expressing progenitors [233]. Therefore, it is likely that not only one cell type is affected by the *Brg1* loss. To examine the abundance and location of the different cerebellar cells, we stained for NeuN, Pax6, Pax2, Sox2 and Calbindin. These are markers for differentiated GCs, maturing GCs, inhibitory neurons (basket, stellate, and Golgi cells), BGs and PCs, respectively. We further stained for Ki67 to investigate proliferation. Granule neurons are the most abundant cells in the cerebellum [235]. At P7, there were significantly less maturing and differentiated granule neurons in *hGFAP-cre::Brg1^{fl/fl}* mice compared to control mice: Pax6 and NeuN were expressed by 70 % of all cells in control

cerebella corresponding to 432 cells per $5 \times 10^4 \mu\text{m}^2$ and 488 per $5 \times 10^4 \mu\text{m}^2$, respectively (Figure 8 M, N, KK). In contrast, only 33 % of cells in *hGFAP-cre::Brg1^{fl/fl}* mice were positive for Pax6 (75 cells per $5 \times 10^4 \mu\text{m}^2$) and 26 % (57 cells per $5 \times 10^4 \mu\text{m}^2$) stained for NeuN (Figure 8 P, Q, KK). The number of NeuN positive cells appeared to be normal at P13, but their distribution was disorganized in mutant mice compared to controls (Figure 8 EE, HH). Therefore, it was likely that the loss of Brg1 did not inhibit differentiation of granule neurons entirely but caused a delay in differentiation. Ki67 stainings were congruent with this hypothesis, as it appeared that there were less proliferating GNPCs at P0 and especially at P7 in *hGFAP-cre::Brg1^{fl/fl}* mice (Figure 8 C, F, O, R). However, at P13, the proportion of Ki67 positive cells seemed similar compared to controls (Figure 8 AA, DD).

Layering in the cerebellar cortex is highly dependent on the function of BGs. Sox2 is not only expressed by neural progenitors but also by glia cells, including BGs [236, 237]. Therefore, we used Sox2 to examine their numbers and location. In *hGFAP-cre::Brg1^{fl/fl}* cerebella, about 40 % of cells were positive for Sox2, whereas in controls, only 20 % expressed the marker at P7. In relation to the surface, however, there were no differences between these two groups. In controls, 128 Sox2 positive cells per $5 \times 10^4 \mu\text{m}^2$ and in Brg1 deficient mice, 106 Sox2 positive cells per $5 \times 10^4 \mu\text{m}^2$ were found at P7 (Figure 8 T, W, KK). Also at P13, the numbers of Sox2 expressing cells seemed comparable between both groups (Figure 8 FF, II).

Although PCs were not directly affected by the Brg1 loss and their final mitosis happens prior to E13.5, we were interested whether their morphology and distribution were altered in *hGFAP-cre::Brg1^{fl/fl}* cerebella [29, 30]. Normally, PCs form a monolayer above the IGL, have large cell bodies and characteristic dendritic branches. This can be seen in Calbindin stainings of control brains at P7 and P13 (Figure 8 U, GG). In Brg1 deficient cerebella, not only the location of PCs was altered as they did not form a monolayer but they also lacked any visible dendrites at P7 (Figure 8 X). This might indicate improper maturation of PCs as a result of a Brg1 deprived environment. In *hGFAP-cre::Brg1^{fl/fl}* cerebella both, the proportion of PCs (19 % of cells) and numbers in relation to area (44 per $5 \times 10^4 \mu\text{m}^2$), were increased compared to controls in which only 2 % of cells corresponding to 9 cells per $5 \times 10^4 \mu\text{m}^2$ were Calbindin positive (Figure 8 KK). At P13, a fraction of PCs had developed dendritic branches in *hGFAP-cre::Brg1^{fl/fl}* cerebella, but their location was still disturbed, hinting towards a migration deficit of PCs (Figure 8 JJ).

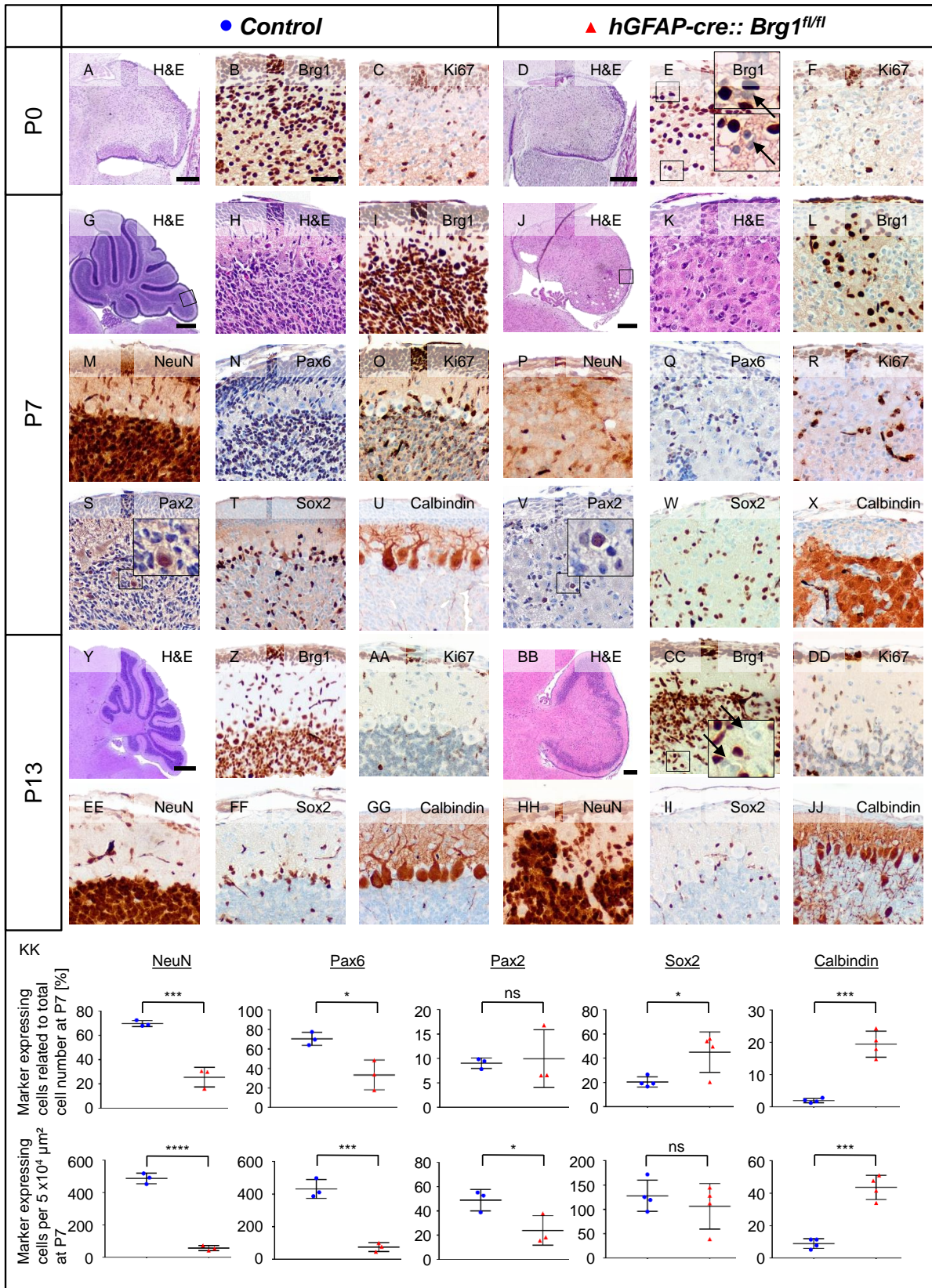


(Figure legend is found on the next page.)

Figure 8 *hGFAP* dependent *Brg1* loss results in a hypoplastic cerebellum without proper foliation and lamination. Cerebella of control and *hGFAP-cre::Brg1^{fl/fl}* mice are shown at P0, P7 and P13. *Brg1* deficient mice lack any foliation and there is no discrete layering present (D, J, K, BB) compared to control mice (A, G, H, Y) as visualized by H&E stains. *Brg1* is present in all cells of control cerebelli (B, I, Z), but absent in a subset of cells in mutant cerebelli (E, L, CC). Proliferation at P0 and P7 is pronounced in the EGL and downregulated at P13 in control mice (C, O, AA) as indicated by Ki67 stainings but reduced in mutant mice at P0 and P7 (F, R). Proliferation at P13 is similar in control and mutant mice (AA, DD). The number of NeuN positive cells at P7 is significantly decreased and the location of these cells at P13 is abnormal in mutant mice (P, HH) compared to controls (M, EE, KK). Likewise, the number of Pax6 positive cells is reduced in *hGFAP-cre::Brg1^{fl/fl}* mice at P7 (N, Q, KK). The proportion of Pax2 expressing cells in relation to the total cell number is unaltered, but the number per area is decreased (S, V, KK). BGs are visualized by Sox2 stainings. Their number compared to total cell number is increased in mutant mice (W, II) compared to control mice (T, FF, KK) but unchanged in relation to area of the cerebellum. Calbindin stainings PCs that are organized in a monolayer in controls (U, GG), but are randomly distributed and in some cases miss the dendritic tree in mutant mice (X, JJ). Their number is increased in mutants at P7 (KK). All controls include *hGFAP*, *Brg1^{fl/wt}* and *Brg1^{fl/fl}* mice. Scale bars correspond to 200 μm in panels A, D, J and V, to 400 μm in panels G and S and to 40 μm in all other panels. Arrows indicate *Brg1* negative cells. Graphs show mean \pm standard deviation. $n=3$ or $n=4$, ns: not significant/ $p \geq 0.05$, * $p < 0.05$, *** $p < 0.001$, **** $p < 0.0001$

The last cell population we investigated were Pax2 expressing inhibitory interneurons (immature basket, stellate and Golgi neurons). The proportion of Pax2 positive cells in *hGFAP-cre::Brg1^{fl/fl}* and control cerebella was almost equal (10 % and 9 %, respectively). Only the cell numbers in relation to area were significantly reduced upon *Brg1* loss (24 and 49 per $5 \times 10^4 \mu\text{m}^2$, respectively) at P7 (Figure 8 S, V, KK). This indicates that *Brg1* deprivation might cause a slight decrease in inhibitory cell numbers, but it is unlikely to be the major cause for the massive hypoplasia observed in *hGFAP-cre::Brg1^{fl/fl}* cerebella.

Since neuronal migration is essential for all parts of CNS development including layering of the cerebellar cortex, we investigated whether the migration of CGNPs is disturbed upon *Brg1* loss by cultivating cerebellar explants *in vitro*. Cerebella of P3 *hGFAP-cre::Brg1^{fl/fl}* or control pups were cultured for 7 days. As CGNPs migrate along BG fibers, the latter were stained for GFAP and all GFAP negative nuclei outside the explant were counted in relation to the distance to the explant (Figure 9). There were significantly less late-migrating cells, which had only travelled $< 100 \mu\text{m}$ in *hGFAP-cre::Brg1^{fl/fl}* compared to control explants (405 and 544 cells/explant, respectively; Figure 9 B). However, the number of cells which had left the explant early in culture were similar in both groups: In mutant explants 415 and 451 cells/explant were found in a distance of 100-200 μm and more than 200 μm , respectively. Likewise, in average 440 cells migrated 100-200 μm and 329 cells travelled more than 200 μm in controls. These results indicate that *Brg1* is essential during late stages of CGNP migration.

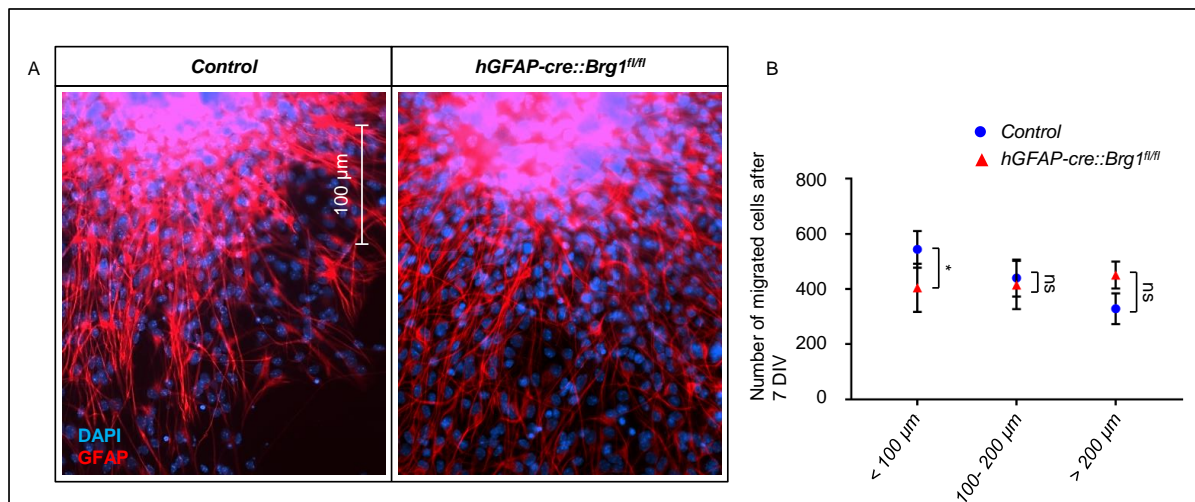


Figure 9 Brg1 is important for late stages of CGNPs migration *in vitro*. Cerebellar explants from controls and *hGFAP-cre::Brg1^{fl/fl}* mice were cultured for 7 days and glia cell fibers (red) were stained by using an anti-GFAP antibody. DAPI was used to counterstain all nuclei (A). All GFAP negative cells were counted in relation to the distance to the explant. Only cells which left the explant late in culture and migrated less than 100 µm travelled significantly shorter distances in *hGFAP-cre::Brg1^{fl/fl}* derived explants compared to controls (B). All controls include explants from *hGFAP-cre*, *Brg1^{fl/wt}* and *Brg1^{fl/fl}* mice. Graph shows mean +/- standard deviation. n=3. ns: not significant/p ≥ 0.05, *p < 0.05, DIV: days *in vitro*.

4.1.3 Stem cells in the SVZ survive less in the absence of Brg1

The different alterations in all major parts of the brains in *hGFAP-cre::Brg1^{fl/fl}* mice pointed towards a problem in the stem cell compartment due to the Brg1 deficiency. One of the main germinal zones after birth is the SVZ, which is located subjacent to the ependymal cell layer of (predominantly) the lateral ventricles [7]. In the SVZ neural progenitors develop into neuroblasts. They, in turn, travel through the rostral migratory stream towards the olfactory bulb, where they mature into interneurons [238, 239]. In order to investigate morphology, the extent of Brg1 loss as well as the numbers of NSCs, proliferating and apoptotic cells in the SVZ, we performed H&E stains and IHC for Brg1, Sox2, Ki67 and cleaved Caspase 3, respectively (Figure 10). There were no morphological alterations visible in H&E stains, but Brg1 was lost in almost all cells of the SVZ in *hGFAP-cre::Brg1^{fl/fl}* mice, whereas in controls, all SVZ cells were Brg1 positive (Figure 10 A-E, G). Only 86.34 % of cells in the Brg1 deprived SVZ were Sox2 positive, which was significantly less compared to control SVZ cells of which 98.61 % expressed Sox2 (Figure 10 F, H, M). Furthermore, the survival capacities of SVZ cells in *hGFAP-cre::Brg1^{fl/fl}* mice were decreased as significantly less cells were proliferating (29.63 %) opposed to control SVZ cells, which were almost entirely Ki67 positive (88.40 %, Figure 10 I, K, N). Likewise, significantly more cells were positive for the apoptosis indicator cleaved caspase 3 in the SVZ of *hGFAP-cre::Brg1^{fl/fl}* mice compared to control mice (4.27 % and 0.24 %, respectively, Figure 10 J, L, O). Taken together, the stem cell pool in the SVZ of

hGFAP-cre::Brg1^{fl/fl} mice is severely impaired as less NSCs are present and the cell survival is decreased.

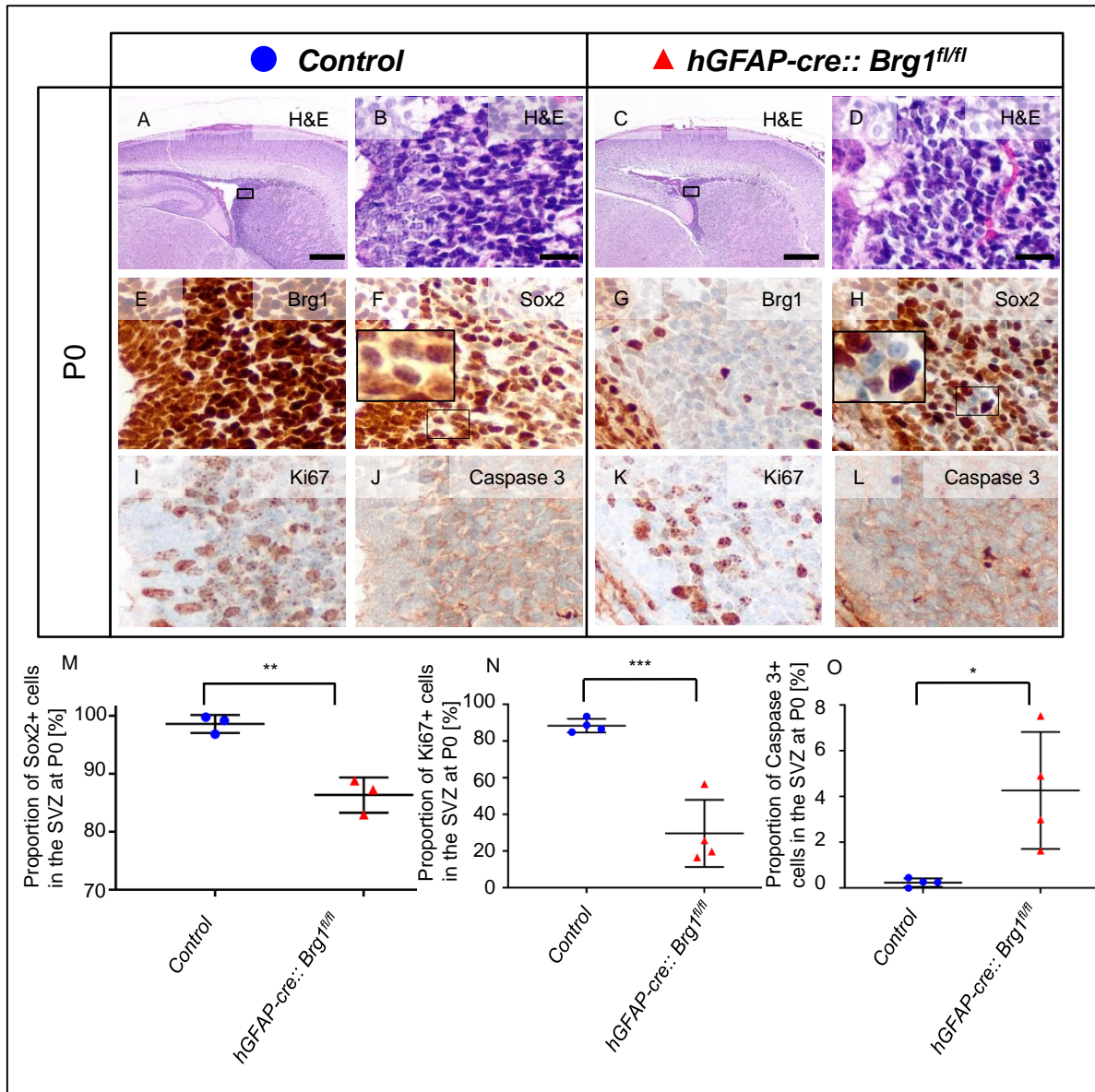


Figure 10 The SVZ is highly affected by the loss of Brg1 and loses stem cell capacities. The SVZ of control and *hGFAP-cre::Brg1^{fl/fl}* mice is shown at P0. There are no morphological alterations found in H&E stains of controls and mutants (A-E). All SVZ cells express Brg1 in control mice (E), but almost the entire SVZ has lost its expression in mutant mice (G). This loss is accompanied by significantly reduced number of Sox2 positive (H, M) and Ki67 positive (K, N) as well as an increased number of cleaved Caspase 3 positive cells (L, O) compared to controls (F, I, J). Controls include *hGFAP-cre*, *Brg1^{fl/wt}* and *Brg1^{fl/fl}* mice. Scale bars correspond to 400 μ m (A, C) and 20 μ m (B, D-L). n=4 (M, N) and n=3 (O). Graphs show mean +/- standard deviation. *p<0.05, **p<0.01, ***p<0.001.

4.1.4 The upper layers of the cerebral cortex are thinner, and neurons display pathological dendrites

Another striking phenotype of *hGFAP-cre::Brg1^{fl/fl}* mice was the severely thinned cerebral cortex, which was already visible during dissection of the brains. Eighty percent of the cells in the cerebral cortex had lost Brg1 expression (Figure 11 A-C). This resulted in a significant decrease in the thickness of the cortex. Yet, the cell density was unchanged (Figure 11 D, E).

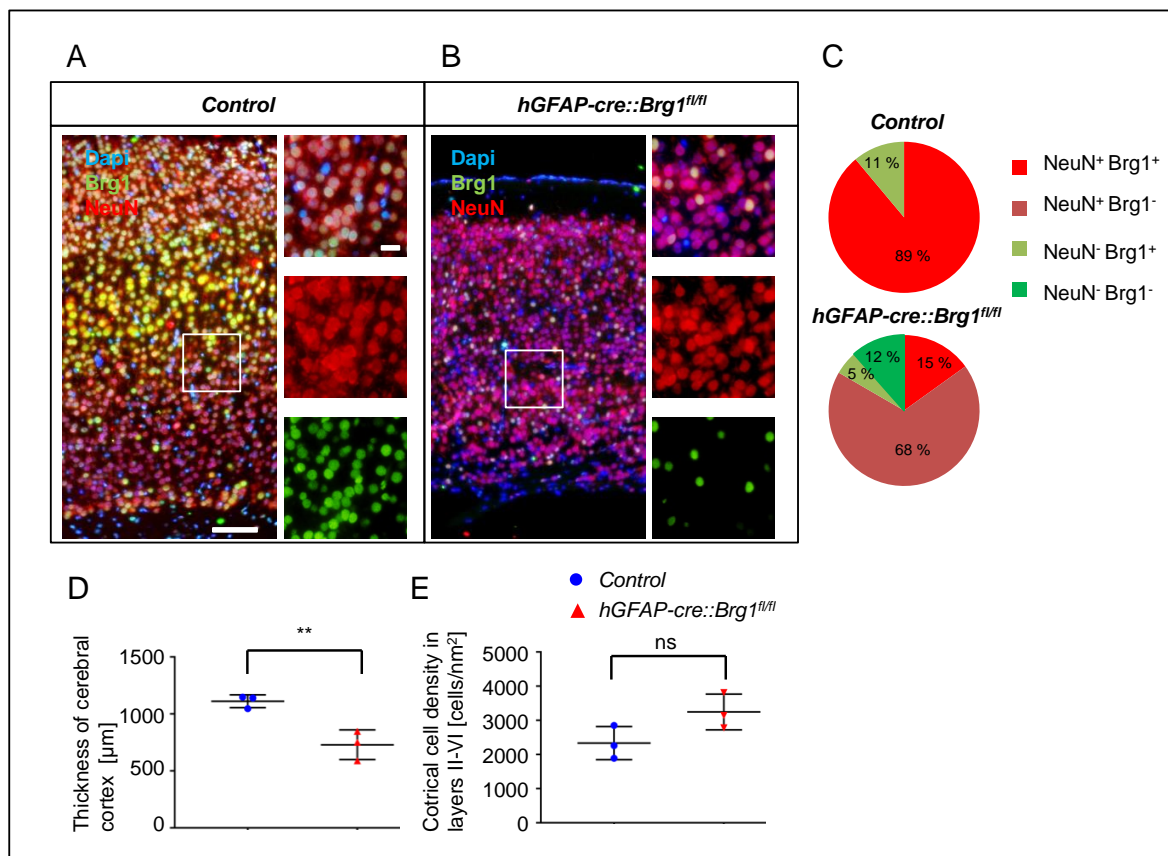


Figure 11 The cerebral cortex is severely thinner upon Brg1 loss. All stainings and quantifications were performed on P7 cerebral cortices. The proportion of postmitotic NeuN positive neurons is unaltered and Brg1 negative cells are found in both NeuN positive and NeuN negative cells in *hGFAP-cre::Brg1^{fl/fl}* mice compared to controls (A-C). Loss of *Brg1* results in significantly thinner cortices (D) with normal cell densities (E). Scale bars in A and B correspond to 100 μ m and 50 μ m for overview and high power panels, respectively. All controls include *hGFAP-cre*, *Brg1^{fl/wt}* and *Brg1^{fl/fl}* mice. Graphs show mean +/- standard deviation. n=3, ns: not significant/ $p \geq 0.05$, ** $p < 0.01$.

As both neuronal and non-neuronal cells derive from *hGFAP* expressing neural precursors, we were interested, whether the ratio of neuronal and non-neuronal cells had shifted upon loss of Brg1. For this purpose, we quantified NeuN positive (neuronal cells) and NeuN negative cells (non-neuronal cells) across all cortical layers (Figure 11 A-C). Although there were slightly more non-neuronal cells in *hGFAP-cre::Brg1^{fl/fl}* mice (17 %) compared to controls (11%), this increase was not significant. Therefore, we concluded that the neurogenic-to-gliogenic-switch was not affected by the Brg1 deficiency.

In order to investigate whether layering was disturbed in *hGFAP-cre::Brg1^{fl/fl}* cerebral cortices, we performed costainings of Cux1 and Ctip2, which mark layers II-IV and V-VI, respectively (Figure 12 A). The layers were present and distinct in the Brg1 deficient cortices but compared to controls the proportion of layers II-IV seemed to be decreased.

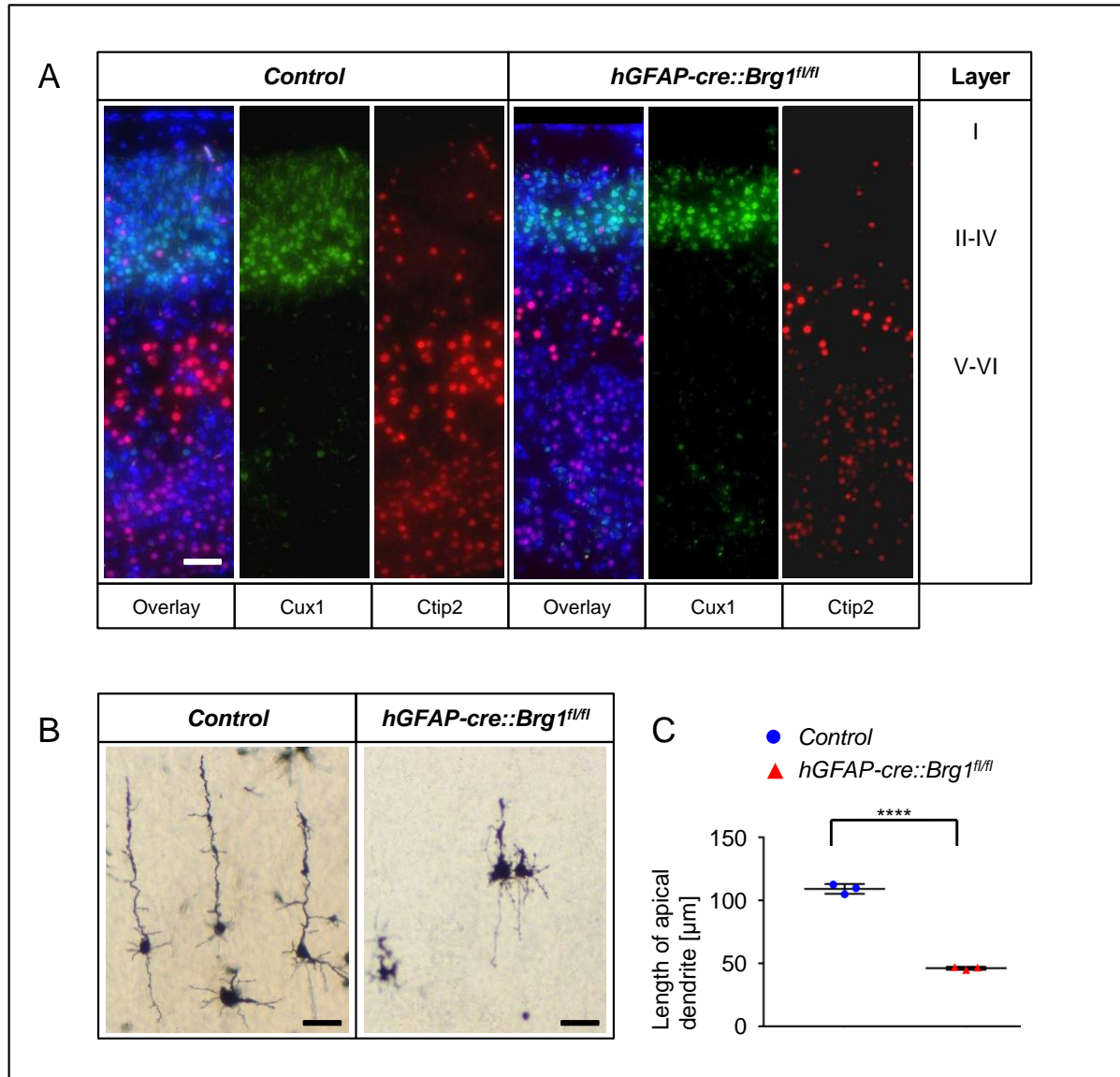


Figure 12 Cortical layers II-IV are thinner and pyramidal neurons have an altered morphology in *hGFAP-cre::Brg1^{fl/fl}* mice at P7. All stainings and quantifications were performed on P7 cerebral cortices. Cortical layering as shown by Cux1 and Ctip2 stainings is not affected in *hGFAP-cre::Brg1^{fl/fl}* mice (A), but neurons display significantly reduced lengths of apical dendrites as visualized by Golgi-Cox stainings (B, C). In A and B, the scale bars correspond to 50 μm and to 20 μm, respectively. All controls include *hGFAP-cre*, *Brg1^{fl/wt}* and *Brg1^{fl/fl}* mice. Graph shows mean +/- standard deviation. n=3, ****p > 0.0001.

Of note, presence and location of Cajal-Retzius cells were not disrupted in *hGFAP-cre::Brg1^{fl/fl}* cerebral cortices, as they were located in layer I like in controls (Supplementary Figure 2). In a last step to characterize the cerebral cortex of *hGFAP-cre::Brg1^{fl/fl}* mice, we analyzed the neuronal morphology utilizing Golgi-Cox stainings (Figure 12 B). In the cerebral cortex,

pyramidal neurons are the most abundant neuronal subtype. These excitatory neurons can be recognized by their soma, which is shaped like a pyramid or a tear drop, and by their long apical dendrites [240]. In *hGFAP-cre::Brg1^{fl/fl}* mice, the apical dendrites were significantly shorter than in control animals (109 μm and 46 μm , respectively) (Figure 12 C).

In summary, Brg1 deficiency in *hGFAP* expressing cells results in a thinned cerebral cortex, presumably due to diminished cell numbers in layers II-IV. Additionally, the morphology of pyramidal neurons is altered upon Brg1 loss.

4.1.5 Brg1 deficiency causes a severely underdeveloped hippocampus

One striking phenotype, which was already visible in H&E stains of P0 animals, was the severely underdeveloped hippocampus in *hGFAP-cre::Brg1^{fl/fl}* mice (Figure 7 G, K, O). It was only visible in a very limited number of sections as it was not only hypoplastic but also caudally shifted (Figure 13). At P7, the hippocampus of Brg1 deficient mice appeared less cell dense and the subdivision into dentate gyrus (DG) and cornu ammonis (CA), which can be seen in controls, was hardly recognizable (Figure 13 A-D). In order to investigate the presence and location of distinct cell populations in the hippocampus, we stained for Prox1 (DG granule cells), Sox2 (neural progenitors), NeuN (postmitotic neurons), Ctip2 (DG granule cells, CA1, CA2), Reelin (Cajal-Retzius cells), and Zbtb20 (pyramidal and granule neurons) by IHC [241-245]. In H&E stains, especially the DG was hardly detectable. However, Prox1 positive granule cells in the DG were detectable not only in controls but also in the mutant hippocampus (Figure 13 E, H). The number of Sox2 expressing neural progenitors in the subgranular zone of the DG seemed reduced in the latter in comparison with controls (Figure 13 F, I). NeuN positive postmitotic neurons were less dense in *hGFAP-cre::Brg1^{fl/fl}* mice, particularly in the CA regions (Figure 13 G, J). Ctip2 is also expressed in postmitotic neurons, but only in CA1 and DG regions as demonstrated in controls (Figure 13 K). In Brg1 deprived hippocampi, there were almost no Ctip2 positive neurons detectable (Figure 13 N). In healthy controls, Cajal-Retzius cells were located in the *stratum lacunosum-moleculare* as well as in the outer ML of the DG (Figure 13 L). In contrast, they were also detectable by Reelin stainings in the CA1 *stratum pyramidale* of *hGFAP-cre::Brg1^{fl/fl}* mice (Figure 13 O). Nonetheless, the number of Cajal-Retzius cells seemed to be unaffected in case of Brg1 deficiency. Last, we examined Zbtb20 stainings, which are present in all regions of the hippocampus, but most pronounced in the upper row of the CA1 *stratum pyramidale* in control animals (Figure 13 M). In contrast, there was no clear division into upper row and deep row neurons of the CA1 *stratum pyramidale* in *hGFAP-cre::Brg1^{fl/fl}* hippocampi. This observation was accompanied by a general reduction of Zbtb20 expressing cells in these mice (Figure 13 P).

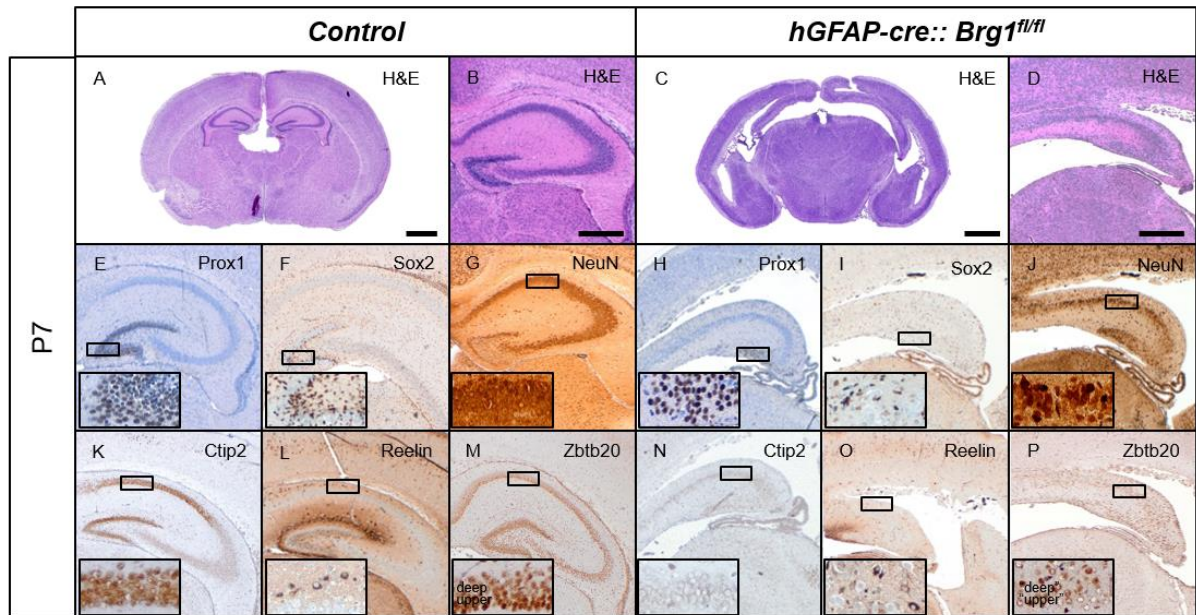


Figure 13 The hippocampus is highly underdeveloped in *hGFAP-cre::Brg1^{fl/fl}* mice. H&E stains show a caudally shifted and hypoplastic hippocampus in mutant mice compared to controls (A-D). Prox1 positive granule cells indicate the presence of the DG (E, H), which harbors a reduced number of Sox2 positive stem cells in *hGFAP-cre::Brg1^{fl/fl}* mice compared to controls (F, I). In mutants, CA regions show decreased densities of NeuN and Zbtb20 positive and almost complete loss of Ctip2 positive cells as opposed to controls (G, J, K, M, N, P). Reelin expression is unaltered in mutant mice compared to controls, but the location of Reelin expressing cells seems to be abnormal (L, O). All controls include *hGFAP*, *Brg1^{fl/wt}* and *Brg1^{fl/fl}* mice (A, B, E-G, K-M). Scale bars correspond to 1 mm in A and C and to 400 μ m in B, D -P.

To sum up, the hypoplasia in the hippocampus of *hGFAP-cre::Brg1^{fl/fl}* mice was particularly severe in CA regions. In the DG, granule cells and neural progenitors were present, even though the cell number of the latter was reduced. Likewise, the number of postmitotic neurons was diminished in the CA and they were less densely packed. Specifically, there were less Zbtb20 and almost no Ctip2 expressing neurons found in mutants. Furthermore, the lamination into *strata* in the hippocampus of *hGFAP-cre::Brg1^{fl/fl}* mice was disturbed, since Cajal-Retzius cells were located in the *stratum pyramidale* and the subdivision into upper and deep row neurons within the *stratum pyramidale* was abolished in Zbtb20 stainings.

4.2 A postnatal knockout of Brg1 in GNPCs results in a transient increase in proliferation

Chromatin modifiers can have temporal specific roles: An embryonic loss of CREB-binding protein (Cbp) results in an underdeveloped cerebellum, whereas a postnatal Cbp deficiency in CGNPs accelerates tumor formation in a murine model of medulloblastoma [224]. Since Brg1 is part of the SWI/SNF chromatin remodeling complex, we were interested if the protein might have similar functions during the development of the cerebellum.

An earlier study illustrated that a chronic Brg1 loss in *Math1-cre::Brg1^{fl/fl}* mice results in a hypoplastic cerebellum [176]. To investigate whether Brg1 continues to be essential during the development of the cerebellum after birth, we generated *Math1-creER^{T2}::Brg1^{fl/fl}* mice and deleted Brg1 by tamoxifen injections at P3. After birth, *Math1* expression in the cerebellum is restricted to the GNPCs in the EGL [246]. GNPCs first proliferate heavily in the EGL before they migrate along the BG fibers to form the IGL [247]. We selected P3 as the time point for Brg1 deletion to investigate the impact on GNPCs right before these cells are at the peak of proliferation at around P8 [27]. *Brg1^{fl/fl}* mice were also injected with tamoxifen and served as controls.

4.2.1 An acute Brg1 loss in *Math1* expressing cells at P3 enhances proliferation at P8

To investigate the short-term effect of Brg1 deficiency on proliferation, we sacrificed the mice at P8. In order to determine the number of proliferating cells, we injected the mice with BrdU, a thymidine analog which is incorporated during the S-phase of the cell cycle, two hours prior to the sacrifice. H&E stains of *Math1-creER^{T2}::Brg1^{fl/fl}* and *Brg1^{fl/fl}* mice cerebella revealed no differences at P8. In both groups, the cerebellum was divided into distinct lobuli and all layers (EGL, ML, PCL and IGL) were present (Figure 14 A). Brg1 stainings showed that about 51 % of the cells in the EGL of *Math1-creER^{T2}::Brg1^{fl/fl}* mice were negative for Brg1, whereas all cells in the control group expressed the protein as expected (Figure 14 A, B). This decrease in Brg1 positive cell numbers was significant and confirmed the function of the system. BrdU stainings revealed that in *Math1-creER^{T2}::Brg1^{fl/fl}* mice 32 % of cells in the EGL were proliferating, which was significantly more than in *Brg1^{fl/fl}* mice. Here, 26 % were positive for BrdU (Figure 14 A, C).

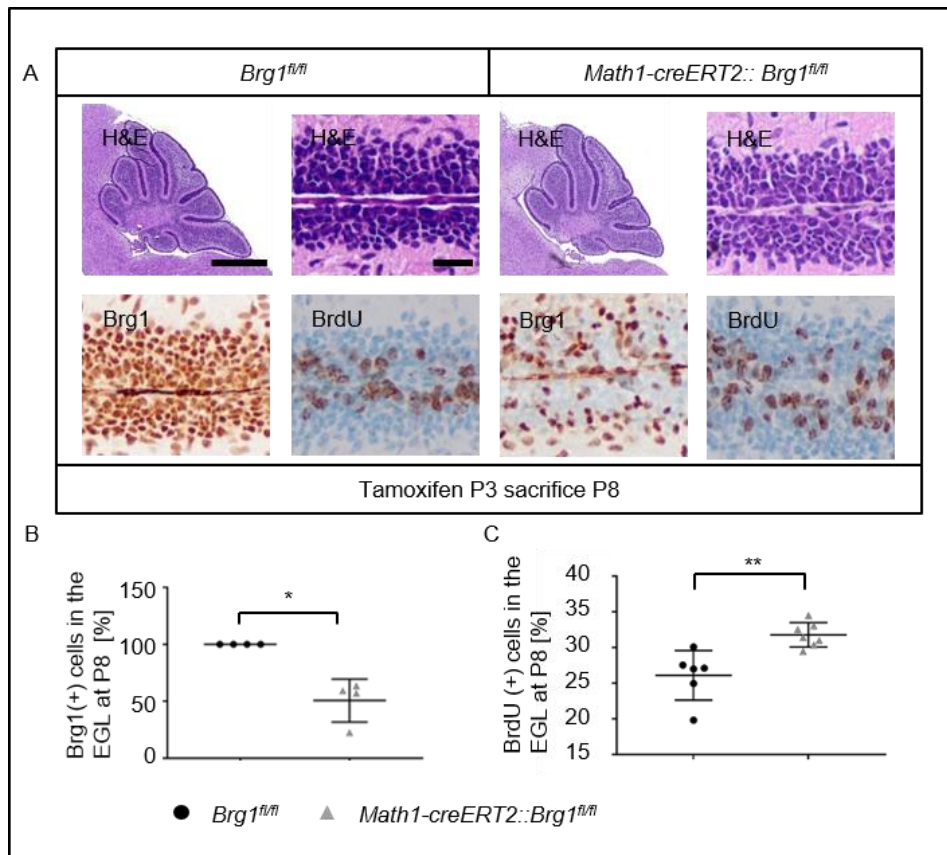


Figure 14 Postnatal knockout of *Brg1* in *Math1* expressing cells increases the proliferation of cells in the EGL. *Brg1^{fl/fl}* and *Math1-creERT2::Brg1^{fl/fl}* mice received tamoxifen at P3 and were sacrificed at P8. Two hours before death, they were treated with BrdU. H&E stains of sagittally cut cerebella appear similar between both groups (A). Fraction of Brg1 negative and proliferating (BrdU positive) cells were determined by IHC (A). Quantifications revealed a significant decrease in Brg1 positive and an increase in BrdU expressing cells due to tamoxifen induced Brg1 loss (B, C). Graphs show mean +/- standard deviation. *p<0.05, **p < 0.01, n≥4.

4.2.2 *Brg1* deprivation at P3 in *Math1* expressing cells does not obstruct cerebellar development

Furthermore, we were interested whether the increase in proliferation changed the cerebellar architecture in the adult or even drove tumor formation. Therefore, we observed *Math1-creERT2::Brg1^{fl/fl}* and *Brg1^{fl/fl}* mice after tamoxifen administration at P3 for half a year. In both groups, some animals died in the first 30 days of life. Only 31 % of *Math1-creERT2::Brg1^{fl/fl}* and 63 % of *Brg1^{fl/fl}* mice survived. However, the overall survival was not significantly different (p=0.1312) between both groups and the deaths were likely caused by side effects of the tamoxifen treatment (Figure 15 A). After half a year, the surviving *Math1-creERT2::Brg1^{fl/fl}* mice had body and brain weights of 29 g and 444 mg, respectively. *Brg1^{fl/fl}* mice had an average body weight of 24 g and an average brain weight of 435 mg, which was not significantly different from *Math1-creERT2::Brg1^{fl/fl}* mice (Figure 15 B, C). Analyses of the brains of adult mice by H&E stains showed no alterations in cerebellar architecture and no tumor development in any of the mice (Figure 15 D, E). Brg1 negative

cells had remained in the brain and migrated normally into the IGL in *Math1-creERT2::Brg1^{fl/fl}* mice. A few Brg1 deficient cells were found in the ML. Ki67 stainings were performed to check for adverse proliferation, but the distribution and number of proliferating cells in both groups were similar.

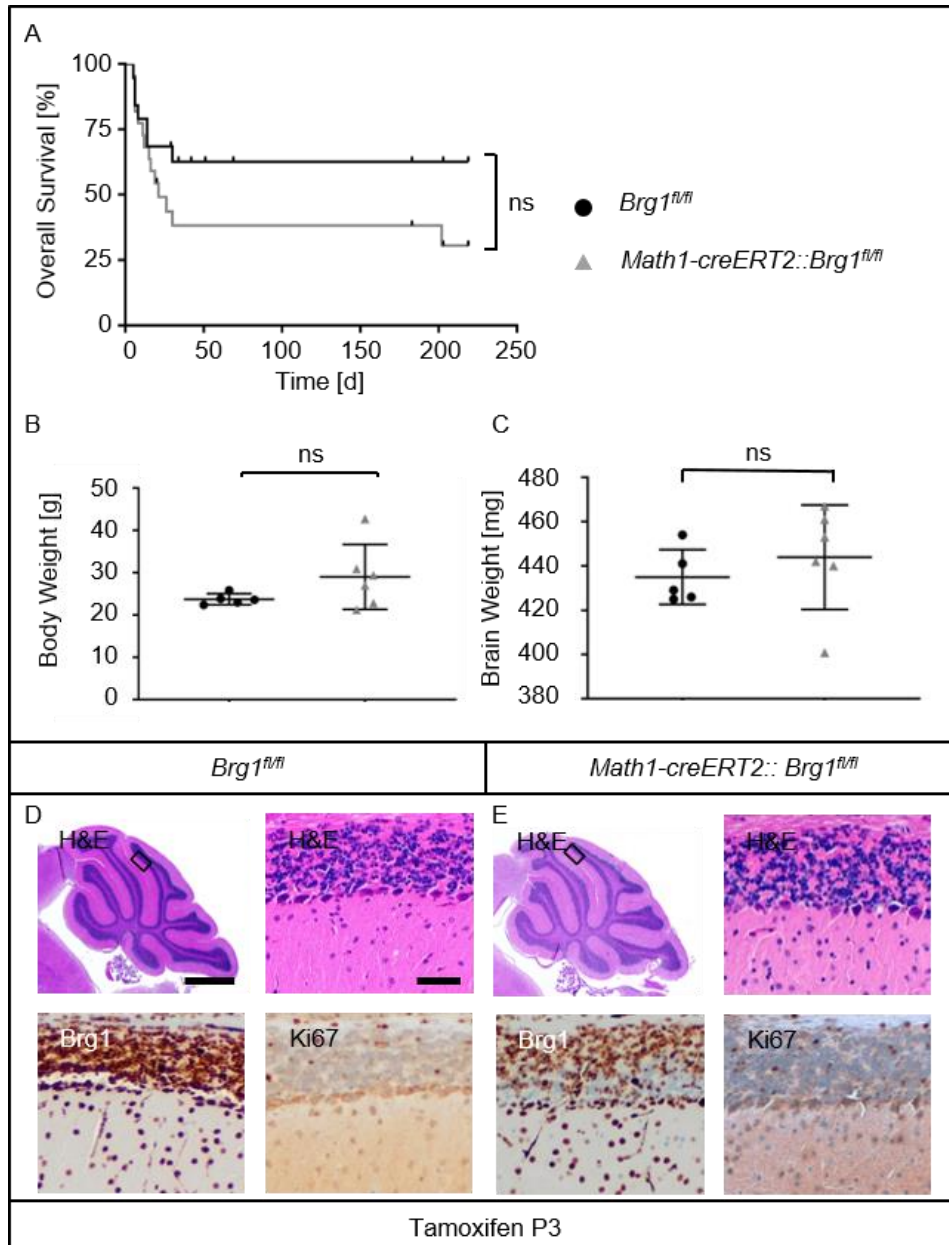


Figure 15 A postnatal Brg1 loss in GNPCs does not hinder normal brain development. *Brg1^{fl/fl}* and *Math1-creERT2::Brg1^{fl/fl}* mice received tamoxifen at P3. Overall survival was observed until they were at least 6 months old and is shown as a Kaplan-Meier curve (A). Body and brain weights were unchanged in Brg1 deficient animals (B, C). H&E stains revealed no differences in cerebellar morphology, but Brg1 deficient cells were still detectable in IHC (D, E). Ki67 stainings indicated no differences between *Brg1^{fl/fl}* and *Math1-creERT2::Brg1^{fl/fl}* cerebella (D, E). Graphs show mean +/- standard deviation. ns: not significant/ $p \geq 0.05$, $n \geq 5$.

In conclusion, a postnatal knockout of Brg1 in GNPCs leads to an increase of proliferation. However, this increase is only transient and does not alter cerebellar development or causes tumor formation in adult mice.

4.3 Brg1 has time point specific roles in Sox2 positive NSCs and is essential for brain and eye development

In 2016, Han *et al.* proposed that Sox2 might be a marker for cells from which AT/RTs originate. The study further illustrated that the cell(s) of origin are only susceptible to oncogenic transformation in a restricted time period. To model Ini1 deficient AT/RTs, the gene had to be deleted between E6 and E10 in mice [103]. Based on these observations, we established the following mouse model (Figure 16): Male *Sox2-creER^{T2}::Brg1^{fl/fl}* mice were bred with female *Brg1^{fl/fl}* mice. Successful mating was confirmed by the observation of a post-coital vaginal plug. In order to activate the cre recombinase in the offspring, the pregnant mothers received a single dose of tamoxifen by i.p. injections between E6.5 and E14.5. In theory, 50 % of the offspring had the genotype *Sox2-creER^{T2}::Brg1^{fl/fl}* (mutants) and 50 % *Brg1^{fl/fl}* (controls). Furthermore, the mothers were not affected by the *Brg1* loss because they did not harbor the *creER^{T2}* transgene.

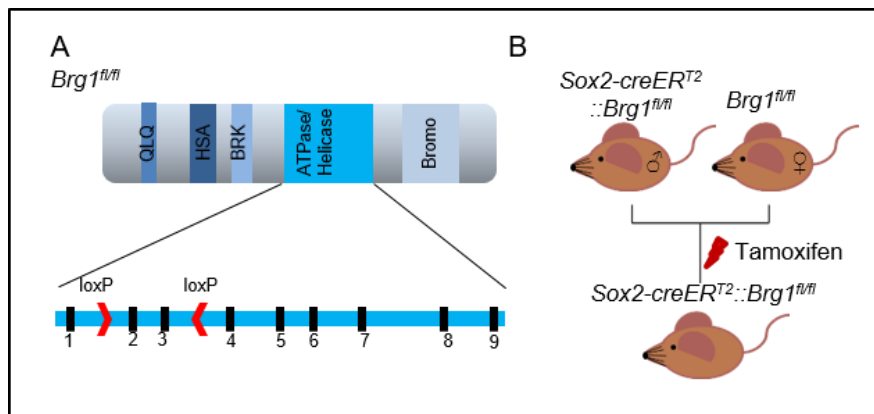


Figure 16 Experimental design to investigate time point specific roles of Brg1 in Sox2 expressing NSCs. The loxP sites are located upstream of exon 2 and downstream of exon 3 of the ATPase domain in the murine *Brg1* gene [226]. Male *Sox2-creER^{T2}::Brg1^{fl/fl}* mice are mated with female *Brg1^{fl/fl}* mice to ensure that 50 % of the offspring have the genotype *Sox2-creER^{T2}::Brg1^{fl/fl}*. Cre negative littermates serve as controls. During pregnancy, tamoxifen is injected i.p. to induce cre-mediated recombination of the loxP sites.

4.3.1 A Brg1 loss between E7.5 and E12.5 causes morphological abnormalities in the embryonic brain

After tamoxifen induced Brg1 loss between E6.5 and E14.5, the embryos were sacrificed at different embryonic stages and their brains were analyzed by H&E stains (Figure 17 C-K). For reasons of simplicity, only *Brg1^{fl/fl}* brains, which received tamoxifen at E7.5 are depicted. For all other time points of tamoxifen injections, control brains looked alike and are therefore not shown. *Sox2-creER^{T2}::Brg1^{fl/fl}* embryos presented morphological alterations in the embryonic brain (until E21.5), when the loss of Brg1 was induced by tamoxifen injections at E7.5, E8.5, E9.5, E10.5 or E12.5 with a penetrance of 100 %, 91 %, 65 %, 79 % and 100 %, respectively.

respectively (Figure 17 A). Induction of Brg1 deficiency at E6.5 or E14.5 resulted in normal prenatal brain development (Figure 17 A, E, F, K). In detail, all *Sox2-creER^{T2}::Brg1^{fl/fl}* embryos which received tamoxifen at E7.5 developed a lesion close to the basal part of the cerebrum (Figure 17 B). The lesion was already present at E14.5 and became very prominent at E18.5 (Figure 17 G, H). It consisted of a part with high cell densities, surrounded by more loosely packed cells (Figure 17 Gii, Hi). About 63 % showed additional abnormalities in the SVZ, often with rosette-like structures (Figure 17 B, Hii). *Sox2-creER^{T2}::Brg1^{fl/fl}* embryos, in which Brg1 deprivation was induced at E8.5 showed features like the basal lesion (70 %) or the involvement of the SVZ (80 %) (Figure 17 B). In case of an induced Brg1 loss at E9.5, the alterations were located in the SVZ (88 %) and the cerebral cortex (12 %). Furthermore, the embryos presented with a hydrocephalus (12 %) or a combination of these phenotypes (Figure 17 B, I, J). The abnormalities in the SVZ usually involved rosette-like structures and the layering of the cerebral cortex seemed disturbed as shown in H&E stains at E14.5 or E18.5 (Figure 17 Ii, Ji, Jii). Furthermore, in some animals the neural retina presented with rosettes (Figure 17 Iii). Initiation of Brg1 loss at E10.5 or E12.5 resulted primarily in a disrupted SVZ with rosette forming structures (73 % and 100 % of embryos, respectively) very similar to those observed after tamoxifen injections at E9.5 (Figure 17 B).

Taken together, Brg1 deficiency in *Sox2* expressing cells causes architectural alterations in the embryonic brain, when the loss is induced between E7.5 and E12.5. The type of abnormality depends on the time point of tamoxifen injections, since the lesion close to the basal cerebrum only occurred in animals induced at E7.5 and E8.5. However, alterations in the SVZ were found after Brg1 loss between E7.5 and E12.5, indicating that the cells forming the SVZ are dependent on proper *Brg1* expression for a longer period of time.

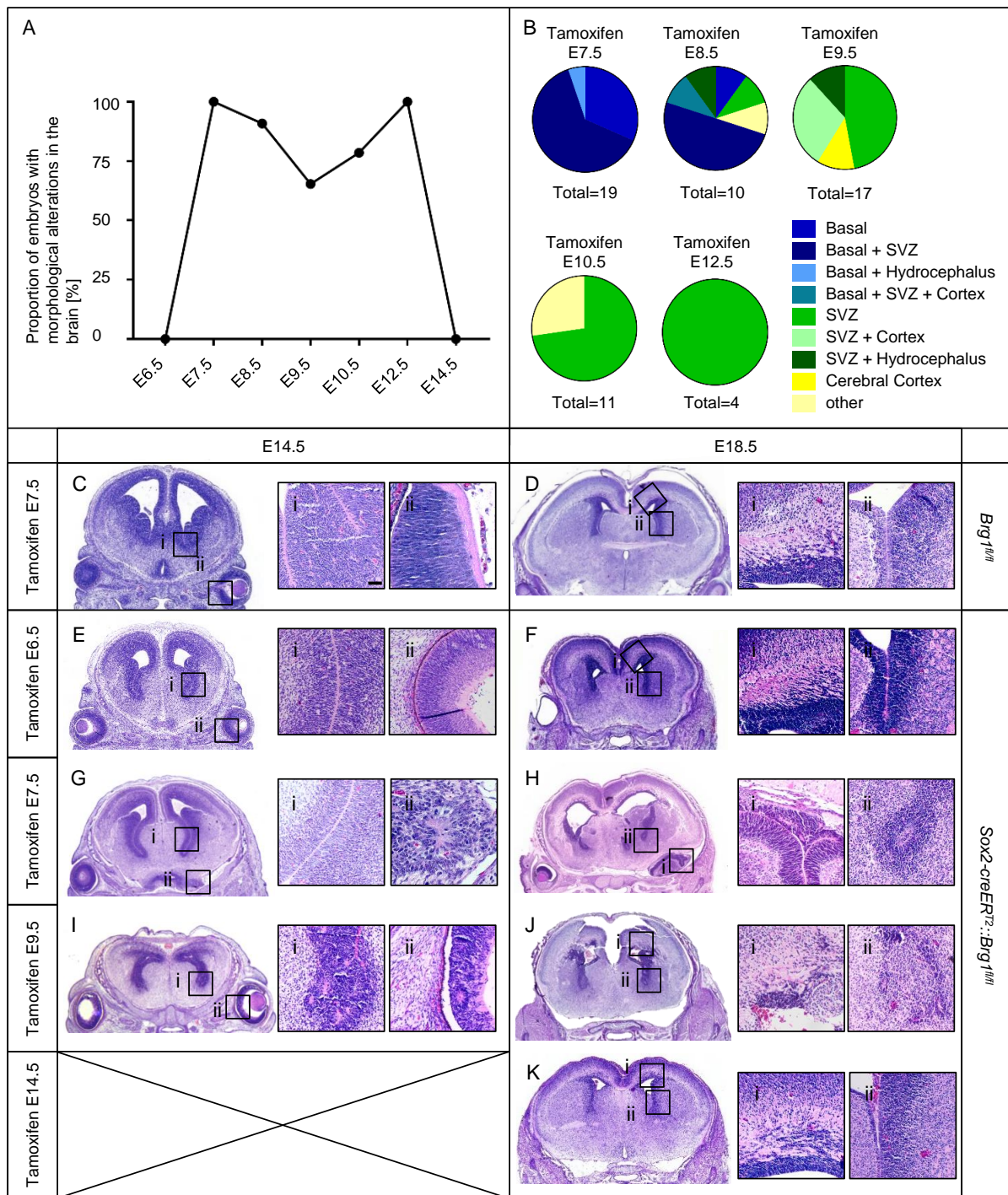
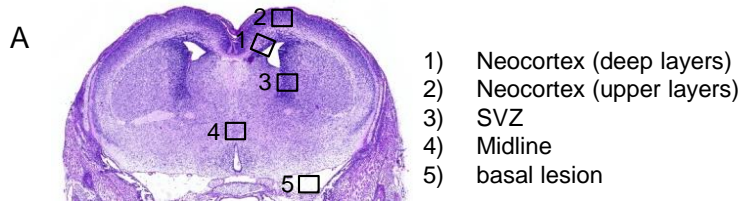


Figure 17 Loss of Brg1 in Sox2 expressing NSCs causes architectural alterations in the brain. A single dose of tamoxifen was injected into pregnant mice between E6.5 and E14.5. *Sox2-creER^{T2}::Brg1^{fl/fl}* embryos presented with morphological abnormalities only when tamoxifen was administered between E7.5 and E12.5 and with varying penetrance of the phenotypic alterations (A). They developed different types of morphological alterations in the embryonic brain (B). Frontal H&E stains of E14.5 and E18.5 embryos serve as representative images for each of the different time points of tamoxifen injections (C-K). High power images show the respective region marked in the overview images, i.e. SVZ, eye, basal lesion or cortex (i, ii). H&E stains of *Brg1^{fl/fl}* after tamoxifen at E7.5 serve as controls (C, D). Embryos between E14.5 and E21.5 were analyzed in A and B. Scale bar in Ci corresponds to 50 μ m and is representative for Ci-Kii. Whole embryo heads are shown in C-K. n= 6, n=19, n=11, n=26, n=14, n=4, n=3 *Sox2-creER^{T2}::Brg1^{fl/fl}* embryos were analyzed after tamoxifen administration at E6.5, E7.5, E8.5, E9.5, E10.5, E12.5 and E14.5, respectively.

4.3.2 Morphological altered regions in *Sox2-creER^{T2}::Brg1^{fl/fl}* embryos are formed primarily by Brg1 positive cells and show no increase in proliferation

We were interested if the brain regions with architectural disruptions were formed by those cells which had lost Brg1 earlier in embryonic development. Therefore, we performed IHC and stained for Brg1. Furthermore, we stained for Ki67 to investigate if the morphological alterations were associated with changes in proliferation.

We examined E18.5 old *Sox2-creER^{T2}::Brg1^{fl/fl}* embryos after tamoxifen treatment at E7.5 or E9.5 because all brain anomalies occurring following Brg1 loss between E7.5 and E12.5 were present in those animals. *Brg1^{fl/fl}* embryos which received tamoxifen at E7.5 were chosen as controls. We investigated Brg1 and Ki67 stainings in the deep and upper layers of the neocortex, in the SVZ, the midline and (if present) in the basal lesion close to the cerebrum (Figure 18 A). All cells in control brains were positive for Brg1 as expected (Figure 18 B-E). In *Sox2-creER^{T2}::Brg1^{fl/fl}* embryos after tamoxifen-induced loss of Brg1 at E7.5 were some Brg1 negative cells occasionally found in the deep and upper layers of the neocortex (Figure 18 J, K). In these animals, the SVZ often presented with a disrupted morphology, but the rosette-like structures were primarily formed by Brg1 expressing cells (Figure 18 L). Even though the midline did not show any architectural abnormalities in H&E stains, Brg1 deficient cells were frequently found in this region (Figures 17 G, H, 18 M). The basal lesion close to the cerebrum which was only detectable in *Sox2-creER^{T2}::Brg1^{fl/fl}* embryos after tamoxifen exposure at E7.5 (and occasionally E8.5) consisted of two distinct cell populations: The more cell dense structure was Brg1 positive and surrounded by another Brg1 negative cell population (Figure 18 N). Proliferation as indicated by Ki67 stainings was normal in the neocortex of these embryos compared to the controls. In the deeper neocortical layers, especially the cells lining the ventricle were Ki67 positive, whereas those located in the upper layers did not proliferate (Figure 18 F, G, O, P). At E18.5, the cells of the SVZ normally proliferate heavily as demonstrated in controls (Figure 18 H). However, the rosette-forming cells in *Sox2-creER^{T2}::Brg1^{fl/fl}* embryos after tamoxifen exposure at E7.5 were composed of several Ki67 negative cells (Figure 18 Q). The cells located in the midline proliferated normally in comparison with controls (Figure 18 I, R). Again, the structure at the basal part of the cerebrum was composed of two parts: The Brg1 positive elements were proliferating and the Brg1 negative cells were not mitotically active (Figure 18 N, S).



		Neocortex (deep layers)	Neocortex (upper layers)	SVZ	Midline	Basal lesion	
<i>Brg1^{fl/fl}</i>	Tamoxifen E7.5	B	C	D	E		Brg1
		F	G	H	I		Ki67
<i>Sox2-creER^{T2}::Brg1^{fl/fl}</i>	Tamoxifen E7.5	J	K	L	M	N	Brg1
		O	P	Q	R	S	Ki67
	Tamoxifen E9.5	T	U	V	W		Brg1
		X	Y	Z	AA		Ki67

Figure 18 Regions of altered morphology are predominantly formed by Brg1 competent cells. Schematic overview of all regions with morphological alterations and/or Brg1 negative cells in mutants is shown in A. In control brains all cells stain positive for Brg1 (B-E) and show moderate, almost no, high and low proliferation in the deep and upper layers of the neocortex, the SVZ and the midline, respectively, indicated by Ki67 stainings (F-I). After tamoxifen injection at E7.5 only very few Brg1 negative cells are found in the neocortex and the SVZ, whereas about 50 % of cells in the lesion at the basal part of the cerebrum have lost its expression (J-N). In mutants, in which Brg1 loss was introduced at E9.5, the number of Brg1 negative cells in the neocortex is more pronounced, but the majority retained its expression (T, U). The knockout in the SVZ is similar to the E7.5 mutants (V). In both mutant groups, there are Brg1 negative cells in the midline (N, W). Neither in the neocortex nor in the SVZ or the midline there seems to be a correlation of Brg1 knockout and a change in proliferation, but in the basal lesion of at E7.5 tamoxifen receiving embryos, the Brg1 deficient cells show less Ki67 reactivity (O-S, X-AA). All panels show representative images of E18.5 frontal brain sections. Red arrows highlight Brg1 negative cells. Scale bar in B is representative for all panels and corresponds to 20 μ m.

The expression patterns of Brg1 and Ki67 in *Sox2-creER^{T2}::Brg1^{fl/fl}* embryos induced at E9.5 were similar as in the ones induced at E7.5: In the neocortex, Brg1 negative cells were scattered in both deeper and superficial layers. However, it seemed as if slightly more Brg1 deficient cells were present in than in embryos in which Brg1 loss was induced at E7.5 (Figure

18 T, U). The rosette-like structures were formed primarily by Brg1 competent cells (Figure 18 V). In the midline, Brg1 deprived cells were present as well (Figure 18 W). The architecture of the neocortex was disturbed when Brg1 deficiency was induced at E9.5, but there was no alteration in Ki67 expressing cells in neither the deeper nor the upper layers (Figure 18 X, Y). Rosette-like structures in the SVZ appeared to proliferate less compared to control and cells in the midline seemed to proliferate normally (Figure 18 Z, AA).

All in all, even though there were different morphological alterations found in the embryonic brain after loss of Brg1 at E7.5 and E9.5 in Sox2 expressing NSCs, the abundance of Brg1 negative cells and proliferative behavior was similar. The regions with architectural abnormalities were not primarily formed by Brg1 negative cells and they proliferated normally or less compared to the respective regions in control brains. The unphysiological region close to the basal cerebrum in embryos which lost Brg1 at E7.5 was composed of two parts: a proliferating Brg1 positive and a not proliferating Brg1 negative structure.

4.3.3 Brg1 deprivation decreases cell survival and causes distinct changes in gene expression

In order to characterize the Brg1 deficient cells better, we developed fate-mapping mice. In this approach, all cells and their progeny in which the cre recombinase was activated by tamoxifen were marked by RFP expression (Figure 19). *Sox2-creER^{T2}::lsIRFP^{fl/fl}* mice were used to generate control cells. Here, all cells and their descendants that expressed Sox2 at the time point of tamoxifen injection were marked by RFP. In *Sox2-creER^{T2}::Brg1^{fl/fl}::lsIRFP^{fl/fl}* mice, tamoxifen exposure additionally caused a loss of Brg1. Pregnant mothers were injected with tamoxifen at either E7.5 or E9.5 and embryos were sacrificed at E14.5. RFP expressing cells were sorted using FACS. Afterwards, they were used for neurosphere assays or their RNA was isolated for transcriptome analysis.

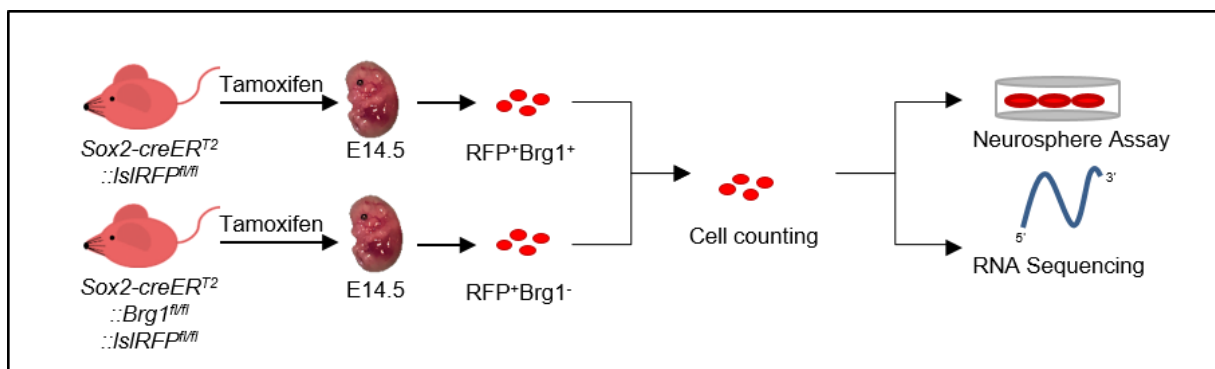


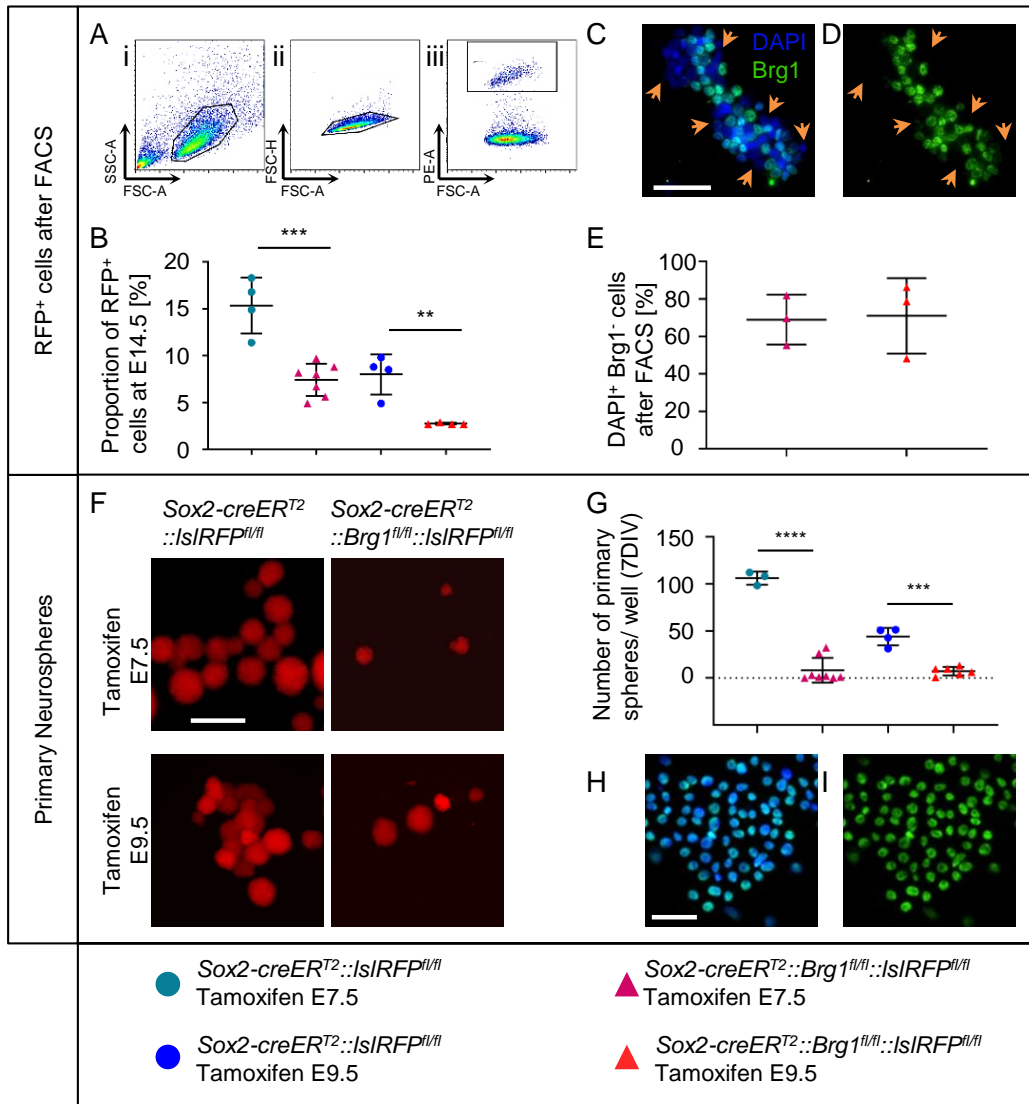
Figure 19 Experimental setup of fate-mapping experiments. In order to specifically investigate Brg1 deficient cells, fate-mapping mice were generated, in which all cells with active cre recombinase were marked with an RFP reporter. Mutant (*Sox2-creER^{T2}::lsIRFP^{fl/fl}::Brg1^{fl/fl}*) and control (*Sox2-creER^{T2}::lsIRFP^{fl/fl}*) embryos received tamoxifen either at E7.5 or E9.5 and were sacrificed at E14.5. RFP positive cells were used for a neurosphere assay and for transcriptome analysis.

4.3.3.1 Brg1 deficiency prevents formation of neurospheres

Brg1 loss significantly decreased the yield of cells which were obtained from E14.5 brains by FACS (Figure 20 Ai-iii). After tamoxifen exposure at E7.5 and E9.5, only 7.41 % and 2.75 % of RFP positive cells were isolated from *Sox2-creER^{T2}::Brg1^{fl/fl}::lsIRFP^{fl/fl}* brains, respectively. In comparison, 15.35 % and 8.00 % cells were received from *Sox2-creER^{T2}::lsIR26tdRFP^{fl/fl}* embryos after tamoxifen treatment at E7.5 and E9.5, respectively (Figure 20 B). In theory, all RFP positive cells isolated from *Sox2-creER^{T2}::Brg1^{fl/fl}::lsIRFP^{fl/fl}* brains should be Brg1 deficient after exposure to tamoxifen. To validate the efficiency of the system, we did an IF staining of the cells after FACS and stained for Brg1 (Figure 20 C-E). A representative staining of RFP positive cells derived from *Sox2-creER^{T2}::Brg1^{fl/fl}::lsIRFP^{fl/fl}* embryos after tamoxifen exposure at E9.5 is shown in Figure 20 C and D. For both time points of tamoxifen induction at least 48 % and a maximum of 86 % of RFP positive cells were negative for Brg1 (Figure 20 E). These results suggest that the efficiency of the cre enzyme is reduced, when two floxed transgenes have to be recombined simultaneously.

We cultured the RFP positive cells to investigate if they were able to form neurospheres. The ability to form primary neurospheres indicates that NSCs are able to proliferate *in vitro*, whereas the capacity to form secondary neurospheres after passage is an indicator for self-renewal [248]. After 7 days, neurospheres were present in the wells of all 4 conditions (Figure 20 F). However, in wells with cells derived from *Sox2-creER^{T2}::Brg1^{fl/fl}::lsIRFP^{fl/fl}* brains, there were significantly less spheres found (Figure 20 G). RFP expressing cells from *Sox2-creER^{T2}::lsIRFP^{fl/fl}* embryos after tamoxifen at E7.5 and E9.5 formed in average 106 and 44 neurospheres/well after 7 days in culture, respectively. In wells containing cells obtained from *Sox2-creER^{T2}::Brg1^{fl/fl}::lsIRFP^{fl/fl}* embryos which were treated with tamoxifen at E7.5 or E9.5, only 8 or 7 neurospheres were found, respectively. After passage of the primary neurospheres, secondary neurospheres could be generated from all 4 conditions (data not shown).

In order to investigate if these spheres were formed by Brg1 positive or negative cells, we used IF to stain for the protein. A representative image of a primary neurosphere grown from cells derived from embryos that were exposed to tamoxifen at E9.5 is shown in Figure 20 H and I. The neurospheres contained almost exclusively Brg1 positive cells. This suggests that in culture, Brg1 expressing cells were selected and form neurospheres, whereas Brg1 deficiency hinders formation of neurospheres. Taken together, loss of Brg1 at either E7.5 or E9.5 decreases the abundance of the respective cells at E14.5. Furthermore, these cells are probably not able to form neurospheres *in vitro*.



4.3.3.2 Transcriptome analysis indicates decreased neuronal function in absence of Brg1

Brg1 is the ATPase of the SWI/SNF chromatin remodeling complex, which regulates gene expression leading to increased or repressed transcription in a context dependent manner. Therefore, we used RNA sequencing to analyze global changes in gene expression upon loss of Brg1. We used the same experimental set-up as for the neurosphere assay and isolated the RNA immediately after FACS (Figure 19).

Unsupervised hierarchical clustering of significant DEGs (FDR < 0.1; log₂ fold change < +/- 0.6) revealed four distinct clusters (Figure 21 A). These clusters corresponded with the four treatment groups: *Sox2-creER^{T2}::Brg1^{fl/fl}::lsIRFP^{fl/fl}* and *Sox2-creER^{T2}::lsIRFP^{fl/fl}* embryos, both treated at E7.5 or E9.5 to activate the cre recombinase. The Brg1 loss at E7.5 resulted in 172 downregulated and 115 upregulated genes (Figure 21 B; Supplementary Table 1). In comparison, tamoxifen induced Brg1 deficiency at E9.5 led to 18 downregulated and 97 upregulated genes (Figure 21 C; Supplementary Table 2).

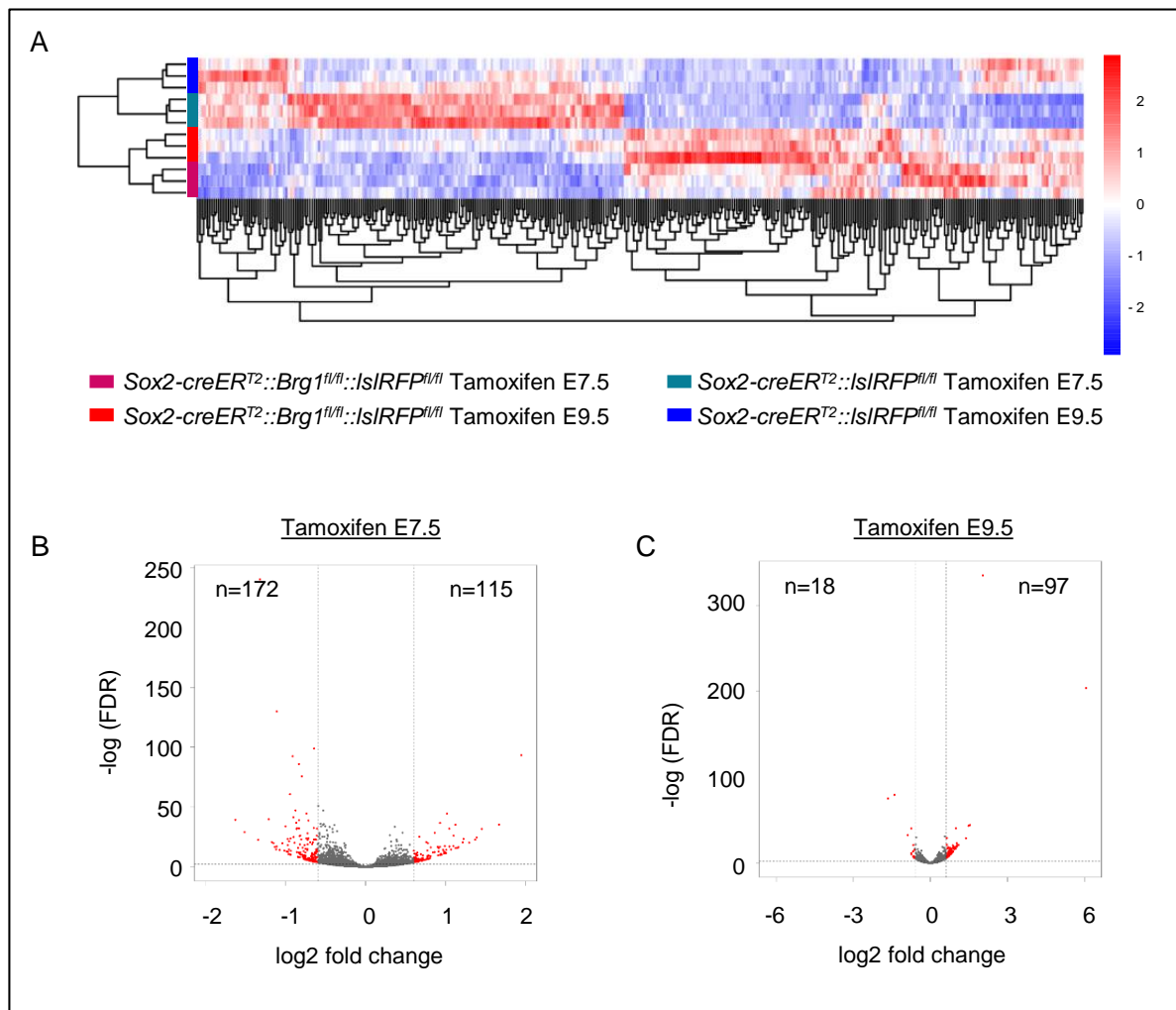


Figure 21 Loss of *Brg1* results in distinct changes in gene expression. Hierarchical cluster analysis of DEGs reveals four distinct transcriptional clusters correlating with the four treatment groups: *Brg1* deficiency induced at E7.5 or E9.5 and respective controls (A). Volcano plots show 172 (tamoxifen E7.5) and 18 (tamoxifen E9.5) downregulated as well as 115 (tamoxifen E7.5) and 97 (tamoxifen E9.5) upregulated genes in *Brg1* deficient compared to *Brg1* competent cells (B, C). Red dots mark DEGs, defined by a \log_2 fold change $> \pm 0.6$ and a $FDR < 0.1$.

In order to interpret these results functionally, we performed GO term enrichment analyses. Significantly enriched terms involving DEGs with a \log_2 fold change $> \pm 0.6$ were visualized as GOchords (Figure 22, 23). Functionally related terms were summarized as their lowest common denominator derived from the ten most significant terms per category (i.e. "Molecular Function", "Cellular Component" and "Biological Process"). In the GOchords, the respective GO terms are shown on the right half of the circle, connected by "chords" to the involved DEGs, which are depicted on the left side of the circle. Loss of *Brg1* at both investigated time points (E7.5 or E9.5) resulted in downregulation of the GO terms "cation channel complex" (GO: 0034703) and "metal ion transmembrane transporter activity (GO:0046873). The other GO terms downregulated upon *Brg1* loss differed between the groups. Still, they were all related to the function of neurons, indicating that independent of the time point, NSCs are dependent on *Brg1* to give rise to functional neurons.

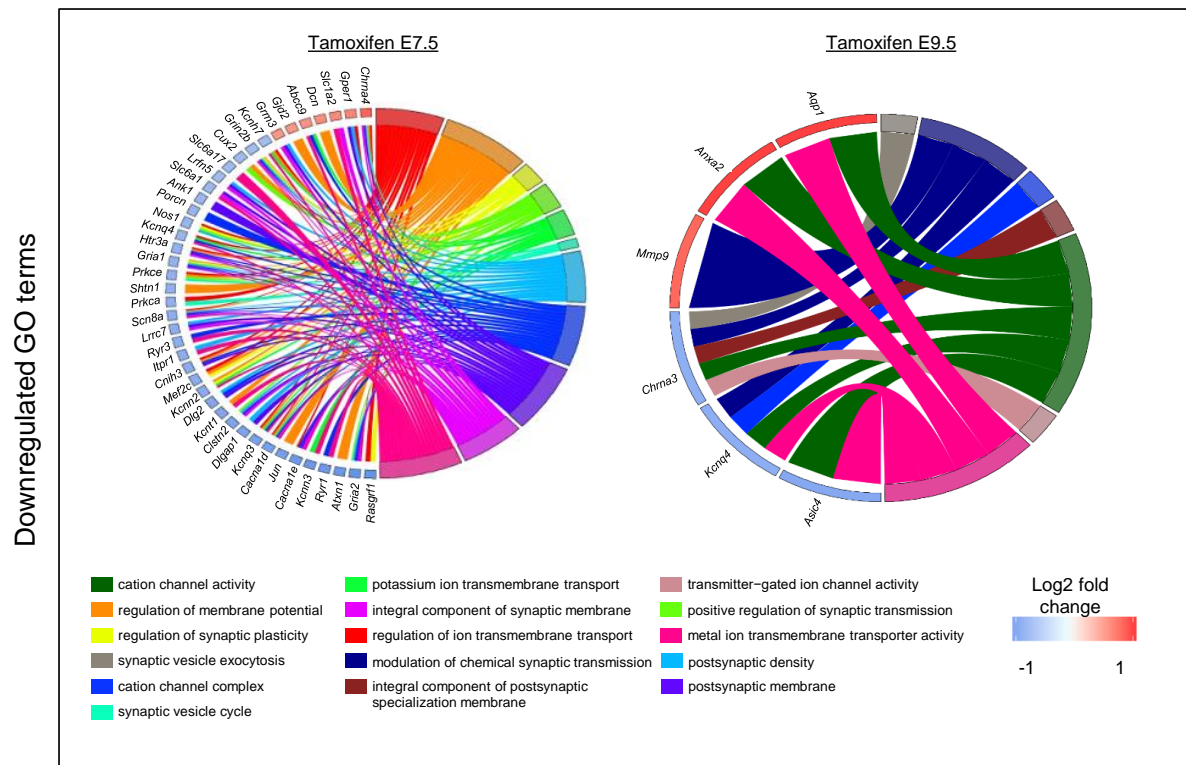


Figure 22 Downregulated GO terms are related to neuronal function. GOchords of significantly enriched downregulated GO terms after loss of Brg1 at E7.5 or E9.5 depict involved DEGs sorted according to log₂ fold change on the left side of the circle and GO terms on the right.

Using this method to identify enriched GO terms upon Brg1 loss at E7.5 resulted only in two upregulated GO terms: “antioxidant activity” (GO: 0016209) and “extracellular matrix structural constituent” (GO: 00052011) (Figure 23). However, when Brg1 deficiency was introduced at E9.5 several GO terms were upregulated, including processes involved in the cell cycle, vascular development and extracellular matrix (ECM) functions. Of note, genes encoding collagens were significantly upregulated as a result of both, Brg1 deprivation at E7.5 or E9.5 (Figure 23; Supplementary Tables 1, 2). Additionally, after Brg1 loss at E9.5, further genes encoding other ECM components such as *vitronectin*, *fibronectin 1*, *heparan sulfate proteoglycan 2* (*Hspg2*, *perlecan*), *laminin α4* (*Lama4*) and *laminin γ3* (*Lamc3*) were significantly upregulated. Concordantly, as laminins and integrins interact, *integrin α1* expression was enhanced upon induced Brg1 deficiency at E9.5 [249]. Other upregulated DEGs after Brg1 loss at E9.5 involved genes such as *Bmp7*, *Tgfβ receptor II* (*Tgfr2*) or the stem cell marker *Nestin* (Supplementary Table 2).

Taken together, Brg1 deprivation at either E7.5 or E9.5 results in the upregulation of genes and GO terms associated with the ECM. However, tamoxifen treatment at E7.5 mainly causes

enhanced expression of collagen encoding genes, whereas treatment at E9.5 additionally increases a variety of other ECM related genes.

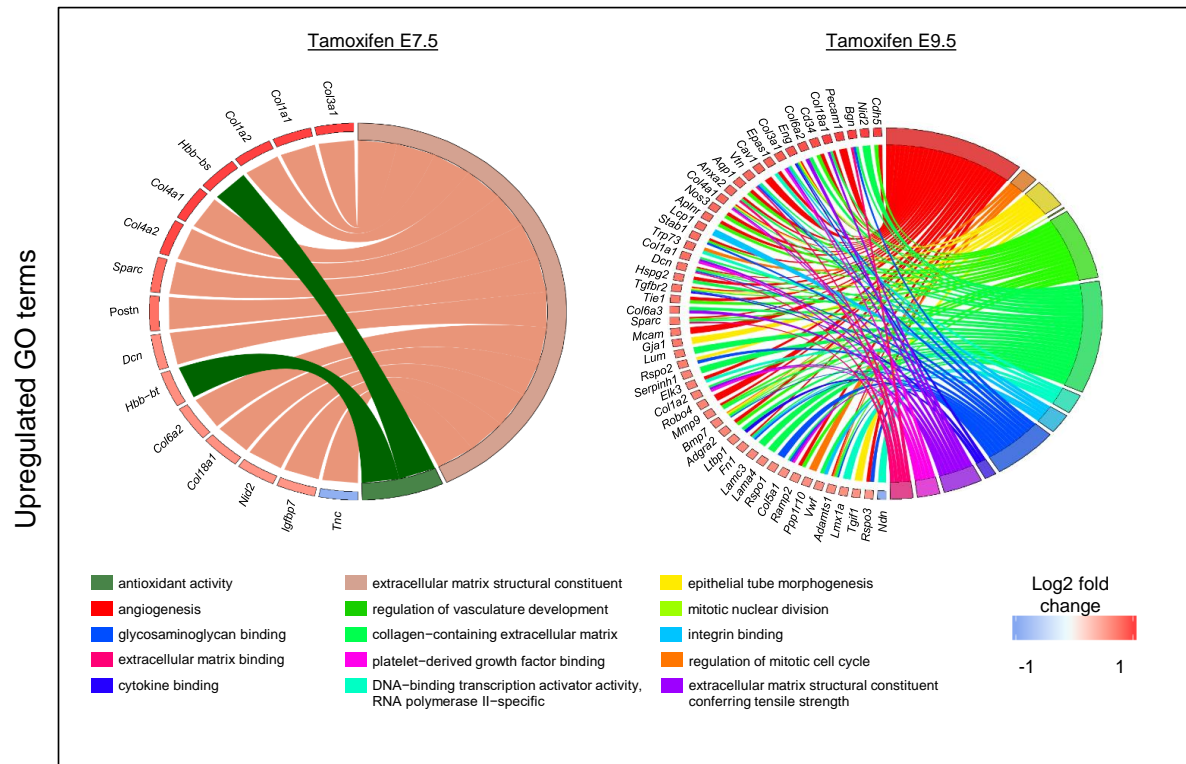


Figure 23 ECM related GO terms are upregulated upon loss of Brg1. Gochords of significantly enriched upregulated GO terms after loss of Brg1 at E7.5 or E9.5 depict involved DEGs on the left side of the circle and GO terms on the right. Especially, collagen encoding genes (e.g. *Col1a1* or *Col18a1*) or other genes coding for ECM related proteins (e.g. *Vitronectin: Vtn*, *Fibronectin: Fn1*, *heparan sulfate proteoglycan 2: Hspg2*, *perlecan*, *laminin α4: Lama4* and *laminin γ3: Lamc3*) are upregulated.

4.3.3.3 Loss of Brg1 at E7.5 hinders proper eye formation and likely causes RPE to retina transdifferentiation

Transcriptome analysis revealed 115 DEGs which were upregulated upon tamoxifen induced Brg1 loss at E7.5 (Figure 21 B; Supplementary Table 1). However, analysis of GO term enrichment did only identify two upregulated GO terms that merely included 15 of the DEGs. Therefore, we took a closer look at the individual upregulated DEGs. In this way, we recognized many genes which are normally expressed during the development of the eye, such as *Fgf15*, *Pituitary homeobox 2 (Pitx2)*, *Otx2*, *Iroquois homeobox gene 5 (Irx5)*, *POU domain class 4 transcription factor 1 (Pou4f1)* and *Lhx9* [40, 62, 250-253] (Figure 24 A). *Fgf15*, *Otx2* and *Lhx9* counts increased more than two-fold in *Sox2-creER^{T2}::Brg1^{fl/fl}::lsIRFP^{fl/fl}* compared to *Sox2-creER^{T2}::lsIRFP^{fl/fl}* derived RFP expressing cells (573.8 vs 241.8, 962.9 vs. 438.8 and 1876 vs 872.6, respectively). *Pou4f1* expression showed a three-fold increase from 228.9 reads/gene to 717.4 reads/gene in case of Brg1 deprivation. *Irx5* and *Pitx2* counts were elevated almost by the factor 4 in *Sox2-creER^{T2}::Brg1^{fl/fl}::lsIRFP^{fl/fl}* compared to *Sox2-creER^{T2}::lsIRFP^{fl/fl}* derived RFP expressing cells (196.9 vs 53.58 and 150.4 vs 38.59,

respectively). It is known that increased FGF signaling can induce transdifferentiation of RPE cells to retina *in vitro* [254]. Furthermore, in a mouse model investigating RPE development, it was shown that specifically *Fgf15* was upregulated in case of RPE to retina transdifferentiation [62]. Therefore, we speculated that the lesion we observed in 100 % of *Sox2-creER^{T2}::Brg1^{fl/fl}* embryos after tamoxifen exposure at E7.5 might be ectopic retina caused by RPE to retina transdifferentiation (Figure 17 Gii, Hi). Indeed, when we investigated the eyes of these mutants using H&E stains, we observed multiple folds of retina resembling structures around the lens (Figure 24 B). Higher magnifications suggested the transition of RPE to retina in some regions (Figure 24 C). Based on these results, we hypothesized that *Brg1* loss at E7.5 in *Sox2* expressing cells resulted in the dysregulation of genes which are essential for normal eye development. As a consequence, the RPE, at least parts of it, did not develop normally but instead gave rise to an ectopic retina.

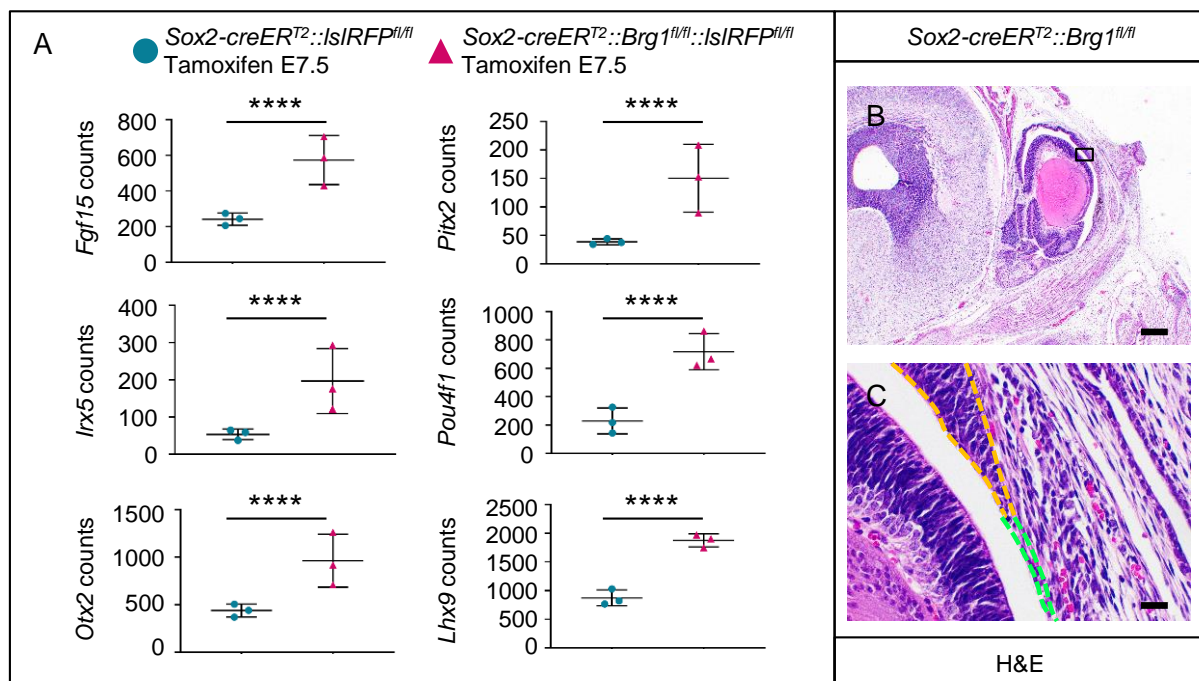


Figure 24 *Brg1* is likely indispensable for normal eye development at E7.5 in *Sox2* expressing NSCs. RNA sequencing results show a significant increase of counts in RFP expressing cells derived from *Sox2-creER^{T2}::Brg1^{fl/fl}::IsIRFP^{fl/fl}* brains for selected genes (A). All selected genes have a log₂ fold change of $\geq \pm 0.6$ and a FDR of < 0.1 . A representative H&E stain of a *Sox2-creER^{T2}::Brg1^{fl/fl}* head at E18.5 indicates a RPE to retina transdifferentiation (B, C). Potential ectopic retina is highlighted in orange dotted lines and remaining RPE in green dotted lines. All results were acquired from embryos that were treated with tamoxifen at E7.5. Scale bar in B corresponds to 200 μm and in C to 20 μm. Graphs show mean \pm standard deviation. $n \geq 3$, **** $p < 0.0001$

To validate whether the lesion in close proximity to the basal parts of the cerebrum was formed by an ectopic retina, we compared this structure with retina of healthy controls by IHC marker expression (Figure 25). The adult neural retina is composed of three layers: outer nuclear layer, inner nuclear layer and the ganglion cell layer (GCL). However, at E18.5, mainly two layers are visible, the neuroblast layer (NBL) and the GCL [253]. Both were easily recognizable

in H&E stains of retina in healthy controls (Figure 25 A, B). The NBL was composed of densely packed cells, whereas the cells in the GCL were arranged more loosely. Based on morphology, the basal lesion in *Sox2-creER^{T2}::Brg1^{fl/fl}* embryos showed similar structures resembling NBL and GCL (Figure 25 H, I). *Sox2* is a marker for retinal progenitor cells, Müller glial cells, retinal astrocytes, and a subset of cholinergic amacrine cells and therefore mainly found in the NBL [255]. The corresponding expression pattern was found in both, the NBL of the retina in *Brg1^{fl/fl}* mice as well as in the NBL resembling structure in the basal lesion of *Brg1* deprived animals (Figure 25 C, J). *Pax6* was predominantly expressed in the inner part of the NBL and cells in the GCL in controls (Figure 25 D). Even though it seemed as if more cells in the basal regions of *Sox2-creER^{T2}::Brg1^{fl/fl}* embryos were *Pax6* positive, the general expression pattern appeared similar (Figure 25 K). In the embryonic retina, *Otx2* marks post-mitotic retinal progenitor daughter cells [256]. In control retinas, *Otx2* was found in the NBL, especially in the outer parts (Figure 25 E). In the basal lesion of *Brg1* deficient animals it was found in the corresponding regions (Figure 25 L). Oligodendrocyte transcription factor 2 (*Olig2*) is expressed during retinal development in retinal progenitor cells and is exclusively found in the NBL [257]. In both, the NBL of *Brg1^{fl/fl}* retinas and the NBL-like structure in *Sox2-creER^{T2}::Brg1^{fl/fl}* cerebra, *Olig2* was expressed in a subset of cells (Figure 25 F, M). Early born retinal neurons express neuron-specific class III beta-tubulin (*TuJ1*) [258]. *TuJ1* is often used as a marker for the retinal ganglion cells in the GCL [259]. As expected, the GCL of our control retinas were *TuJ1* positive and this expression pattern was also seen in GCL-like structures of the basal lesion in *Sox2-creER^{T2}::Brg1^{fl/fl}* mice (Figure 25 G, N).

Taken together, the results of the IHC marker comparison suggest that the lesion close to the basal parts of the cerebrum in *Sox2-creER^{T2}::Brg1^{fl/fl}* mice in which *Brg1* loss was induced at E7.5, shares many characteristics with the retina in *Brg1^{fl/fl}* mice at E18.5.

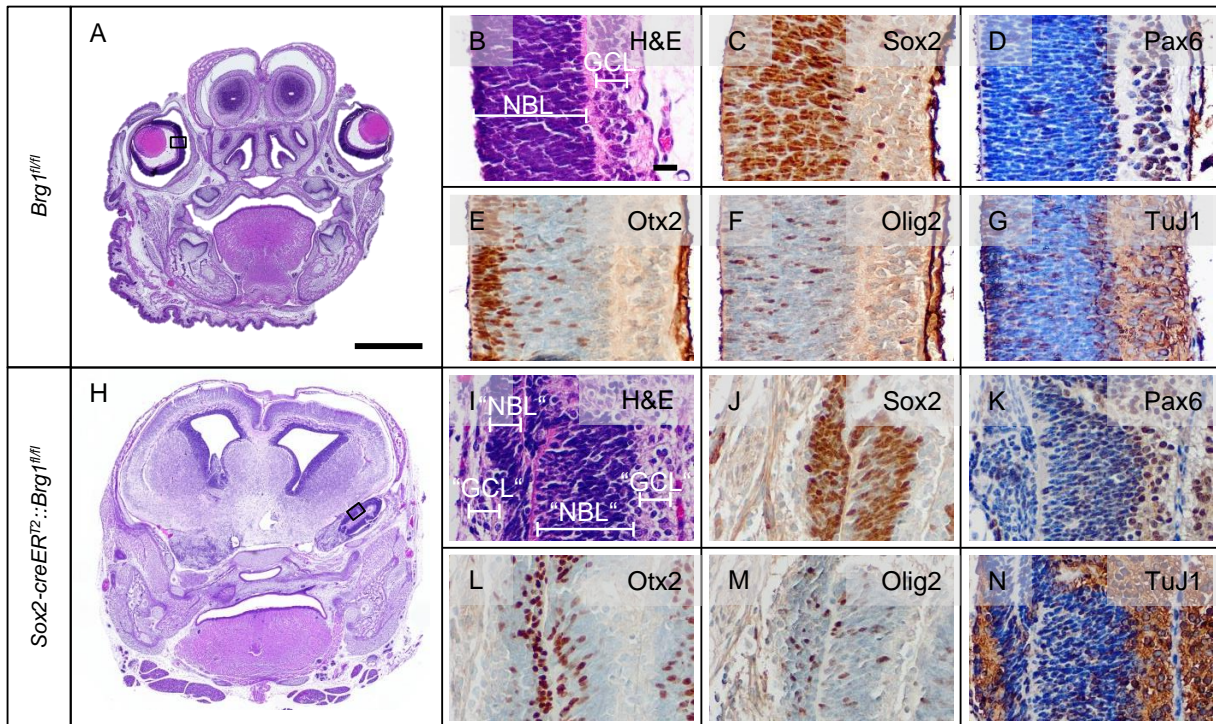


Figure 25 IHC analysis reveals similarities of the basal lesion in *Brg1* deprived embryos and physiological retina. All images show representative regions of E18.5 heads from either *Brg1^{fl/fl}* (A-G) or *Sox2-creERT2::Brg1^{fl/fl}* (H-N) embryos treated with tamoxifen at E7.5. NBL and GCL as well as NBL-like and GCL-like structures are marked in H&E stains of controls and mutants (B, I). Expression patterns of Sox2, Pax6, Otx2, Olig2 and TuJ1 in *Brg1^{fl/fl}* and *Sox2-creERT2::Brg1^{fl/fl}* mice indicate that the basal lesion close to the basal parts of the cerebrum shares many characteristics with neural retina (C-G, J-N). Scale bar in A corresponds to 1 mm and in B to 20 μ m.

4.3.4 Early loss of *Brg1* in *Sox2* positive NSCs does not result in tumor formation in young mice

One drawback of the system we used to induce *Brg1* deficiency at different time points in *Sox2* expressing NSCs were the side effects of tamoxifen. Embryonal application of 1 mg tamoxifen lead to *uterine inertia* impeding the analysis of postnatal animals. In rare occasions, tamoxifen treatment lead to abortions from E15.5 onwards. To circumvent this problem, we reduced the dosage to 0.75 mg tamoxifen and placed foster mothers in the breeding cages for support during birth and rearing of the offspring. Thereby, we were able to deliver *Sox2-creERT2::Brg1^{fl/fl}* animals after tamoxifen exposure at E6.5 and E7.5 (n=12 and n=11, respectively; Table 11). They were born after 19-20 days of pregnancy. Three (tamoxifen E6.5, 25 %) and two (tamoxifen E7.5, 18 %) mice died in the first 24 h. Unfortunately, they were either cannibalized or their brains had already started to degrade. Therefore, we could not analyze the brains histologically. However, we hypothesized that their brains would look similar as at E18.5 (Figure 17 F, H) since it seemed unlikely that 1-2 days were enough to cause severe changes. Of note, no *Brg1^{fl/fl}* animal died (tamoxifen E6.5: n=10; tamoxifen E7.5:

n=16), but 2 pups were cannibalized before their genotype could be determined. We observed all mice for at least 15 weeks, but no animal developed a tumor or tumor-specific symptoms.

Table 11 Overview of born mice after embryonal tamoxifen exposure.

Tamoxifen	Genotype	n	average days of pregnancy	number of deaths in the first 24 h	tumor free survival (≥ 15 weeks)
E6.5	<i>Brg1</i> ^{fl/fl}	10	19.5	0	10
E6.5	<i>Sox2-creER</i> ^{T2} :: <i>Brg1</i> ^{fl/fl}	12	19.5	3	9
E6.5	n/a	1	19.5	1	0
E7.5	<i>Brg1</i> ^{fl/fl}	16	19.7	0	16
E7.5	<i>Sox2-creER</i> ^{T2} :: <i>Brg1</i> ^{fl/fl}	11	19.7	2	9
E7.5	n/a	1	19.7	1	0

Unfortunately, the reduced tamoxifen dosage did not prevent *uterine inertia* when it was injected at E9.5 into pregnant mothers (n_{litters}=3). Therefore, we did not observe any postnatal *Sox2-creER*^{T2}::*Brg1*^{fl/fl} mice in which *Brg1* loss was introduced at E9.5.

5 Discussion

In this study, we examined the spatial and temporal role of Brg1 regarding neural development and brain tumorigenesis by establishing three independent mouse models. First, we used *hGFAP-cre::Brg1^{fl/fl}* mice to investigate the impact of an embryonal loss of Brg1 in multipotent NSCs on brain development. Second, we deleted *Brg1* in postnatal GNPCs to analyze its role in cerebellar development and to assess whether the Brg1 deficiency was enough to drive tumor formation. Last, we employed *Sox2-creER^{T2}::Brg1^{fl/fl}* mice and induced Brg1 deprivation at different time points during embryonal development. Thereby, we investigated the role of Brg1 in brain and eye development as well as in brain tumor formation.

5.1 *hGFAP* mediated Brg1 loss causes multiple brain alterations and causes death during adolescence

A homozygous *Brg1* deficiency in *hGFAP* expressing NSCs resulted in decreased body and brain weights accompanied by a hydrocephalus and death at an age of about two weeks. The brains of *hGFAP-cre::Brg1^{fl/fl}* mice presented with several morphological alterations including a hypoplastic cerebellum, a severely thinned cerebral cortex and an underdeveloped hippocampus. In comparison, *hGFAP-cre::Brg1^{fl/wt}* mice developed without any signs of histological abnormalities in the brain and survived normally. Many of the phenotypic alterations in *hGFAP-cre::Brg1^{fl/fl}* mice resembled those of *Nestin-cre::Brg1^{fl/fl}* mice [126]. In these mice, Brg1 is lost in neural progenitors from E10.5 onwards, which causes a decreased brain size, a thinning of the neocortex and midbrain, an underdeveloped cerebellum and death during birth. The similar phenotypes in *Nestin-cre::Brg1^{fl/fl}* and *hGFAP-cre::Brg1^{fl/fl}* mice suggest that Brg1 facilitates analogous essential functions during early and late neural development, marked by *Nestin* and *hGFAP* expression, respectively. However, the mice in our mouse model survived longer and the hippocampal phenotype was not as obvious in *Nestin-cre::Brg1^{fl/fl}* mice, indicating that Brg1 facilitates additional cell type specific roles.

It was already reported by Cao and Wu that Brg1 loss can cause a congenital hydrocephalus [260]. They generated *Camk2a-cre::Brg1^{fl/fl}* mice, in which Brg1 is lost in forebrain neurons. These mice developed a hydrocephalus, likely because the subcommissural organs were smaller and the Sylvian aqueducts narrowed. We did not observe similar alterations in our *hGFAP-cre::Brg1^{fl/fl}* mice and concluded that they developed a hydrocephalus due to a lack of cells in the thinned cerebral cortices.

One major phenotype in *hGFAP-cre::Brg1^{fl/fl}* mice were their ataxic movements caused by a hypoplastic cerebellum with disrupted layering. The general importance of Brg1 for cerebellar development has been reported previously [176]. In *Math1-cre::Brg1^{fl/fl}* mice, the proliferation in CGNPs is disturbed, resulting in a hypoplastic cerebellum. However, the Brg1 deficiency in

hGFAP-cre::Brg1^{fl/fl} mice did not only decrease CGNP proliferation but also delayed their maturation. Furthermore, *hGFAP-cre::Brg1^{fl/fl}* cerebella presented with foliation and layering disturbances. Taken together, the cerebellar phenotype of *hGFAP-cre::Brg1^{fl/fl}* mice was stronger compared with *Math1-cre::Brg1^{fl/fl}* mice, likely because more cell types were affected by the loss of Brg1. The same phenomenon has been shown for an *Ini1* deficiency in *hGFAP-cre::Ini1^{fl/fl}* and *Math1-cre::Ini1^{fl/fl}* mice [176]. Zhan and colleagues have demonstrated that *Brg1* expression in CGNPs is essential for their ability to respond to SHH [177]. Since SHH signaling induces CGNP proliferation and, consequently, is a prerequisite for cerebellar foliation, this might be one underlying cause for the phenotype observed in *hGFAP-cre::Brg1^{fl/fl}* mice.

Cerebellar layering is dependent on proper neuronal migration, including migration of GCs along BG fibers from the EGL to the IGL [247]. Our *in vitro* data from cultured cerebellar explants revealed that a fraction of late-migrating cells did not leave the explant derived from *hGFAP-cre::Brg1^{fl/fl}* mice, suggesting that Brg1 is essential for their proper migration. Furthermore, our *in vivo* findings suggested that PCs were not arranged in a monolayer above the IGL. They were rather found in random patches, indicating that their migration was also disturbed. However, PCs are not descendants of *hGFAP* expressing NSCs. Therefore, Brg1 deficiency in other cell types probably had indirect effects on PC migration. Still, we did not elucidate how the Brg1 deficiency in *hGFAP-cre::Brg1^{fl/fl}* mice contributed to the migration deficit in PCs. Additionally, maturation of PCs seemed disturbed in *hGFAP-cre::Brg1^{fl/fl}* mice as they developed their characteristic dendritic branches later than in controls. Notably, also another component of the SWI/SNF complex, B-cell lymphoma/leukemia protein 7 A (Bcl7a), has been identified to be essential for normal dendritic development in PCs [261]. This implies that a functional SWI/SNF complex is important for proper maturation of PCs in general. The development of PC dendrites is dependent on the presence of BGs [262]. Even though the proportion of BGs doubled in *hGFAP-cre::Brg1^{fl/fl}* mice compared to controls, the fraction of PCs increased almost 10-fold. Therefore, the numbers of BGs were likely insufficient to support dendritic outgrowth of PCs. This is congruent with the observation that in some PCs, development of the dendritic branches was only delayed. In contrast, a fraction of PCs never developed dendrites. Of note, the expansion of BG and especially PC proportions was likely the consequence of reduced abundance of CGNPs and GNs. An actual increase in cell numbers seems unlikely. Inhibitory interneurons (immature basket, stellate, and Golgi cells) were decreased in relation to cerebellar area, but their proportion in regard to total cell numbers were equal in *hGFAP-cre::Brg1^{fl/fl}* mice and respective controls. Therefore, Brg1 deficiency might cause a decrease in their abundance, but this is unlikely a major cause for the cerebellar phenotype in *hGFAP-cre::Brg1^{fl/fl}* mice. Furthermore, as GABAergic neurons,

including PCs, basket, stellate and Golgi cells, only make up a very small proportion of cerebellar neurons in general, it is improbable that a reduction in their cell numbers causes hypoplasia in the cerebellum [263].

In order to investigate, whether the NSCs in *hGFAP-cre::Brg1^{fl/fl}* mice were altered, we examined survival and NSC marker expression in the SVZ, one of the major germinal zones after birth. SVZ cells were almost entirely affected by the loss of Brg1, which was accompanied by lower proliferation, higher apoptosis and less expression of the NSC marker Sox2. This finding is in agreement with Lessard *et al.*, who proposed that the observed alterations in the brains of *Nestin-cre::Brg1^{fl/fl}* mice were the result of a defect in self-renewal and maintenance of NSCs [126]. They and others have described that embryonic stem cells, neural progenitors and neurons express distinct types of the SWI/SNF complex [133, 264]. Therefore, one possible explanation for the observed phenotype might be that the loss of Brg1 resulted in the mis-expression of the SWI/SNF complex in the NSCs and neural progenitors in the SVZ. As a result, the global gene expression had changed and the cells lost their identity.

The cerebral cortex was severely affected by the loss of Brg1 and was significantly thinner in *hGFAP-cre::Brg1^{fl/fl}* mice compared to controls. Presumably, Brg1 deficient NSCs failed to supply the cortex with a sufficient number of cells. The ratio of neuronal to non-neuronal cells was normal in *hGFAP-cre::Brg1^{fl/fl}* cortices. The cerebral cortex is formed in an inside-out fashion, resulting in early born neurons residing in the deeper and later born neurons in the upper layers [10, 12, 14]. We investigated whether the layering was impaired by IF staining of Cux1 (layers II-IV) and Ctip2 (layers V-VI). The neocortex of *hGFAP-cre::Brg1^{fl/fl}* mice presented with distinct layers, but layers II-IV seemed to be thinner than in controls. This indicates that the deeper layers were generated before the cre recombinase became active. However, the upper layers were formed when the NSCs were already Brg1 deprived and unable to generate enough neural progenitors for layers II-IV.

We also investigated whether neuronal morphology was altered in *hGFAP-cre::Brg1^{fl/fl}* mice by Golgi-Cox impregnations. The apical dendrites of pyramidal neurons were significantly shorter in case of Brg1 deficiency. This finding was in agreement with a study of Wu *et al.*, who uncovered that the loss of SWI/SNF complex member BAF53b causes impaired dendritic development [265]. Furthermore, Brg1 is essential for the maintenance of dendrites in murine spinal cord derived motor neurons [266].

Finally, hippocampal development was severely impaired in *hGFAP-cre::Brg1^{fl/fl}* mice. The DG and CA regions were hypoplastic and only visible in a limited number of brain sections. There were less NSCs in the subgranular zone of the DG, but the proportion of granule neurons appeared normal. Especially the number of neurons expressing Zbtb20 or Ctip2 in the CA

regions was decreased. In addition, the organization of the CA regions into distinct *strata* seemed disrupted in Brg1 deficient animals. This indicates that the CA regions of the hippocampus in *hGFAP-cre::Brg1^{fl/fl}* mice might be more affected than the DG. Of note, a similar hippocampal phenotype has been described previously for another mouse model [267]. In *hGFAP-cre::Baf155^{fl/fl}::Baf170^{fl/fl}* mice, the entire SWI/SNF complex is lost in *hGFAP* expressing multipotent stem cells, thus hindering normal hippocampal development. The authors proposed that the deprivation of the SWI/SNF complex caused a dysregulation of the WNT signaling pathway. As Brg1 has been described as an interactor of this pathway in other contexts as well, disrupted WNT signaling might also be the underlying cause for the observed phenotype in our mouse model [268-270]. Consequently, Brg1 deficiency might also be the cause for the underdeveloped hippocampus in *hGFAP-cre::Baf155^{fl/fl}::Baf170^{fl/fl}* mice.

5.2 A Brg1 deficiency in GNPC increases proliferation but is not enough to drive tumor formation

A chronic loss of Brg1 in *Math1* positive cells results in the development of a hypoplastic cerebellum in mice [176]. Likewise, as discussed earlier, *hGFAP* expressing multipotent NSCs depend on Brg1 for proper formation of all major brain structures, including the cerebellum. However, chromatin modifying enzymes facilitate not only cell type specific functions but can also have time point dependent roles: Like a Brg1 deprivation, a loss of Cbp, a transcriptional co-activator with histone acetyltransferase activity, in *Math1* expressing cells causes hypoplasia in the developing cerebellum [224]. Nevertheless, a postnatal loss of Cbp in *Math1* positive cells accelerates tumor formation in a mouse model for SHH medulloblastoma. Therefore, we were interested how a postnatal knockout of Brg1 influenced cerebellar development and if it might cause tumor formation in mice. In *Math1-creER^{T2}::Brg1^{fl/fl}* mice, Brg1 deletion at P3 resulted in an increase in proliferating cells in the EGL at P8. This result contradicted an observation of Zhan *et al.* [177]. They cultured CGNPs derived from *Actin-creER^{T2}::Brg1^{fl/fl}* mice, induced Brg1 loss by the treatment with 4-OH-tamoxifen and observed that the SHH induced increase in proliferation was reduced upon Brg1 deficiency. The authors also tested the influence of a Brg1 loss *in vivo* by injecting tamoxifen at P0 into *Nestin-creER^{T2}::Brg1^{fl/fl}* mice. They noticed smaller cerebella and less proliferating CGNPs. However, in addition to NSCs and BGs only a *Math1* negative subset of CGNPs expresses *Nestin* [271-273]. Accordingly, Zhan *et al.* not only induced Brg1 at a different time point but also in different cells. This highlights the temporal and spatial dependent function of Brg1.

Even though we observed a proliferation increase due to Brg1 loss in early postnatal cerebellar development, this boost in proliferation did not result in any morphological alterations in the adult cerebellum. Hence, the proliferation enhancement was only transient and did not result

in increased cell numbers or disturbed cerebellar development. Therefore, we concluded that in Brg1 competent cerebella, CGNP proliferation caught up to their Brg1 deficient counterparts after P8. Since Brg1 negative cells were present in the adult cerebellum, the possibility of their exclusion from the brain by apoptosis or other forms of programmed cell death seemed unlikely.

Based on these results, we hypothesized that in addition to the loss of Brg1, the activation of a proto-oncogene is needed to drive tumor formation in mice. In human *BRG1* mutated AT/RTs, the loss of the Brg1 protein is regarded as the sole tumor-initiating event [87, 91]. However, in medulloblastoma the role of *BRG1* mutations in tumorigenesis is not understood, but they are always accompanied by additional mutations in other genes [208-212]. Thus, the combination of an activated proto-oncogene with the Brg1 deficiency is not likely to resemble human AT/RT formation but would rather serve as a model for medulloblastoma. Another study uncovered that Brg1 deletion could prevent tumor formation in a mouse model of SHH medulloblastoma [222]. Nevertheless, *BRG1* mutations are usually found in WNT and Group 3 and only seldom in SHH medulloblastoma [208-212]. Therefore, a combination of Brg1 loss with a second driver mutation could be a starting point for future studies to model WNT and Group 3 medulloblastoma, respectively.

5.3 Brg1 has time point dependent functions in Sox2 expressing NSCs

The initial aim of the third part of this project was to investigate whether a Brg1 loss at different time points during embryonal development in NSCs marked by *Sox2* expression leads to oncogenic transformation of these cells. *Sox2* positive NSCs were considered to be the potential cells of origin for AT/RTs based on murine and human transcriptome data proposed by Han *et al.* [103]. They also presented data revealing that in mice, *Ini1* deficient AT/RTs arise only when the loss is introduced between E6.5 and E10.5. In our experiments, we expanded this period of time because we could not rule out that the timespan during which cells are susceptible to oncogenic transformation were different in case of *Ini1* and Brg1 loss. However, we did not induce Brg1 deficiency earlier than E6.5 because the gene is essential during peri-implantation and gastrulation [165, 167]. As *Sox2* is expressed in the presumptive neuroectoderm right before the onset of gastrulation, we hypothesized that a Brg1 loss before E6.5 may result in embryonic lethality [274]. Consequently, we induced Brg1 loss in *Sox2-creER^{T2}::Brg1^{fl/fl}* embryos between E6.5 and E14.5. Since Brg1 is of high importance for neural development, we did not only focus on tumor formation but also investigated if Brg1 deprivation resulted in neurodevelopmental changes. Therefore, in a first step we examined

whether *Sox2-creER^{T2}::Brg1^{fl/fl}* animals displayed any morphological alterations in the embryonic brain.

The Brg1 deficiency did not alter embryonic brain development, when it was induced at E6.5 or E14.5. However, a deletion between E7.5 and E12.5 caused diverse architectural abnormalities in the brains and eyes of *Sox2-creER^{T2}::Brg1^{fl/fl}* embryos. The type of alteration was dependent on the time point of tamoxifen-induced Brg1 deficiency. In addition to the morphological characterization of the embryos, we also performed transcriptome analysis using fate-mapping mice to identify the changes in gene expression responsible for the alterations observed in H&E and IHC stainings. We compared the transcriptomes of cells after Brg1 deprivation at either E7.5 or E9.5 with respective control cells. We did not only observe distinct changes in gene expression between Brg1 negative and Brg1 competent cells but also between Brg1 deficient cells that had received tamoxifen at E7.5 or E9.5. Based on this data, we concluded that Brg1 facilitates important functions in Sox2 expressing NSCs and that, in addition, the ATPase has distinct roles at different stages during early neural development.

As the SVZ is one of the germinal zones harboring mainly NSCs, it seemed likely that this region was highly affected by the NSC-specific loss of Brg1. Unexpectedly, the SVZ, including the rosette like structures, were mainly composed of Brg1 positive cells and Brg1 deficient cells were found only occasionally. Furthermore, as NSCs in the SVZ are usually dividing, we expected the rosettes to be highly proliferative. Instead, they displayed decreased Ki67 reactivity. Therefore, we concluded that even though Brg1 is not lost in the majority of SVZ cells, the NSCs residing there still show a disturbed behavior as they were arranged in rosette like structures and proliferated less. This phenotype might be explained by the fact that cells essential for the integrity of the SVZ were lacking. Concordantly, using a fate-mapping approach, we could show that upon loss of Brg1 at either E7.5 or E9.5, Brg1 deficient cells are less abundant at E14.5 compared to their Brg1 competent controls. Previous studies have already demonstrated that Brg1 knockdown can result in enhanced apoptosis. Cultivated hippocampal neurons displayed decreased survival upon Brg1 loss in an *in vitro* model for cerebral ischemia and reperfusion injury [275]. Likewise, induction of Brg1 deficiency at E6.5 in *Rosa26-creER^{T2}::Brg1^{fl/fl}* mice resulted in enhanced apoptosis, leading to embryonic death of the animals [167]. However, ectopic Brg1 expression caused cell cycle arrest accompanied by increased apoptosis in cultured mesenchymal stem cells [142]. These studies illustrate that Brg1 is indeed involved in apoptosis and that balanced Brg1 expression is essential for cell survival or cell death. Therefore, we conclude that Brg1 loss at E7.5 or E9.5 in *Sox2-creER^{T2}::Brg1^{fl/fl}* embryos decreased cell survival presumably by increased apoptosis. As a consequence, a fraction of cells were lacking in *Sox2-creER^{T2}::Brg1^{fl/fl}* embryos, contributing to the observed SVZ phenotype upon Brg1 loss.

Another cause for the disrupted SVZ might be found in the microenvironment of the stem cell niche. The ECM contributes to maintaining stem cell identity, for example by, providing a reservoir of growth factors, BMPs or TGF β [276, 277]. We recognized that the expression of collagen encoding genes were upregulated upon Brg1 loss at either E7.5 or E9.5. Notably, induction of Brg1 deficiency at E9.5 additionally resulted in enhanced expression of other ECM associated genes, including *vitronectin*, *fibronectin 1*, *perlecan*, *Lama4*, and *Lamc3*. Many of these upregulated genes are found in fractones, a basement membrane resembling structure found exclusively in the SVZ [278-280]. Even though fractones have so far only been described to be present in the adult SVZ, to our knowledge there is no evidence that they are not already present in the embryonic SVZ. They have been associated to provide NSCs with growth factors, supporting their stem cell function. Therefore, a disbalance in the expression of fractone associated genes might interfere with facilitating these functions. Additionally, *Bmp7* expression was increased upon Brg1 loss at E9.5. *Bmp7* has been proposed to bind to heparin sulfates in fractones and thereby inhibit cell proliferation in the SVZ [281]. To sum up, the dysregulation of ECM associated genes might also contribute to the observed SVZ phenotype observed in *Sox2-creER^{T2}::Brg1^{fl/fl}* embryos, especially when Brg1 deficiency was induced at E9.5. However, it remains elusive whether the upregulation of these genes was the cause or only the consequence of the observed phenotype. Furthermore, the ECM facilitates also important functions in NSC differentiation, neuronal migration, the formation of axonal tracts, and the maturation and function of synapses [277]. Therefore, the upregulation of ECM associated genes and GO terms might also have an impact on these processes.

In order to investigate if Brg1 influenced the stem cell capacities in this model, we employed a fate mapping approach to track cells and their progeny. *Sox2-creER^{T2}::lsIRFP^{fl/fl}* and *Sox2-creER^{T2}::Brg1^{fl/fl}::lsIRFP^{fl/fl}* embryos were injected with tamoxifen at either E7.5 or E9.5 to generate Brg1 competent and Brg1 negative cells, respectively. All cells in which the cre recombinase was activated were marked by RFP expression, which could be employed for FACS based isolation of Brg1 positive and negative cells. We isolated the Brg1 deficient and competent cells to perform a neurosphere assay. All conditions were able to form primary and secondary neurospheres, which correlates with the ability of NSCs to proliferate and self-renew, respectively [248]. However, Brg1 stainings of neurospheres revealed that all neurospheres contained only Brg1 expressing cells. This was not expected as theoretically no Brg1 positive cells should have been present in cultures derived from *Sox2-creER^{T2}::Brg1^{fl/fl}::lsIRFP^{fl/fl}* embryos. To validate whether the recombination efficiency of the cre recombinase was decreased in the presence of two transgenes, we performed IF stainings immediately after FACS. This demonstrated that not all RFP positive cells isolated from *Sox2-creER^{T2}::Brg1^{fl/fl}::lsIRFP^{fl/fl}* embryos were Brg1 negative. Therefore, we concluded

that Brg1 competent cells were selected in culture and were able to form neurospheres unlike their Brg1 deficient counterparts. The reduced neurosphere numbers in cultures derived from *Sox2-creER^{T2}::Brg1^{fl/fl}::lsIRFP^{fl/fl}* embryos were in line with this hypothesis. Here, less Brg1 competent cells that were able to proliferate and form neurospheres were seeded at the beginning of the experiment. In conclusion, stem cell capacities were severely decreased upon loss of Brg1 in *Sox2* expressing NSCs as neurospheres derived only from Brg1 expressing cells. This observation is congruent with observation from *Nestin-cre::Brg1^{fl/fl}* derived neurospheres and neurospheres derived from postnatal NSCs. In both models, number and size of neurospheres were reduced upon Brg1 loss [126, 179].

In the developing cerebral cortex of *Sox2-creER^{T2}::Brg1^{fl/fl}* embryos, Brg1 deficient cells were scattered randomly across all layers. However, only in a fraction of embryos Brg1 deprivation resulted in disrupted layering in the deeper layers (VZ/SVZ), harboring neural progenitors. The upper layers seemed normal in all *Sox2-creER^{T2}::Brg1^{fl/fl}* embryos in the developing brain at E18.5. As already mentioned earlier, maturation of neural progenitors into neurons is accompanied by a switch in the composition of the SWI/SNF complex. This contributes to distinct changes in gene expression needed for correct differentiation and migration of neurons during cortical development [133, 264, 282, 283]. Therefore, the integrity of the SWI/SNF complex is of high importance for cortical development. In addition, the fact that the neocortex was altered in our *hGFAP-cre::Brg1^{fl/fl}* mouse model highlights that also Brg1 itself is essential for normal corticogenesis. However, as only the regions where neural progenitors resides were affected in *Sox2-creER^{T2}::Brg1^{fl/fl}* embryos, this phenotype might not reflect issues in cortical development. It is rather another example that the knockout of Brg1 caused disruption of the NSC niche as already discussed for the SVZ.

One of the most striking phenotypes in the *Sox2-creER^{T2}::Brg1^{fl/fl}* embryos, was the ectopic basal lesion that exclusively occurred after Brg1 loss between E7.5 and E8.5. One half of this structure was composed of Brg1 competent, highly proliferating cells and the other half consisted of Brg1 deficient, Ki67 negative cells. Transcriptome analysis revealed that genes that are normally expressed during eye development were upregulated upon Brg1 loss at E7.5. For example, *Irx5* is essential for the development of retinal cone bipolar cells [252]. *Otx2* facilitates the differentiation of post-mitotic retinal progenitors into photoreceptors and bipolar cells [256]. Furthermore, *Pitx2* is essential for the development of peri-ocular mesenchyme [250, 284, 285]. *Pouf41* was one of the DEGs with the highest log2 fold change and is physiologically expressed in the embryonic retina starting at E12.5 [286]. Strikingly, *Fgf15* expression was also significantly upregulated upon Brg1 loss at E7.5. In another mouse model, *Fgf15* transcription was enhanced in case of RPE to retina transdifferentiation [62]. Therefore, we hypothesized that the basal lesion close to the cerebrum was in fact ectopic

retina and not part of the brain. In H&E stains of the eyes of *Sox2-creER^{T2}::Brg1^{fl/fl}* embryos, we discovered regions appearing like transitions from RPE to retina. To validate our hypothesis, we compared the basal lesion with neural retina of control littermates. Similar to the embryonic retina, which consisted of two layers at E18.5 (NBL and GCL), the basal lesion consisted of two different structures. Furthermore, the expression profiles of *Sox2*, *Pax6*, *Otx2*, *Olig2* and *TuJ1* in IHC were congruent in the neural retina and the basal lesion. Therefore, we concluded that loss of *Brg1* in *Sox2* positive cells at E7.5 resulted in the transdifferentiation of parts of the RPE to retina. Several mouse models have already demonstrated that dysregulation of one gene such as *Mitf*, β *Catenin*, *transcription factor AP-2 α* or *Yes-associated protein (Yap)* can result in RPE to retina transdifferentiation [61, 287-289]. So far, *Brg1* has not been associated with this process in mice. However, the interaction of *Brg1* itself or the SWI/SNF complex with many of the before-mentioned genes has already been reported elsewhere [290-292]. Additionally, *Brg1* has been described to be involved in retinogenesis in mice [218]. Furthermore, occasionally we detected rosette-like structures in the retina of *Sox2-creER^{T2}::Brg1^{fl/fl}* embryos that received tamoxifen at E9.5, even though the basal lesion resembling neural retina was not found in these animals. Finally, patients with CSS associated with *SMARCA4* mutations occasionally present with ophthalmological anomalies including microphthalmia, strabismus or retinal dystrophy [184-186]. In conclusion, *Brg1* expression is likely essential for proper eye development. However, the temporal window seems very limited as we did not observe RPE to retina transdifferentiation, when *Brg1* loss was induced earlier than E7.5 or later than E8.5.

Our transcriptome analysis suggested that the function of neurons might be disturbed in case of *Brg1* loss in *Sox2* expressing NSCs as several downregulated GO terms were associated with the synapses. We did not conduct any further experiments to examine morphology or functionality of the neurons in *Sox2-creER^{T2}::Brg1^{fl/fl}* embryos. However, as the morphology of the pyramidal neurons in the cortices of *hGFAP-cre::Brg1^{fl/fl}* mice was severely altered, we hypothesized that *Brg1* is important in both, *hGFAP* and *Sox2* expressing NSCs for giving rise to functional neurons.

One main idea to develop the *Sox2-creER^{T2}::Brg1^{fl/fl}* mouse model was to investigate whether *Sox2* expressing NSCs were susceptible to oncogenic transformation when *Brg1* deficiency was induced between E6.5 and E14.5. However, as the embryos at E18.5 had not developed any tumors, the next logical step would have been to examine these mice after birth. Unfortunately, the treatment with tamoxifen did not only cause side effects in *Math1-creER^{T2}::Brg1^{fl/fl}* mice and respective controls in which it was injected at P3 but also during pregnancy in the *Sox2-creER^{T2}::Brg1^{fl/fl}* mouse model. This observation has also been reported by others [293, 294]. Therefore, we were only able to generate postnatal

Sox2-creER^{T2}::Brg1^{fl/fl} mice that were exposed to reduced dosages of tamoxifen at E6.5 or E7.5. Unfortunately, these mice did not develop any tumors in the first months of life. As AT/RTs arise in young children, this mouse model might probably not recapitulate human AT/RTs even if these mice developed a tumor later in life. Therefore, either Sox2 is not a marker for the cell of origin in murine Brg1 deficient AT/RTs or E6.5 and E7.5 are not the correct time points for Brg1 deletion. Another explanation could be that the reduced tamoxifen dosage is not enough to induce Brg1 deficiency in a sufficient number of cells. Apart from the issues concerning embryonal tamoxifen applications, another obstacle is that many embryonal cell types are dependent on Brg1 expression for normal organ development [126, 180, 295]. Therefore, it might be challenging to identify the right cell of origin for *BRG1* deficient AT/RTs using mouse models.

6 Outlook

In the data presented here, we show that Brg1 is essential for normal brain and eye development in NSCs at different time points during murine embryonic development. Brg1 deficiency in *hGFAP* expressing cells resulted in early postnatal death accompanied by malformations in all major brain regions. *Sox2* positive NSCs depended on Brg1 between E7.5 and E12.5. In these cells, knockout of Brg1 caused distinct changes in gene expression, leading to morphological alterations in the SVZ, the cerebral cortex and transdifferentiation of RPE to retina. Still, a loss of Brg1 at E6.5 or E7.5 in *Sox2* expressing cells did not result in tumor formation in the first months of life. *Math1* expressing GNPCs showed enhanced proliferation after a postnatally induced Brg1 deficiency. However, these mice did not develop a tumor either. Therefore, the introduction of a second driver might be needed to induce oncogenesis in these mice. As *BRG1* mutations are frequently found in human WNT and Group 3 medulloblastoma, we suggest the combination of Brg1 loss with simultaneous activating mutations in *Ctnnb1* or *cMyc* [208-212].

The *hGFAP-cre::Brg1^{fl/fl}* mice displayed many different alterations in the brain. For example, the cells in the SVZ lost their stem cell characteristics due to the loss of Brg1. However, we did not investigate the underlying mechanisms causing this alteration. Brg1 is part of the SWI/SNF chromatin remodeling complex that controls global gene expression in a spatial and temporal specific manner. Therefore, transcriptome analysis of the Brg1 deprived SVZ, for example by RNA sequencing analysis, might help to identify candidate genes contributing to the observed phenotype. We hypothesized that prenatally Brg1 deprived NSCs were unable to produce sufficient numbers of cells that formed the cerebral cortex, causing a severe thinning of this structure. Still, we did not examine what kind of cells, glutamatergic neurons, GABAergic neurons, astrocytes or oligodendrocytes, were mainly affected. We demonstrated that the apical dendrites of the pyramidal neurons were significantly shorter in *hGFAP-cre::Brg1^{fl/fl}* mice compared to controls. Number and types of dendritic spines could be analyzed in a next step to further characterize neuronal function. For example, electron microscopy could be applied in order to examine whether the synapses were affected in this model. The cerebellum was hypoplastic with disrupted layering in *hGFAP-cre::Brg1^{fl/fl}* mice. We hypothesized that the decreased proliferation and migration of CGNPs were the main causes for this phenotype. However, also PC migration and maturation appeared disturbed even though these cells are not descendant from *hGFAP* expressing progenitors. Hence, exocrine factors or interaction with other cell types are likely responsible for this PC phenotype. Consequently, identifying these factors might be interesting in further studies.

The Brg1 deficiency in *Sox2* expressing NSCs caused different alterations in the embryonic brain. Using RNA sequencing analysis, we identified several DEGs after loss of Brg1 at either

E7.5 or E9.5. Unfortunately, in the fate-mapping approach we used to isolate the Brg1 deprived cells, the recombination efficiency of the cre recombinase was reduced due to the presence of two transgenes, i.e. *Brg1^{fl/fl}* and *lsIRFP^{fl/fl}*. Therefore, we did not only sequence the RNA of Brg1 negative but also of Brg1 competent cells. Consequently, single cell RNA sequencing would be the only applicable method to analyze the transcriptome of exclusively Brg1 deprived cells. However, even though we probably did not determine all genes that were differentially expressed upon loss of Brg1, we were still able to identify many downregulated genes involved in regulating the function of neurons. To further characterize if this change in gene expression resulted in actual consequences for the function of neurons, we could analyze dendritic spines or synapses similarly as proposed for the *hGFAP-cre::Brg1^{fl/fl}* mouse model. In addition to the downregulation of GO terms related to neuronal functions, we identified that several genes associated with the ECM were upregulated upon loss of Brg1. Nonetheless, it has to be examined whether the enhanced expression of these genes resulted in altered abundance of the respective proteins in *Sox2-creER^{T2}::Brg1^{fl/fl}* mice. For this purpose, we could employ IHC stainings or western blot analysis.

We demonstrated that the yields of RFP positive cells derived from *Sox2-creER^{T2}::Brg1^{fl/fl}::lsIRFP^{fl/fl}* mice was decreased compared to their respective controls. Furthermore, we identified that Brg1 negative cells did not form neurospheres *in vitro*. Finally, the SVZ in *Sox2-creER^{T2}::Brg1^{fl/fl}* embryos displayed less reactivity for Ki67 in IHC stainings. Consequently, we hypothesized that Brg1 loss decreased proliferation and enhanced apoptosis. Nevertheless, we need to perform further analyses to confirm this assumption.

In the *Sox2-creER^{T2}::Brg1^{fl/fl}* mouse model, one drawback were the side effects of the tamoxifen application during pregnancy. Due to them, we were not able to investigate whether a loss of Brg1 at E9.5 in *Sox2* expressing NSCs results in tumor formation after birth. In order to examine whether a tumor would arise later during development, another approach than investigating postnatal mice could be to transplant the embryonic brains of induced *Sox2-creER^{T2}::Brg1^{fl/fl}* mice into the flanks of recipient mice. This procedure has been established in the laboratory of Franck Bourdeaut [personal communication]. Alternatively, the Brg1 deficient cells, we obtained in the fate-mapping experiments, could be transplanted into healthy recipients. However, as we demonstrated in this study, the recombination efficiency of the cre recombinase in the presence of two transgenes is reduced. Therefore, we would lose a proportion of Brg1 negative cells in this second experimental setup. A third option to analyze whether *Sox2* expressing NSCs give rise to Brg1 deficient brain tumors is to use conditional *Sox2-cre::Brg1^{fl/wt}* mice. In this approach, it would not be necessary to treat pregnant mice with tamoxifen. However, the disadvantage of this strategy is that the temporal influence of the Brg1 loss cannot be examined. Additionally, we could probably only examine

the impact of a heterozygous Brg1 loss as a homozygous Brg1 knockout would likely cause embryonic death. Still, in other mouse models a heterozygous Brg1 deficiency was sufficient to drive tumor formation [165, 166, 217].

Finally, as *Sox2* expression might not mark the cell of origin for Brg1 deficient AT/RTs, Brg1 loss in other cell types should be investigated. In order to define candidates, we could use DNA methylation data derived from *BRG1* mutated AT/RTs, since it has been demonstrated that the methylation profile of tumors resembles the methylation profile of the cell of origin [296]. Furthermore, we could employ RNA sequencing data of *BRG1* mutated AT/RTs to determine potential cells of origin. This method has previously been demonstrated by Jessa *et al.* who used transcriptome data to identify possible cells of origin for WNT medulloblastoma and for embryonal tumors with multilayered rosettes [297].

7 Summary

Brahma homolog 1 (Brg1) is part of the switch/sucrose non-fermentable (SWI/SNF) chromatin remodeling complex that controls global gene expression by altering the positions of histones along the DNA. It has been proposed that Brg1 is essential in the development of diverse organs, including the brain. Furthermore, several tumors harbor missense or truncating mutations in the *BRG1* gene.

Here, we were interested in both, the function of Brg1 in neural development and in brain tumorigenesis. Therefore, we established three independent mouse models. In *hGFAP-cre::Brg1^{fl/fl}* mice, Brg1 was lost at embryonic day 13.5 (E13.5) in multipotent neural stem cells (NSCs). The Brg1 deficiency resulted in early postnatal death accompanied by severely reduced body and brain weights. Histological examination revealed several alterations in all major brain structures, including the cerebellum, the cerebral cortex, the subventricular zone (SVZ) and the hippocampus.

In a second mouse model, we investigated whether a postnatal loss of Brg1 in *Math1* expressing cerebellar granular neuron precursors (CGNPs) altered cerebellar development. Brg1 deficiency resulted in a short-term increase in proliferation in the external granular layer. However, this did not alter physiological brain development, as adult mice did not show any cerebellar abnormalities or tumor formation.

In the third part of the project, we induced loss of Brg1 in *Sox2* positive NSCs between E6.5 and E14.5. By investigating the effect on the embryonic brain at E18.5, we observed that Brg1 deficiency between E7.5 and E12.5 resulted in disruptions in the SVZ, the developing neocortex and a transdifferentiation of retinal pigment epithelium to retina. The latter was only observed when Brg1 was lost at E7.5 or E8.5. These histological alterations were accompanied by distinct changes in gene expression revealed by RNA sequencing analysis. Extracellular matrix associated genes were upregulated especially upon Brg1 loss at E9.5, whereas a deficiency from E7.5 onwards resulted in the upregulation of genes involved in eye development. In contrast, genes linked to neuronal functions were downregulated upon Brg1 loss at either E7.5 or E9.5. Last, we investigated whether an early loss of Brg1 at E6.5 or E7.5 resulted in tumorigenesis after birth. However, we did not observe any tumor formation in the first 15 weeks of life.

Taken together, these results suggest that Brg1 is essential in embryonic NSCs for normal brain and eye development, whereas postnatal CGNPs are not dependent on Brg1 for normal development. Furthermore, a Brg1 loss at E6.5 or E7.5 in NSCs is not sufficient to drive tumor formation in young mice.

8 Zusammenfassung

Brahma homolog 1 (Brg1) ist eine Untereinheit des switch/sucrose non-fermentable (SWI/SNF) chromatin remodeling complex, der die globale Genexpression regulieren kann, indem er die Position der Histone entlang der DNS verändert. Verschiedene Studien konnten zeigen, dass Brg1 an der Entstehung vieler Organe beteiligt ist. So sind zahlreiche Prozesse in der frühen Embryonal- und auch der Hirnentwicklung von einer korrekten Brg1 Expression abhängig. Zusätzlich haben andere Untersuchungen gezeigt, dass *BRG1* in vielen Tumoren mutiert vorliegt.

In dieser Doktorarbeit wurde anhand drei verschiedener Mausmodelle die Rolle von Brg1 in der neuralen Entwicklung und in der Entstehung von pädiatrischen Hirntumoren untersucht. Zunächst konnte gezeigt werden, dass der homozygote Verlust von Brg1 in *hGFAP* exprimierenden multipotenten neuralen Vorläuferzellen zum Tod der Tiere in den ersten zwei Lebenswochen führt. Die Mäuse zeigten ein verringertes Körper- und Hirngewicht, einen Wasserkopf und verschiedene Veränderungen in allen wichtigen Hirnregionen, einschließlich des Kleinhirns, des zerebralen Kortex, der Subventrikulärzone (SVZ) und des Hippocampus.

In einem zweiten Mausmodell untersuchten wir, ob ein postnataler Brg1 Verlust in zerebellären Vorläuferzellen die Entwicklung des Kleinhirns verändert oder sogar zur Tumorentstehung führen kann. Obwohl ein paar Tage nach dem Brg1 Verlust die Proliferation erhöht war, entwickelte sich das Kleinhirn normal und wir konnten keine Tumorentstehung beobachten.

Zu guter Letzt untersuchten wir, ob sich ein Brg1 Verlust in *Sox2* positiven Stammzellen zwischen Embryonaltag 6.5 (E6.5) und E14.5 verändernd auf die Hirnentwicklung auswirkt oder sogar zur Tumorentstehung führt. Zunächst evaluierten wir embryonale Hirne an E18.5 und entdeckten histologische Veränderungen in der SVZ, dem zerebralen Kortex und, dass das retinale Pigmentepithel teilweise zur Retina transdifferenziert war. Transkriptomanalysen wiesen darauf hin, dass durch den Brg1 Verlust an E7.5 vor allem Gene, die mit der Entwicklung des Auges assoziiert sind, hochreguliert waren. Gene, die in der extrazellulären Matrix exprimiert werden, waren nach Brg1 Verlust an E7.5 und vor allem nach Brg1 Defizienz an E9.5 verstärkt exprimiert. Die fehlende Brg1 Expression an beiden Zeitpunkten führte zur verringerten Transkription von Genen, die in der Funktion von Neuronen eine Rolle spielen. Ein Brg1 Verlust an E6.5 oder E7.5 führte zu keiner Tumorentstehung in den ersten 15 Wochen nach der Geburt.

Zusammenfassend spielt Brg1 sowohl in *hGFAP* als auch in *Sox2* positiven Stammzellen essenzielle Rollen bezüglich der Hirnentwicklung, wohingegen das Protein nach der Geburt in zerebellären Vorläuferzellen weniger ausschlaggebende Funktionen zu erfüllen scheint.

9 Abbreviations

Table 12 List of abbreviations

°C	Degree Celsius
ASD	Autism spectrum disorder
AT	Austria
AT/RT	Atypical teratoid/rhaboid tumor
Atoh1, Math1	Atonal Homolog 1
BAF	BRM/BRG1-associated factor
BG	Bergmann glia cell
bHLH	basic helix-loop-helix
BMP	bone morphogenic protein
bp	Base pair
Bcl7a	B-cell lymphoma/leukemia protein 7 A
Brg1	Brahma homolog 1
Brm	Brahma
c	Concentration
cBAF	Canonical BAF
Cbp	CREB-binding protein
CHD	Chromodomain helicase DNA-binding
CNS	Central nervous system
COSMIC	Catalogue Of Somatic Mutations In Cancer
Cre	Cyclization Recombinatio
CSS	Coffin Siris Syndrom
CT	Computed tomography
Ctrl	Control
cVZ	Cerebellar ventricular Zone
d	Days
ddH ₂ O	Double distilled water
DE	Germany
DEG	Differentially expressed gene
DEPC	Diethyl pyrocarbonate
DG	Dentate gyrus
DMEM	Dulbecco's Modified Eagle Medium
DNA	Deoxyribonucleic acid
DOX	Doxorubicin, intra-ventricular methotrexate
E	Embryonic day
ECM	Extracellular matrix
EDTA	Ethylenediaminetetraacetic acid
EFTF	Eye field transcription factor
EGL	External granular layer
EMA	Epithelial membrane antigen
EU-RHAB	European Rhabdoid Registry
FACS	Fluorescence-activated cell sorting
FBS	Fetal bovine serum
FDR	False discovery rate
FGF	Fibroblast growth factor

FGFR	Fibroblast growth factor receptor
fl	Flanked by loxP, floxed
fw	Forward
FSC-A	Forward scatter area
FSC-H	Forward scatter height
g	Gram
GABA	gamma-Aminobutyric acid
GC	Granule cell
GCL	Ganglion cell layer
GEMM	Genetically engineered mouse model
GFAP	Glial fibrillary acidic protein
GNPC	Granule neuron precursor cell
GO	Gene Ontology
h	Hour(s)
H&E	Hematoxylin and eosin
HBSS	Hank's balanced salt solution
Hspg2	Heparan sulfate proteoglycan 2
HH	Hedgehog
HRP	Horseradish peroxidase
ICE	Ifosfamide, carboplatinum, etoposide, intra-ventricular methotrexate
IF	Immunofluorescence
i.p.	Intraperitoneal
IGL	Inner granule cell layer
IHC	Immunohistochemistry
Ini1	Integrase interactor 1
INO80	Inositol Requiring 80
ISWI	Imitation switch
kDa	Kilo Dalton
l	Liter
Isl	loxP STOP loxP
Lama4	Laminin α 4
Lamc3	Laminin γ 3
L-Gln	L-Glutamine
Lhx2	LIM Homeobox 2
loxP	Locus of crossing [xing]- over bacteriophage P1
min	Minute(s)
Mitf	Microphthalmia-associated transcription factor
ml	Milliliter
ML	Molecular layer
MRI	Magnetic resonance imaging
MRT	Malignant rhabdoid tumor
NBL	Neuroblast layer
ncBAF	Non-canonical BAF
NFP	Neurofilament protein
ng	Nanogram
ns	Not significant
NSC	Neural stem cell

Otx2	Orthodenticle homeobox 2
P	Postnatal day
Pax6	Paired box protein 6
pBAF	Polybromo-associated BAF
PBS	Phosphate-buffered saline
PC	Purkinje cell
PCL	Purkinje cell layer
PDX	Patient-derived xenografts
PE-A	Phycoerythrin area
PFA	Paraformaldehyde
PHD10	PHD finger protein 10
PS	Penicillin and streptomycin
Ptf1	Pancreas transcription factor 1a
Rax, Rx	Retinal homeobox protein
RFP	Red fluorescent protein
RPE	Retinal pigment epithelium
rpm	Rounds per minute
RT	Rhabdoid tumor
RTK	rhabdoid tumor of the kidney
rv	Reverse
s	Second(s)
SCCOHT	Small cell carcinoma of the ovary hypercalcemic type
SHH	Sonic Hedgehog
Six3	Sine oculis-related homeobox 3
SMA	α smooth muscle actin
SmarcA2	SWI/SNF-related matrix-associated actin-dependent regulator of chromatin subfamily A, member 2
SmarcA4	SWI/SNF-related matrix-associated actin-dependent regulator of chromatin subfamily A, member 4
SmarcB1	SWI/SNF-related matrix-associated actin-dependent regulator of chromatin subfamily B, member 1
Sox2	Sex determining region Y-box 2
SSC-A	Side scatter Area
SVZ	Subventricular zone
SWI/SNF	Switch/ sucrose non-fermentable
TBS-T	Tris-buffered saline – Tween
TGF β	Transforming growth factor β
UK	United Kingdom
US	United States
VCA	Vincristine, cyclophosphamide, actinomycin-D, intra-ventricular methotrexat
Vsx2, Chx10	Visual system homeobox 2
VZ	Ventricular zone
WHO	World Health Organization
WNT	Wingless
x g	Force of gravity (9.81 m/s ²)
μ	Micro

10 References

1. Chen, V.S., et al., *Histology Atlas of the Developing Prenatal and Postnatal Mouse Central Nervous System, with Emphasis on Prenatal Days E7.5 to E18.5*. Toxicol Pathol, 2017. **45**(6): p. 705-744.
2. Beccari, L., R. Marco-Ferrerres, and P. Bovolenta, *The logic of gene regulatory networks in early vertebrate forebrain patterning*. Mech Dev, 2013. **130**(2-3): p. 95-111.
3. Graham, V., et al., *SOX2 functions to maintain neural progenitor identity*. Neuron, 2003. **39**(5): p. 749-65.
4. Pakkenberg, B. and H.J. Gundersen, *Neocortical neuron number in humans: effect of sex and age*. J Comp Neurol, 1997. **384**(2): p. 312-20.
5. Adnani, L., et al., *Mechanisms of Cortical Differentiation*. Int Rev Cell Mol Biol, 2018. **336**: p. 223-320.
6. Sidman, R.L. and P. Rakic, *Neuronal migration, with special reference to developing human brain: a review*. Brain Res, 1973. **62**(1): p. 1-35.
7. Bystron, I., C. Blakemore, and P. Rakic, *Development of the human cerebral cortex: Boulder Committee revisited*. Nat Rev Neurosci, 2008. **9**(2): p. 110-22.
8. Rakic, P., *Guidance of neurons migrating to the fetal monkey neocortex*. Brain Res, 1971. **33**(2): p. 471-6.
9. Misson, J.P., et al., *The alignment of migrating neural cells in relation to the murine neopallial radial glial fiber system*. Cereb Cortex, 1991. **1**(3): p. 221-9.
10. Brazel, C.Y., et al., *Roles of the mammalian subventricular zone in brain development*. Prog Neurobiol, 2003. **69**(1): p. 49-69.
11. Noctor, S.C., et al., *Cortical neurons arise in symmetric and asymmetric division zones and migrate through specific phases*. Nat Neurosci, 2004. **7**(2): p. 136-44.
12. Angevine, J.B., Jr. and R.L. Sidman, *Autoradiographic study of cell migration during histogenesis of cerebral cortex in the mouse*. Nature, 1961. **192**: p. 766-8.
13. Marin-Padilla, M., *Cajal-Retzius cells and the development of the neocortex*. Trends Neurosci, 1998. **21**(2): p. 64-71.
14. Greig, L.C., et al., *Molecular logic of neocortical projection neuron specification, development and diversity*. Nat Rev Neurosci, 2013. **14**(11): p. 755-69.
15. Miller, F.D. and A.S. Gauthier, *Timing is everything: making neurons versus glia in the developing cortex*. Neuron, 2007. **54**(3): p. 357-69.
16. Lui, J.H., D.V. Hansen, and A.R. Kriegstein, *Development and evolution of the human neocortex*. Cell, 2011. **146**(1): p. 18-36.
17. Hashimoto, M. and M. Hibi, *Development and evolution of cerebellar neural circuits*. Dev Growth Differ, 2012. **54**(3): p. 373-89.
18. Sillitoe, R.V. and A.L. Joyner, *Morphology, molecular codes, and circuitry produce the three-dimensional complexity of the cerebellum*. Annu Rev Cell Dev Biol, 2007. **23**: p. 549-77.
19. Hatten, M.E. and N. Heintz, *Mechanisms of neural patterning and specification in the developing cerebellum*. Annu Rev Neurosci, 1995. **18**: p. 385-408.
20. Wingate, R.J., *The rhombic lip and early cerebellar development*. Curr Opin Neurobiol, 2001. **11**(1): p. 82-8.
21. Machold, R. and G. Fishell, *Math1 is expressed in temporally discrete pools of cerebellar rhombic-lip neural progenitors*. Neuron, 2005. **48**(1): p. 17-24.
22. Wang, V.Y., M.F. Rose, and H.Y. Zoghbi, *Math1 expression redefines the rhombic lip derivatives and reveals novel lineages within the brainstem and cerebellum*. Neuron, 2005. **48**(1): p. 31-43.
23. Hoshino, M., et al., *Ptf1a, a bHLH transcriptional gene, defines GABAergic neuronal fates in cerebellum*. Neuron, 2005. **47**(2): p. 201-13.
24. Pascual, M., et al., *Cerebellar GABAergic progenitors adopt an external granule cell-like phenotype in the absence of Ptf1a transcription factor expression*. Proc Natl Acad Sci U S A, 2007. **104**(12): p. 5193-8.

25. Alder, J., N.K. Cho, and M.E. Hatten, *Embryonic precursor cells from the rhombic lip are specified to a cerebellar granule neuron identity*. *Neuron*, 1996. **17**(3): p. 389-99.
26. Ben-Arie, N., et al., *Math1 is essential for genesis of cerebellar granule neurons*. *Nature*, 1997. **390**(6656): p. 169-72.
27. Fujita, S., M. Shimada, and T. Nakamura, *H3-thymidine autoradiographic studies on the cell proliferation and differentiation in the external and the internal granular layers of the mouse cerebellum*. *J Comp Neurol*, 1966. **128**(2): p. 191-208.
28. Lewis, P.M., et al., *Sonic hedgehog signaling is required for expansion of granule neuron precursors and patterning of the mouse cerebellum*. *Dev Biol*, 2004. **270**(2): p. 393-410.
29. Hashimoto, M. and K. Mikoshiba, *Mediolateral compartmentalization of the cerebellum is determined on the "birth date" of Purkinje cells*. *J Neurosci*, 2003. **23**(36): p. 11342-51.
30. Miale, I.L. and R.L. Sidman, *An autoradiographic analysis of histogenesis in the mouse cerebellum*. *Exp Neurol*, 1961. **4**: p. 277-96.
31. Xu, H., et al., *Bergmann glia function in granule cell migration during cerebellum development*. *Mol Neurobiol*, 2013. **47**(2): p. 833-44.
32. Fuhrmann, S., C. Zou, and E.M. Levine, *Retinal pigment epithelium development, plasticity, and tissue homeostasis*. *Exp Eye Res*, 2014. **123**: p. 141-50.
33. Zuber, M.E., et al., *Specification of the vertebrate eye by a network of eye field transcription factors*. *Development*, 2003. **130**(21): p. 5155-67.
34. Bailey, T.J., et al., *Regulation of vertebrate eye development by Rx genes*. *Int J Dev Biol*, 2004. **48**(8-9): p. 761-70.
35. Yun, S., et al., *Lhx2 links the intrinsic and extrinsic factors that control optic cup formation*. *Development*, 2009. **136**(23): p. 3895-906.
36. Heavner, W. and L. Pevny, *Eye development and retinogenesis*. *Cold Spring Harb Perspect Biol*, 2012. **4**(12).
37. Tétreault, N., M.-P. Champagne, and G. Bernier, *The LIM homeobox transcription factor Lhx2 is required to specify the retina field and synergistically cooperates with Pax6 for Six6 trans-activation*. *Developmental biology*, 2009. **327**(2): p. 541-550.
38. Cavodeassi, F., et al., *Early stages of zebrafish eye formation require the coordinated activity of Wnt11, Fz5, and the Wnt/beta-catenin pathway*. *Neuron*, 2005. **47**(1): p. 43-56.
39. Maurus, D., et al., *Noncanonical Wnt-4 signaling and EAF2 are required for eye development in Xenopus laevis*. *Embo j*, 2005. **24**(6): p. 1181-91.
40. Danno, H., et al., *Molecular links among the causative genes for ocular malformation: Otx2 and Sox2 coregulate Rax expression*. *Proc Natl Acad Sci U S A*, 2008. **105**(14): p. 5408-13.
41. Beccari, L., et al., *Sox2-mediated differential activation of Six3.2 contributes to forebrain patterning*. *Development*, 2012. **139**(1): p. 151-64.
42. Bielen, H. and C. Houart, *BMP signaling protects telencephalic fate by repressing eye identity and its Cxcr4-dependent morphogenesis*. *Dev Cell*, 2012. **23**(4): p. 812-22.
43. Svoboda, K.K. and K.S. O'Shea, *An analysis of cell shape and the neuroepithelial basal lamina during optic vesicle formation in the mouse embryo*. *Development*, 1987. **100**(2): p. 185-200.
44. Chow, R.L. and R.A. Lang, *Early eye development in vertebrates*. *Annu Rev Cell Dev Biol*, 2001. **17**: p. 255-96.
45. Bharti, K., et al., *The other pigment cell: specification and development of the pigmented epithelium of the vertebrate eye*. *Pigment Cell Res*, 2006. **19**(5): p. 380-94.
46. Hyer, J., T. Mima, and T. Mikawa, *FGF1 patterns the optic vesicle by directing the placement of the neural retina domain*. *Development*, 1998. **125**(5): p. 869-77.
47. Gage, P.J., et al., *Fate maps of neural crest and mesoderm in the mammalian eye*. *Invest Ophthalmol Vis Sci*, 2005. **46**(11): p. 4200-8.

48. Kagiya, Y., et al., *Extraocular dorsal signal affects the developmental fate of the optic vesicle and patterns the optic neuroepithelium*. *Dev Growth Differ*, 2005. **47**(8): p. 523-36.
49. Fuhrmann, S., *Eye morphogenesis and patterning of the optic vesicle*. *Curr Top Dev Biol*, 2010. **93**: p. 61-84.
50. Nguyen, M. and H. Arnheiter, *Signaling and transcriptional regulation in early mammalian eye development: a link between FGF and MITF*. *Development*, 2000. **127**(16): p. 3581-91.
51. Andrabi, M., et al., *Comparative, transcriptome analysis of self-organizing optic tissues*. *Sci Data*, 2015. **2**: p. 150030.
52. Yang, X.J., *Roles of cell-extrinsic growth factors in vertebrate eye pattern formation and retinogenesis*. *Semin Cell Dev Biol*, 2004. **15**(1): p. 91-103.
53. Adler, R. and T.L. Belecky-Adams, *The role of bone morphogenetic proteins in the differentiation of the ventral optic cup*. *Development*, 2002. **129**(13): p. 3161-71.
54. Dakubo, G.D., et al., *Indian hedgehog signaling from endothelial cells is required for sclera and retinal pigment epithelium development in the mouse eye*. *Dev Biol*, 2008. **320**(1): p. 242-55.
55. Morcillo, J., et al., *Proper patterning of the optic fissure requires the sequential activity of BMP7 and SHH*. *Development*, 2006. **133**(16): p. 3179-90.
56. Adler, R. and M.V. Canto-Soler, *Molecular mechanisms of optic vesicle development: complexities, ambiguities and controversies*. *Dev Biol*, 2007. **305**(1): p. 1-13.
57. Ashery-Padan, R., et al., *Pax6 activity in the lens primordium is required for lens formation and for correct placement of a single retina in the eye*. *Genes Dev*, 2000. **14**(21): p. 2701-11.
58. Bäumer, N., et al., *Retinal pigmented epithelium determination requires the redundant activities of Pax2 and Pax6*. *Development*, 2003. **130**(13): p. 2903-15.
59. Cai, Z., et al., *Deficient FGF signaling causes optic nerve dysgenesis and ocular coloboma*. *Development*, 2013. **140**(13): p. 2711-23.
60. Yasue, A., et al., *Relationship between somatic mosaicism of Pax6 mutation and variable developmental eye abnormalities-an analysis of CRISPR genome-edited mouse embryos*. *Sci Rep*, 2017. **7**(1): p. 53.
61. Bumsted, K.M. and C.J. Barnstable, *Dorsal retinal pigment epithelium differentiates as neural retina in the microphthalmia (mi/mi) mouse*. *Invest Ophthalmol Vis Sci*, 2000. **41**(3): p. 903-8.
62. Bharti, K., et al., *A regulatory loop involving PAX6, MITF, and WNT signaling controls retinal pigment epithelium development*. *PLoS Genet*, 2012. **8**(7): p. e1002757.
63. Frühwald, M.C., et al., *Atypical teratoid/rhabdoid tumors-current concepts, advances in biology, and potential future therapies*. *Neuro Oncol*, 2016. **18**(6): p. 764-78.
64. Rorke, L.B., R.J. Packer, and J.A. Biegel, *Central nervous system atypical teratoid/rhabdoid tumors of infancy and childhood: definition of an entity*. *J Neurosurg*, 1996. **85**(1): p. 56-65.
65. Rorke, L.B., R. Packer, and J. Biegel, *Central nervous system atypical teratoid/rhabdoid tumors of infancy and childhood*. *J Neurooncol*, 1995. **24**(1): p. 21-8.
66. Bhattacharjee, M., et al., *Central nervous system atypical teratoid/rhabdoid tumors of infancy and childhood*. *Ultrastruct Pathol*, 1997. **21**(4): p. 369-78.
67. Louis, D., et al., *WHO Classification of Tumours of the Central Nervous System*. Revised 4th edition. ed. 2016, France: International Agency for Research on Cancer.
68. Ostrom, Q.T., et al., *Alex's Lemonade Stand Foundation Infant and Childhood Primary Brain and Central Nervous System Tumors Diagnosed in the United States in 2007-2011*. *Neuro Oncol*, 2015. **16 Suppl 10**: p. x1-x36.
69. Woehrer, A., et al., *Incidence of atypical teratoid/rhabdoid tumors in children: a population-based study by the Austrian Brain Tumor Registry, 1996-2006*. *Cancer*, 2010. **116**(24): p. 5725-32.
70. Chan, V., et al., *A Systematic Review of Atypical Teratoid Rhabdoid Tumor in Adults*. *Front Oncol*, 2018. **8**: p. 567.

71. Tulla, M., et al., *Incidence, Trends, and Survival of Children With Embryonal Tumors*. Pediatrics, 2015. **136**(3): p. e623-32.
72. Hilden, J.M., et al., *Central nervous system atypical teratoid/rhabdoid tumor: results of therapy in children enrolled in a registry*. J Clin Oncol, 2004. **22**(14): p. 2877-84.
73. Packer, R.J., et al., *Atypical teratoid/rhabdoid tumor of the central nervous system: report on workshop*. J Pediatr Hematol Oncol, 2002. **24**(5): p. 337-42.
74. Ho, D.M., et al., *Atypical teratoid/rhabdoid tumor of the central nervous system: a comparative study with primitive neuroectodermal tumor/medulloblastoma*. Acta Neuropathol, 2000. **99**(5): p. 482-8.
75. von Hoff, K., et al., *Frequency, risk-factors and survival of children with atypical teratoid rhabdoid tumors (AT/RT) of the CNS diagnosed between 1988 and 2004, and registered to the German HIT database*. Pediatr Blood Cancer, 2011. **57**(6): p. 978-85.
76. Buscariollo, D.L., et al., *Survival outcomes in atypical teratoid rhabdoid tumor for patients undergoing radiotherapy in a Surveillance, Epidemiology, and End Results analysis*. Cancer, 2012. **118**(17): p. 4212-9.
77. Hasselblatt, M., et al., *Nonsense mutation and inactivation of SMARCA4 (BRG1) in an atypical teratoid/rhabdoid tumor showing retained SMARCB1 (INI1) expression*. Am J Surg Pathol, 2011. **35**(6): p. 933-5.
78. Arnhold, V., et al., *Long-term survival of an infant with an atypical teratoid/rhabdoid tumor following subtotal resection and low-cumulative dose chemotherapy: a case report*. Childs Nerv Syst, 2016. **32**(6): p. 1157-61.
79. Bookhout, C., T.W. Bouldin, and D.W. Ellison, *Atypical teratoid/rhabdoid tumor with retained INI1 (SMARCB1) expression and loss of BRG1 (SMARCA4)*. Neuropathology, 2018. **38**(3): p. 305-308.
80. Meyers, S.P., et al., *Primary intracranial atypical teratoid/rhabdoid tumors of infancy and childhood: MRI features and patient outcomes*. AJNR Am J Neuroradiol, 2006. **27**(5): p. 962-71.
81. Biswas, A., et al., *Intracranial atypical teratoid rhabdoid tumor: current management and a single institute experience of 15 patients from north India*. Acta Neurochir (Wien), 2015. **157**(4): p. 589-96.
82. Athale, U.H., et al., *Childhood atypical teratoid rhabdoid tumor of the central nervous system: a meta-analysis of observational studies*. J Pediatr Hematol Oncol, 2009. **31**(9): p. 651-63.
83. Dho, Y.S., et al., *Investigation of the location of atypical teratoid/rhabdoid tumor*. Childs Nerv Syst, 2015. **31**(8): p. 1305-11.
84. Lian, H., et al., *Incidence of metastatic disease and survival among patients with newly diagnosed primary CNS tumors in the United States from 2004-2013*. J Cancer, 2019. **10**(13): p. 3037-3045.
85. Biswas, A., et al., *Atypical teratoid/rhabdoid tumors: challenges and search for solutions*. Cancer Manag Res, 2016. **8**: p. 115-125.
86. Judkins, A.R., et al., *Immunohistochemical analysis of hSNF5/INI1 in pediatric CNS neoplasms*. Am J Surg Pathol, 2004. **28**(5): p. 644-50.
87. Schneppenheim, R., et al., *Germline nonsense mutation and somatic inactivation of SMARCA4/BRG1 in a family with rhabdoid tumor predisposition syndrome*. Am J Hum Genet, 2010. **86**(2): p. 279-84.
88. Capper, D., et al., *DNA methylation-based classification of central nervous system tumours*. Nature, 2018. **555**(7697): p. 469-474.
89. Frühwald, M. and B. Krefeld. *EUROPEAN RHABDOID REGISTRY 2010 18.04.2018*; Available from: https://www.kinderkrebsinfo.de/fachinformationen/studienportal/pohkinderkrebsinfoth erapiestudien/eu_rhab.
90. Hasselblatt, M., et al., *High-resolution genomic analysis suggests the absence of recurrent genomic alterations other than SMARCB1 aberrations in atypical teratoid/rhabdoid tumors*. Genes Chromosomes Cancer, 2013. **52**(2): p. 185-90.

91. Hasselblatt, M., et al., *SMARCA4-mutated atypical teratoid/rhabdoid tumors are associated with inherited germline alterations and poor prognosis*. Acta Neuropathol, 2014. **128**(3): p. 453-6.
92. Lee, R.S., et al., *A remarkably simple genome underlies highly malignant pediatric rhabdoid cancers*. J Clin Invest, 2012. **122**(8): p. 2983-8.
93. Bourdeaut, F., et al., *Frequent hSNF5/INI1 germline mutations in patients with rhabdoid tumor*. Clin Cancer Res, 2011. **17**(1): p. 31-8.
94. Sredni, S.T. and T. Tomita, *Rhabdoid tumor predisposition syndrome*. Pediatr Dev Pathol, 2015. **18**(1): p. 49-58.
95. Johann, P.D., et al., *Atypical Teratoid/Rhabdoid Tumors Are Comprised of Three Epigenetic Subgroups with Distinct Enhancer Landscapes*. Cancer Cell, 2016. **29**(3): p. 379-393.
96. Torchia, J., et al., *Integrated (epi)-Genomic Analyses Identify Subgroup-Specific Therapeutic Targets in CNS Rhabdoid Tumors*. Cancer Cell, 2016. **30**(6): p. 891-908.
97. Ho, B., et al., *Molecular subgrouping of Atypical Teratoid / Rhabdoid Tumors (ATRT) - a reinvestigation and current consensus*. Neuro Oncol, 2019.
98. Frühwald, M.C., et al., *Age and DNA-methylation subgroup as potential independent risk factors for treatment stratification in children with Atypical Teratoid/Rhabdoid Tumors (ATRT)*. Neuro Oncol, 2019.
99. Chun, H.E., et al., *Identification and Analyses of Extra-Cranial and Cranial Rhabdoid Tumor Molecular Subgroups Reveal Tumors with Cytotoxic T Cell Infiltration*. Cell Rep, 2019. **29**(8): p. 2338-2354.e7.
100. Roberts, C.W., et al., *Haploinsufficiency of Snf5 (integrase interactor 1) predisposes to malignant rhabdoid tumors in mice*. Proc Natl Acad Sci U S A, 2000. **97**(25): p. 13796-800.
101. Guidi, C.J., et al., *Disruption of Ini1 leads to peri-implantation lethality and tumorigenesis in mice*. Mol Cell Biol, 2001. **21**(10): p. 3598-603.
102. Ng, J.M., et al., *Generation of a mouse model of atypical teratoid/rhabdoid tumor of the central nervous system through combined deletion of Snf5 and p53*. Cancer Res, 2015. **75**(21): p. 4629-39.
103. Han, Z.Y., et al., *The occurrence of intracranial rhabdoid tumours in mice depends on temporal control of Smarcb1 inactivation*. Nat Commun, 2016. **7**: p. 10421.
104. Pertea, M. and S.L. Salzberg, *Between a chicken and a grape: estimating the number of human genes*. Genome Biol, 2010. **11**(5): p. 206.
105. Ensembl. September 2019 [cited 2019; Ensembl release 98:[Available from: <https://www.ensembl.org>].
106. Bracken, A.P., G.L. Brien, and C.P. Verrijzer, *Dangerous liaisons: interplay between SWI/SNF, NuRD, and Polycomb in chromatin regulation and cancer*. Genes Dev, 2019. **33**(15-16): p. 936-959.
107. Luger, K., et al., *Crystal structure of the nucleosome core particle at 2.8 Å resolution*. Nature, 1997. **389**(6648): p. 251-60.
108. Even-Faitelson, L., et al., *Coming to terms with chromatin structure*. Chromosoma, 2016. **125**(1): p. 95-110.
109. Bannister, A.J. and T. Kouzarides, *Regulation of chromatin by histone modifications*. Cell Res, 2011. **21**(3): p. 381-95.
110. Clapier, C.R., et al., *Mechanisms of action and regulation of ATP-dependent chromatin-remodelling complexes*. Nat Rev Mol Cell Biol, 2017. **18**(7): p. 407-422.
111. Shen, X., et al., *A chromatin remodelling complex involved in transcription and DNA processing*. Nature, 2000. **406**(6795): p. 541-4.
112. Elfring, L.K., et al., *Identification and characterization of Drosophila relatives of the yeast transcriptional activator SNF2/SWI2*. Mol Cell Biol, 1994. **14**(4): p. 2225-34.
113. Varga-Weisz, P.D. and P.B. Becker, *Chromatin-remodeling factors: machines that regulate?* Curr Opin Cell Biol, 1998. **10**(3): p. 346-53.

114. Delmas, V., D.G. Stokes, and R.P. Perry, *A mammalian DNA-binding protein that contains a chromodomain and an SNF2/SWI2-like helicase domain*. Proc Natl Acad Sci U S A, 1993. **90**(6): p. 2414-8.
115. Marfella, C.G. and A.N. Imbalzano, *The Chd family of chromatin remodelers*. Mutat Res, 2007. **618**(1-2): p. 30-40.
116. Stern, M., R. Jensen, and I. Herskowitz, *Five SWI genes are required for expression of the HO gene in yeast*. J Mol Biol, 1984. **178**(4): p. 853-68.
117. Neigeborn, L. and M. Carlson, *Genes affecting the regulation of SUC2 gene expression by glucose repression in Saccharomyces cerevisiae*. Genetics, 1984. **108**(4): p. 845-58.
118. Cote, J., et al., *Stimulation of GAL4 derivative binding to nucleosomal DNA by the yeast SWI/SNF complex*. Science, 1994. **265**(5168): p. 53-60.
119. Imbalzano, A.N., et al., *Facilitated binding of TATA-binding protein to nucleosomal DNA*. Nature, 1994. **370**(6489): p. 481-5.
120. Kwon, H., et al., *Nucleosome disruption and enhancement of activator binding by a human SW1/SNF complex*. Nature, 1994. **370**(6489): p. 477-81.
121. Wang, W., et al., *Purification and biochemical heterogeneity of the mammalian SWI-SNF complex*. Embo j, 1996. **15**(19): p. 5370-82.
122. Wang, W., et al., *Diversity and specialization of mammalian SWI/SNF complexes*. Genes Dev, 1996. **10**(17): p. 2117-30.
123. Alpsy, A. and E.C. Dykhuizen, *Glioma tumor suppressor candidate region gene 1 (GLTSCR1) and its paralog GLTSCR1-like form SWI/SNF chromatin remodeling subcomplexes*. J Biol Chem, 2018. **293**(11): p. 3892-3903.
124. Mashtalir, N., et al., *Modular Organization and Assembly of SWI/SNF Family Chromatin Remodeling Complexes*. Cell, 2018. **175**(5): p. 1272-1288.e20.
125. Ho, L., et al., *An embryonic stem cell chromatin remodeling complex, esBAF, is essential for embryonic stem cell self-renewal and pluripotency*. Proc Natl Acad Sci U S A, 2009. **106**(13): p. 5181-6.
126. Lessard, J., et al., *An essential switch in subunit composition of a chromatin remodeling complex during neural development*. Neuron, 2007. **55**(2): p. 201-15.
127. Ho, P.J., S.M. Lloyd, and X. Bao, *Unwinding chromatin at the right places: how BAF is targeted to specific genomic locations during development*. Development, 2019. **146**(19).
128. de la Serna, I.L., et al., *MyoD targets chromatin remodeling complexes to the myogenin locus prior to forming a stable DNA-bound complex*. Mol Cell Biol, 2005. **25**(10): p. 3997-4009.
129. Takeuchi, J.K. and B.G. Bruneau, *Directed transdifferentiation of mouse mesoderm to heart tissue by defined factors*. Nature, 2009. **459**(7247): p. 708-11.
130. Toto, P.C., P.L. Puri, and S. Albin, *SWI/SNF-directed stem cell lineage specification: dynamic composition regulates specific stages of skeletal myogenesis*. Cell Mol Life Sci, 2016. **73**(20): p. 3887-96.
131. Liu, L., et al., *The chromatin remodeling subunit Baf200 promotes normal hematopoiesis and inhibits leukemogenesis*. J Hematol Oncol, 2018. **11**(1): p. 27.
132. Han, L., et al., *Chromatin remodeling mediated by ARID1A is indispensable for normal hematopoiesis in mice*. Leukemia, 2019. **33**(9): p. 2291-2305.
133. Son, E.Y. and G.R. Crabtree, *The role of BAF (mSWI/SNF) complexes in mammalian neural development*. Am J Med Genet C Semin Med Genet, 2014. **166c**(3): p. 333-49.
134. Tuoc, T., et al., *Ablation of BAF170 in Developing and Postnatal Dentate Gyrus Affects Neural Stem Cell Proliferation, Differentiation, and Learning*. Mol Neurobiol, 2017. **54**(6): p. 4618-4635.
135. Sokpor, G., et al., *Chromatin Remodeling BAF (SWI/SNF) Complexes in Neural Development and Disorders*. Front Mol Neurosci, 2017. **10**: p. 243.
136. Peng, G., et al., *BRIT1/MCPH1 links chromatin remodelling to DNA damage response*. Nat Cell Biol, 2009. **11**(7): p. 865-72.

137. Lee, H.S., et al., *A cooperative activation loop among SWI/SNF, gamma-H2AX and H3 acetylation for DNA double-strand break repair*. *Embo j*, 2010. **29**(8): p. 1434-45.
138. Watanabe, R., et al., *SWI/SNF factors required for cellular resistance to DNA damage include ARID1A and ARID1B and show interdependent protein stability*. *Cancer Res*, 2014. **74**(9): p. 2465-75.
139. Qi, W., et al., *BRG1 promotes the repair of DNA double-strand breaks by facilitating the replacement of RPA with RAD51*. *J Cell Sci*, 2015. **128**(2): p. 317-30.
140. Brownlee, P.M., C. Meisenberg, and J.A. Downs, *The SWI/SNF chromatin remodelling complex: Its role in maintaining genome stability and preventing tumourigenesis*. *DNA Repair (Amst)*, 2015. **32**: p. 127-133.
141. He, L., et al., *Cellular senescence regulated by SWI/SNF complex subunits through p53/p21 and p16/pRB pathway*. *Int J Biochem Cell Biol*, 2017. **90**: p. 29-37.
142. Napolitano, M.A., et al., *Brg1 chromatin remodeling factor is involved in cell growth arrest, apoptosis and senescence of rat mesenchymal stem cells*. *J Cell Sci*, 2007. **120**(Pt 16): p. 2904-11.
143. Moshkin, Y.M., et al., *Functional differentiation of SWI/SNF remodelers in transcription and cell cycle control*. *Mol Cell Biol*, 2007. **27**(2): p. 651-61.
144. Hah, N., et al., *A role for BAF57 in cell cycle-dependent transcriptional regulation by the SWI/SNF chromatin remodeling complex*. *Cancer Res*, 2010. **70**(11): p. 4402-11.
145. Kadoch, C., et al., *Proteomic and bioinformatic analysis of mammalian SWI/SNF complexes identifies extensive roles in human malignancy*. *Nat Genet*, 2013. **45**(6): p. 592-601.
146. Sen, P., et al., *Loss of Snf5 Induces Formation of an Aberrant SWI/SNF Complex*. *Cell Rep*, 2017. **18**(9): p. 2135-2147.
147. Dutta, A., et al., *Composition and Function of Mutant Swi/Snf Complexes*. *Cell Rep*, 2017. **18**(9): p. 2124-2134.
148. Tsurusaki, Y., et al., *Mutations affecting components of the SWI/SNF complex cause Coffin-Siris syndrome*. *Nat Genet*, 2012. **44**(4): p. 376-8.
149. Wieczorek, D., et al., *A comprehensive molecular study on Coffin-Siris and Nicolaides-Baraitser syndromes identifies a broad molecular and clinical spectrum converging on altered chromatin remodeling*. *Hum Mol Genet*, 2013. **22**(25): p. 5121-35.
150. Holsten, T., et al., *Germline variants in SMARCB1 and other members of the BAF chromatin-remodeling complex across human disease entities: a meta-analysis*. *Eur J Hum Genet*, 2018. **26**(8): p. 1083-1093.
151. Neale, B.M., et al., *Patterns and rates of exonic de novo mutations in autism spectrum disorders*. *Nature*, 2012. **485**(7397): p. 242-5.
152. O'Roak, B.J., et al., *Sporadic autism exomes reveal a highly interconnected protein network of de novo mutations*. *Nature*, 2012. **485**(7397): p. 246-50.
153. Michel, B.C., et al., *A non-canonical SWI/SNF complex is a synthetic lethal target in cancers driven by BAF complex perturbation*. *Nat Cell Biol*, 2018. **20**(12): p. 1410-1420.
154. Hodges, C., J.G. Kirkland, and G.R. Crabtree, *The Many Roles of BAF (mSWI/SNF) and PBAF Complexes in Cancer*. *Cold Spring Harb Perspect Med*, 2016. **6**(8).
155. Muchardt, C. and M. Yaniv, *When the SWI/SNF complex remodels...the cell cycle*. *Oncogene*, 2001. **20**(24): p. 3067-75.
156. Romero, O.A. and M. Sanchez-Cespedes, *The SWI/SNF genetic blockade: effects in cell differentiation, cancer and developmental diseases*. *Oncogene*, 2014. **33**(21): p. 2681-9.
157. Kadam, S. and B.M. Emerson, *Transcriptional specificity of human SWI/SNF BRG1 and BRM chromatin remodeling complexes*. *Mol Cell*, 2003. **11**(2): p. 377-89.
158. Giles, K.A., et al., *Integrated epigenomic analysis stratifies chromatin remodellers into distinct functional groups*. *Epigenetics Chromatin*, 2019. **12**(1): p. 12.
159. Raab, J.R., et al., *Co-regulation of transcription by BRG1 and BRM, two mutually exclusive SWI/SNF ATPase subunits*. *Epigenetics Chromatin*, 2017. **10**(1): p. 62.

160. Khavari, P.A., et al., *BRG1 contains a conserved domain of the SWI2/SNF2 family necessary for normal mitotic growth and transcription*. Nature, 1993. **366**(6451): p. 170-4.
161. Witkowski, L., et al., *Germline and somatic SMARCA4 mutations characterize small cell carcinoma of the ovary, hypercalcemic type*. Nat Genet, 2014. **46**(5): p. 438-43.
162. Wu, Q., et al., *The BRG1 ATPase of human SWI/SNF chromatin remodeling enzymes as a driver of cancer*. Epigenomics, 2017. **9**(6): p. 919-931.
163. Trotter, K.W. and T.K. Archer, *The BRG1 transcriptional coregulator*. Nucl Recept Signal, 2008. **6**: p. e004.
164. Shi, J., et al., *Discovery of cancer drug targets by CRISPR-Cas9 screening of protein domains*. Nat Biotechnol, 2015. **33**(6): p. 661-7.
165. Bultman, S., et al., *A Brg1 null mutation in the mouse reveals functional differences among mammalian SWI/SNF complexes*. Mol Cell, 2000. **6**(6): p. 1287-95.
166. Bultman, S.J., et al., *Characterization of mammary tumors from Brg1 heterozygous mice*. Oncogene, 2008. **27**(4): p. 460-8.
167. Singh, A.P., et al., *Brg1 Enables Rapid Growth of the Early Embryo by Suppressing Genes That Regulate Apoptosis and Cell Growth Arrest*. Mol Cell Biol, 2016. **36**(15): p. 1990-2010.
168. Griffin, C.T., J. Brennan, and T. Magnuson, *The chromatin-remodeling enzyme BRG1 plays an essential role in primitive erythropoiesis and vascular development*. Development, 2008. **135**(3): p. 493-500.
169. Vieira, J.M., et al., *BRG1-SWI/SNF-dependent regulation of the Wt1 transcriptional landscape mediates epicardial activity during heart development and disease*. Nat Commun, 2017. **8**: p. 16034.
170. Indra, A.K., et al., *Temporally controlled targeted somatic mutagenesis in embryonic surface ectoderm and fetal epidermal keratinocytes unveils two distinct developmental functions of BRG1 in limb morphogenesis and skin barrier formation*. Development, 2005. **132**(20): p. 4533-44.
171. Banerjee, R., et al., *Non-targeted metabolomics of Brg1/Brm double-mutant cardiomyocytes reveals a novel role for SWI/SNF complexes in metabolic homeostasis*. Metabolomics, 2015. **11**(5): p. 1287-1301.
172. Takada, Y., et al., *Brg1 plays an essential role in development and homeostasis of the duodenum through regulation of Notch signaling*. Development, 2016. **143**(19): p. 3532-3539.
173. Singh, A.P., et al., *A role for BRG1 in the regulation of genes required for development of the lymphatic system*. Oncotarget, 2017. **8**(33): p. 54925-54938.
174. Ronan, J.L., W. Wu, and G.R. Crabtree, *From neural development to cognition: unexpected roles for chromatin*. Nat Rev Genet, 2013. **14**(5): p. 347-59.
175. Matsumoto, S., et al., *Brg1 is required for murine neural stem cell maintenance and gliogenesis*. Dev Biol, 2006. **289**(2): p. 372-83.
176. Moreno, N., et al., *Loss of Smarc proteins impairs cerebellar development*. J Neurosci, 2014. **34**(40): p. 13486-91.
177. Zhan, X., et al., *Dual role of Brg chromatin remodeling factor in Sonic hedgehog signaling during neural development*. Proc Natl Acad Sci U S A, 2011. **108**(31): p. 12758-63.
178. Ninkovic, J., et al., *The BAF complex interacts with Pax6 in adult neural progenitors to establish a neurogenic cross-regulatory transcriptional network*. Cell Stem Cell, 2013. **13**(4): p. 403-18.
179. Petrik, D., et al., *Chromatin Remodeling Factor Brg1 Supports the Early Maintenance and Late Responsiveness of Nestin-Lineage Adult Neural Stem and Progenitor Cells*. Stem Cells, 2015. **33**(12): p. 3655-65.
180. Li, W., et al., *Brg1 governs distinct pathways to direct multiple aspects of mammalian neural crest cell development*. Proc Natl Acad Sci U S A, 2013. **110**(5): p. 1738-43.
181. Yu, Y., et al., *Olig2 targets chromatin remodelers to enhancers to initiate oligodendrocyte differentiation*. Cell, 2013. **152**(1-2): p. 248-61.

182. Weider, M., et al., *Chromatin-remodeling factor Brg1 is required for Schwann cell differentiation and myelination*. Dev Cell, 2012. **23**(1): p. 193-201.
183. Limpert, A.S., et al., *NF-kappaB forms a complex with the chromatin remodeler BRG1 to regulate Schwann cell differentiation*. J Neurosci, 2013. **33**(6): p. 2388-97.
184. Kosho, T., et al., *Clinical correlations of mutations affecting six components of the SWI/SNF complex: detailed description of 21 patients and a review of the literature*. Am J Med Genet A, 2013. **161a**(6): p. 1221-37.
185. Errichiello, E., et al., *SMARCA4 inactivating mutations cause concomitant Coffin-Siris syndrome, microphthalmia and small-cell carcinoma of the ovary hypercalcaemic type*. J Pathol, 2017. **243**(1): p. 9-15.
186. Cappuccio, G., et al., *Retinal dystrophy in an individual carrying a de novo missense variant of SMARCA4*. Mol Genet Genomic Med, 2019. **7**(6): p. e682.
187. Sekiguchi, F., et al., *Genetic abnormalities in a large cohort of Coffin-Siris syndrome patients*. J Hum Genet, 2019. **64**(12): p. 1173-1186.
188. Coffin, G.S. and E. Siris, *Mental retardation with absent fifth fingernail and terminal phalanx*. Am J Dis Child, 1970. **119**(5): p. 433-9.
189. Vergano, S.S. and M.A. Deardorff, *Clinical features, diagnostic criteria, and management of Coffin-Siris syndrome*. Am J Med Genet C Semin Med Genet, 2014. **166c**(3): p. 252-6.
190. De Rubeis, S., et al., *Synaptic, transcriptional and chromatin genes disrupted in autism*. Nature, 2014. **515**(7526): p. 209-15.
191. Pan, Y., et al., *Association of genetic variants of GRIN2B with autism*. Sci Rep, 2015. **5**: p. 8296.
192. Lim, E.T., et al., *Rates, distribution and implications of postzygotic mosaic mutations in autism spectrum disorder*. Nat Neurosci, 2017. **20**(9): p. 1217-1224.
193. Dunaief, J.L., et al., *The retinoblastoma protein and BRG1 form a complex and cooperate to induce cell cycle arrest*. Cell, 1994. **79**(1): p. 119-30.
194. Wong, A.K., et al., *BRG1, a component of the SWI-SNF complex, is mutated in multiple human tumor cell lines*. Cancer Res, 2000. **60**(21): p. 6171-7.
195. Medina, P.P., et al., *Frequent BRG1/SMARCA4-inactivating mutations in human lung cancer cell lines*. Hum Mutat, 2008. **29**(5): p. 617-22.
196. Karnezis, A.N., et al., *Dual loss of the SWI/SNF complex ATPases SMARCA4/BRG1 and SMARCA2/BRM is highly sensitive and specific for small cell carcinoma of the ovary, hypercalcaemic type*. J Pathol, 2016. **238**(3): p. 389-400.
197. Reisman, D.N., et al., *Loss of BRG1/BRM in human lung cancer cell lines and primary lung cancers: correlation with poor prognosis*. Cancer Res, 2003. **63**(3): p. 560-6.
198. Le Loarer, F., et al., *SMARCA4 inactivation defines a group of undifferentiated thoracic malignancies transcriptionally related to BAF-deficient sarcomas*. Nat Genet, 2015. **47**(10): p. 1200-5.
199. Jiang, W., et al., *Immunohistochemistry Successfully Uncovers Intratumoral Heterogeneity and Widespread Co-Losses of Chromatin Regulators in Clear Cell Renal Cell Carcinoma*. PLoS One, 2016. **11**(10): p. e0164554.
200. Jelinic, P., et al., *Recurrent SMARCA4 mutations in small cell carcinoma of the ovary*. Nat Genet, 2014. **46**(5): p. 424-6.
201. Ramos, P., et al., *Small cell carcinoma of the ovary, hypercalcemic type, displays frequent inactivating germline and somatic mutations in SMARCA4*. Nat Genet, 2014. **46**(5): p. 427-9.
202. Nemes, K., et al., *Rhabdoid Tumor Predisposition Syndrome*, in GeneReviews((R)), M.P. Adam, et al., Editors. 2017, University of Washington, Seattle. GeneReviews is a registered trademark of the University of Washington, Seattle. All rights reserved.: Seattle (WA).
203. Stanton, B.Z., et al., *Smarca4 ATPase mutations disrupt direct eviction of PRC1 from chromatin*. Nat Genet, 2017. **49**(2): p. 282-288.
204. Tate, J.G., et al., *COSMIC: the Catalogue Of Somatic Mutations In Cancer*. Nucleic Acids Res, 2019. **47**(D1): p. D941-d947.

205. COSMIC Catalogue Of Somatic Mutations In Cancer. [cited 2020 27/01/2020]; Available from: <https://cancer.sanger.ac.uk/cosmic/>.
206. Love, C., et al., *The genetic landscape of mutations in Burkitt lymphoma*. Nat Genet, 2012. **44**(12): p. 1321-5.
207. Kretzmer, H., et al., *DNA methylome analysis in Burkitt and follicular lymphomas identifies differentially methylated regions linked to somatic mutation and transcriptional control*. Nat Genet, 2015. **47**(11): p. 1316-1325.
208. Jones, D.T., et al., *Dissecting the genomic complexity underlying medulloblastoma*. Nature, 2012. **488**(7409): p. 100-5.
209. Northcott, P.A., et al., *The whole-genome landscape of medulloblastoma subtypes*. Nature, 2017. **547**(7663): p. 311-317.
210. Parsons, D.W., et al., *The genetic landscape of the childhood cancer medulloblastoma*. Science, 2011. **331**(6016): p. 435-9.
211. Pugh, T.J., et al., *Medulloblastoma exome sequencing uncovers subtype-specific somatic mutations*. Nature, 2012. **488**(7409): p. 106-10.
212. Robinson, G., et al., *Novel mutations target distinct subgroups of medulloblastoma*. Nature, 2012. **488**(7409): p. 43-8.
213. Bai, J., et al., *BRG1 expression is increased in human glioma and controls glioma cell proliferation, migration and invasion in vitro*. J Cancer Res Clin Oncol, 2012. **138**(6): p. 991-8.
214. Jubierre, L., et al., *BRG1/SMARCA4 is essential for neuroblastoma cell viability through modulation of cell death and survival pathways*. Oncogene, 2016. **35**(39): p. 5179-90.
215. Chen, Z., et al., *Hepatic SMARCA4 predicts HCC recurrence and promotes tumour cell proliferation by regulating SMAD6 expression*. Cell Death Dis, 2018. **9**(2): p. 59.
216. Muthuswami, R., et al., *BRG1 is a prognostic indicator and a potential therapeutic target for prostate cancer*. J Cell Physiol, 2019.
217. Glaros, S., et al., *Targeted knockout of BRG1 potentiates lung cancer development*. Cancer Res, 2008. **68**(10): p. 3689-96.
218. Aldiri, I., et al., *Brg1 coordinates multiple processes during retinogenesis and is a tumor suppressor in retinoblastoma*. Development, 2015. **142**(23): p. 4092-106.
219. Serber, D.W., et al., *The BRG1 chromatin remodeler protects against ovarian cysts, uterine tumors, and mammary tumors in a lineage-specific manner*. PLoS One, 2012. **7**(2): p. e31346.
220. Tsuda, M., et al., *The BRG1/SOX9 axis is critical for acinar cell-derived pancreatic tumorigenesis*. J Clin Invest, 2018. **128**(8): p. 3475-3489.
221. Laurette, P., et al., *Chromatin remodellers Brg1 and Bptf are required for normal gene expression and progression of oncogenic Braf-driven mouse melanoma*. Cell Death Differ, 2019.
222. Shi, X., et al., *SMARCA4/Brg1 coordinates genetic and epigenetic networks underlying Shh-type medulloblastoma development*. Oncogene, 2016. **35**(44): p. 5746-5758.
223. Matsumoto, S., et al., *Brg1 directly regulates Olig2 transcription and is required for oligodendrocyte progenitor cell specification*. Dev Biol, 2016. **413**(2): p. 173-87.
224. Merk, D.J., et al., *Opposing Effects of CREBBP Mutations Govern the Phenotype of Rubinstein-Taybi Syndrome and Adult SHH Medulloblastoma*. Dev Cell, 2018. **44**(6): p. 709-724.e6.
225. Feil, R., et al., *Regulation of Cre recombinase activity by mutated estrogen receptor ligand-binding domains*. Biochem Biophys Res Commun, 1997. **237**(3): p. 752-7.
226. Sumi-Ichinose, C., et al., *SNF2beta-BRG1 is essential for the viability of F9 murine embryonal carcinoma cells*. Mol Cell Biol, 1997. **17**(10): p. 5976-86.
227. Luche, H., et al., *Faithful activation of an extra-bright red fluorescent protein in "knock-in" Cre-reporter mice ideally suited for lineage tracing studies*. Eur J Immunol, 2007. **37**(1): p. 43-53.

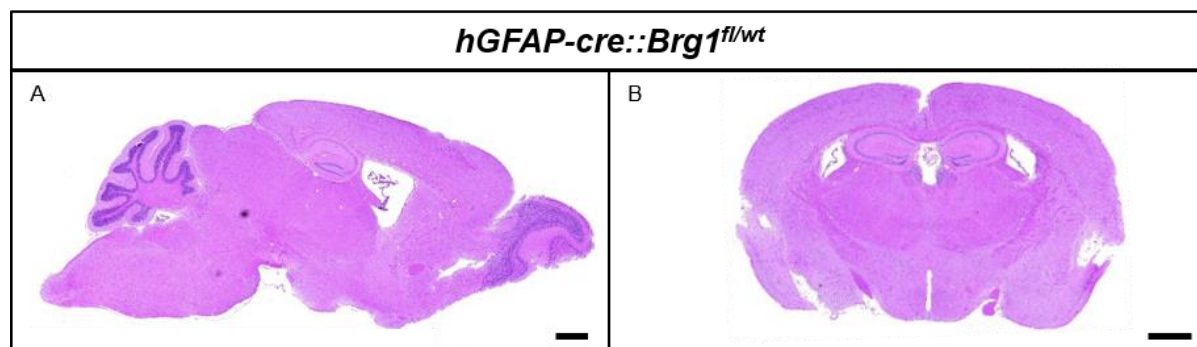
228. Koscheck, T., et al., *Morphological development and neurochemical differentiation of cerebellar inhibitory interneurons in microexplant cultures*. Neuroscience, 2003. **116**(4): p. 973-84.
229. Chomczynski, P., *A reagent for the single-step simultaneous isolation of RNA, DNA and proteins from cell and tissue samples*. Biotechniques, 1993. **15**(3): p. 532-4, 536-7.
230. Andrews, S.; Available from: <https://www.bioinformatics.babraham.ac.uk/projects/fastqc/>.
231. Dobin, A., et al., *STAR: ultrafast universal RNA-seq aligner*. Bioinformatics, 2013. **29**(1): p. 15-21.
232. Love, M.I., W. Huber, and S. Anders, *Moderated estimation of fold change and dispersion for RNA-seq data with DESeq2*. Genome Biol, 2014. **15**(12): p. 550.
233. Zhuo, L., et al., *hGFAP-cre transgenic mice for manipulation of glial and neuronal function in vivo*. Genesis, 2001. **31**(2): p. 85-94.
234. Behesti, H. and S. Marino, *Cerebellar granule cells: insights into proliferation, differentiation, and role in medulloblastoma pathogenesis*. Int J Biochem Cell Biol, 2009. **41**(3): p. 435-45.
235. Wechsler-Reya, R.J. and M.P. Scott, *Control of neuronal precursor proliferation in the cerebellum by Sonic Hedgehog*. Neuron, 1999. **22**(1): p. 103-14.
236. Sottile, V., M. Li, and P.J. Scotting, *Stem cell marker expression in the Bergmann glia population of the adult mouse brain*. Brain Res, 2006. **1099**(1): p. 8-17.
237. Ahlfeld, J., et al., *Neurogenesis from Sox2 expressing cells in the adult cerebellar cortex*. Sci Rep, 2017. **7**(1): p. 6137.
238. Luskin, M.B., *Restricted proliferation and migration of postnatally generated neurons derived from the forebrain subventricular zone*. Neuron, 1993. **11**(1): p. 173-89.
239. Lois, C. and A. Alvarez-Buylla, *Long-distance neuronal migration in the adult mammalian brain*. Science, 1994. **264**(5162): p. 1145-8.
240. Bekkers, J.M., *Pyramidal neurons*. Curr Biol, 2011. **21**(24): p. R975.
241. Xie, Z., et al., *Zbtb20 is essential for the specification of CA1 field identity in the developing hippocampus*. Proc Natl Acad Sci U S A, 2010. **107**(14): p. 6510-5.
242. Iwano, T., et al., *Prox1 postmitotically defines dentate gyrus cells by specifying granule cell identity over CA3 pyramidal cell fate in the hippocampus*. Development, 2012. **139**(16): p. 3051-62.
243. Simon, R., et al., *A dual function of Bcl11b/Ctip2 in hippocampal neurogenesis*. Embo j, 2012. **31**(13): p. 2922-36.
244. Stergiopoulos, A., M. Elkouris, and P.K. Politis, *Prospero-related homeobox 1 (Prox1) at the crossroads of diverse pathways during adult neural fate specification*. Front Cell Neurosci, 2014. **8**: p. 454.
245. Anstötz, M., M. Karsak, and G.M. Rune, *Integrity of Cajal-Retzius cells in the reeler-mouse hippocampus*. Hippocampus, 2018.
246. Helms, A.W., et al., *Autoregulation and multiple enhancers control Math1 expression in the developing nervous system*. Development, 2000. **127**(6): p. 1185-96.
247. Rakic, P., *Neuron-glia relationship during granule cell migration in developing cerebellar cortex. A Golgi and electronmicroscopic study in Macacus Rhesus*. J Comp Neurol, 1971. **141**(3): p. 283-312.
248. Reynolds, B.A. and S. Weiss, *Clonal and population analyses demonstrate that an EGF-responsive mammalian embryonic CNS precursor is a stem cell*. Dev Biol, 1996. **175**(1): p. 1-13.
249. Belkin, A.M. and M.A. Stepp, *Integrins as receptors for laminins*. Microsc Res Tech, 2000. **51**(3): p. 280-301.
250. Gage, P.J., et al., *The canonical Wnt signaling antagonist DKK2 is an essential effector of PITX2 function during normal eye development*. Dev Biol, 2008. **317**(1): p. 310-24.
251. Badea, T.C. and J. Nathans, *Morphologies of mouse retinal ganglion cells expressing transcription factors Brn3a, Brn3b, and Brn3c: analysis of wild type and mutant cells using genetically-directed sparse labeling*. Vision Res, 2011. **51**(2): p. 269-79.

252. Cheng, C.W., et al., *The Iroquois homeobox gene, Irx5, is required for retinal cone bipolar cell development*. Dev Biol, 2005. **287**(1): p. 48-60.
253. Balasubramanian, R., et al., *Expression of LIM-homeodomain transcription factors in the developing and mature mouse retina*. Gene Expr Patterns, 2014. **14**(1): p. 1-8.
254. Zhao, S., S.C. Thornquist, and C.J. Barnstable, *In vitro transdifferentiation of embryonic rat retinal pigment epithelium to neural retina*. Brain Res, 1995. **677**(2): p. 300-10.
255. Saha, A., et al., *Class I histone deacetylases in retinal progenitors and differentiating ganglion cells*. Gene Expr Patterns, 2018. **30**: p. 37-48.
256. Kim, H.T., et al., *Mitochondrial Protection by Exogenous Otx2 in Mouse Retinal Neurons*. Cell Rep, 2015. **13**(5): p. 990-1002.
257. Shibasaki, K., et al., *Expression of the basic helix-loop-factor Olig2 in the developing retina: Olig2 as a new marker for retinal progenitors and late-born cells*. Gene Expr Patterns, 2007. **7**(1-2): p. 57-65.
258. Sharma, R.K. and P.A. Netland, *Early born lineage of retinal neurons express class III beta-tubulin isotype*. Brain Res, 2007. **1176**: p. 11-7.
259. Jiang, S.M., et al., *beta-III-Tubulin: a reliable marker for retinal ganglion cell labeling in experimental models of glaucoma*. Int J Ophthalmol, 2015. **8**(4): p. 643-52.
260. Cao, M. and J.I. Wu, *Camk2a-Cre-mediated conditional deletion of chromatin remodeler Brg1 causes perinatal hydrocephalus*. Neurosci Lett, 2015. **597**: p. 71-6.
261. Wischhof, L., et al., *The SWI/SNF subunit Bcl7a contributes to motor coordination and Purkinje cell function*. Sci Rep, 2017. **7**(1): p. 17055.
262. Sudarov, A. and A.L. Joyner, *Cerebellum morphogenesis: the foliation pattern is orchestrated by multi-cellular anchoring centers*. Neural Dev, 2007. **2**: p. 26.
263. Basson, M.A. and R.J. Wingate, *Congenital hypoplasia of the cerebellum: developmental causes and behavioral consequences*. Front Neuroanat, 2013. **7**: p. 29.
264. Elsen, G.E., et al., *The Epigenetic Factor Landscape of Developing Neocortex Is Regulated by Transcription Factors Pax6--> Tbr2--> Tbr1*. Front Neurosci, 2018. **12**: p. 571.
265. Wu, J.I., et al., *Regulation of dendritic development by neuron-specific chromatin remodeling complexes*. Neuron, 2007. **56**(1): p. 94-108.
266. Tibshirani, M., et al., *Dysregulation of chromatin remodelling complexes in amyotrophic lateral sclerosis*. Hum Mol Genet, 2017. **26**(21): p. 4142-4152.
267. Nguyen, H., et al., *Epigenetic Regulation by BAF Complexes Limits Neural Stem Cell Proliferation by Suppressing Wnt Signaling in Late Embryonic Development*. Stem Cell Reports, 2018. **10**(6): p. 1734-1750.
268. Curtis, C.D. and C.T. Griffin, *The chromatin-remodeling enzymes BRG1 and CHD4 antagonistically regulate vascular Wnt signaling*. Mol Cell Biol, 2012. **32**(7): p. 1312-20.
269. Holik, A.Z., et al., *Brg1 loss attenuates aberrant wnt-signalling and prevents wnt-dependent tumorigenesis in the murine small intestine*. PLoS Genet, 2014. **10**(7): p. e1004453.
270. Li, N., et al., *Brahma related gene 1 (Brg1) contributes to liver regeneration by epigenetically activating the Wnt/beta-catenin pathway in mice*. Faseb j, 2019. **33**(1): p. 327-338.
271. Li, P., et al., *A population of Nestin-expressing progenitors in the cerebellum exhibits increased tumorigenicity*. Nat Neurosci, 2013. **16**(12): p. 1737-44.
272. Lee, A., et al., *Isolation of neural stem cells from the postnatal cerebellum*. Nat Neurosci, 2005. **8**(6): p. 723-9.
273. Sotelo, C., et al., *Molecular plasticity of adult Bergmann fibers is associated with radial migration of grafted Purkinje cells*. J Neurosci, 1994. **14**(1): p. 124-33.
274. Sasai, Y., *Identifying the missing links: genes that connect neural induction and primary neurogenesis in vertebrate embryos*. Neuron, 1998. **21**(3): p. 455-8.
275. Li, F., J. Liang, and D. Tang, *Brahma-related gene 1 ameliorates the neuronal apoptosis and oxidative stress induced by oxygen-glucose deprivation/reoxygenation*

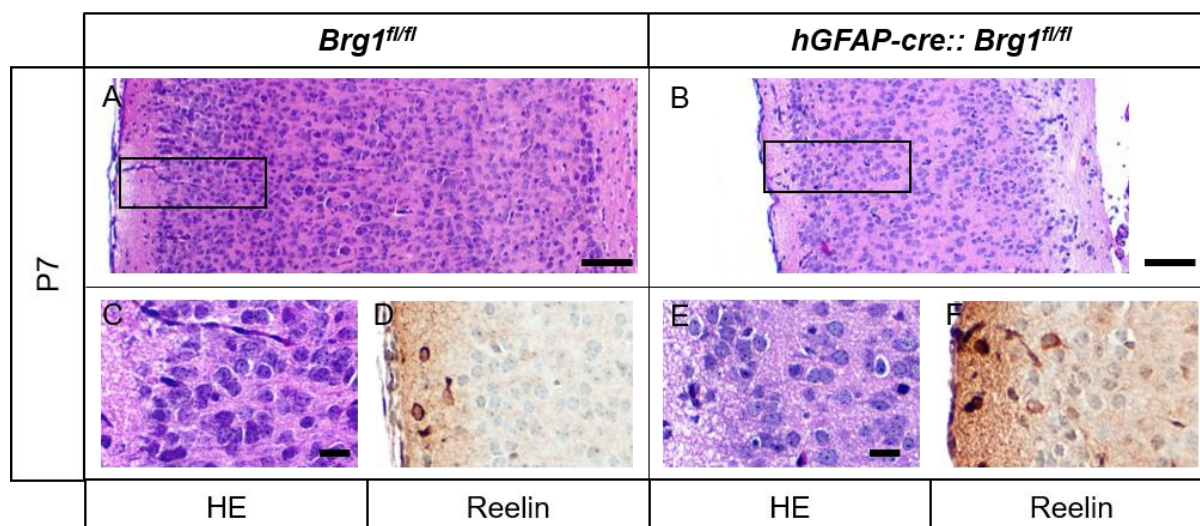
- through activation of *Nrf2/HO-1* signaling. *Biomed Pharmacother*, 2018. **108**: p. 1216-1224.
276. Brizzi, M.F., G. Tarone, and P. Defilippi, *Extracellular matrix, integrins, and growth factors as tailors of the stem cell niche*. *Curr Opin Cell Biol*, 2012. **24**(5): p. 645-51.
 277. Barros, C.S., S.J. Franco, and U. Muller, *Extracellular matrix: functions in the nervous system*. *Cold Spring Harb Perspect Biol*, 2011. **3**(1): p. a005108.
 278. Kerever, A., et al., *Novel extracellular matrix structures in the neural stem cell niche capture the neurogenic factor fibroblast growth factor 2 from the extracellular milieu*. *Stem Cells*, 2007. **25**(9): p. 2146-57.
 279. Mercier, F., *Fractones: extracellular matrix niche controlling stem cell fate and growth factor activity in the brain in health and disease*. *Cell Mol Life Sci*, 2016. **73**(24): p. 4661-4674.
 280. Mercier, F., J.T. Kitasako, and G.I. Hatton, *Anatomy of the brain neurogenic zones revisited: fractones and the fibroblast/macrophage network*. *J Comp Neurol*, 2002. **451**(2): p. 170-88.
 281. Douet, V., E. Arikawa-Hirasawa, and F. Mercier, *Fractone-heparan sulfates mediate BMP-7 inhibition of cell proliferation in the adult subventricular zone*. *Neurosci Lett*, 2012. **528**(2): p. 120-5.
 282. Narayanan, R. and T.C. Tuoc, *Roles of chromatin remodeling BAF complex in neural differentiation and reprogramming*. *Cell Tissue Res*, 2014. **356**(3): p. 575-84.
 283. Sokpor, G., et al., *ATP-Dependent Chromatin Remodeling During Cortical Neurogenesis*. *Front Neurosci*, 2018. **12**: p. 226.
 284. Zhang, R., et al., *Sma- and Mad-related protein 7 (Smad7) is required for embryonic eye development in the mouse*. *J Biol Chem*, 2013. **288**(15): p. 10275-85.
 285. Evans, A.L. and P.J. Gage, *Expression of the homeobox gene Pitx2 in neural crest is required for optic stalk and ocular anterior segment development*. *Hum Mol Genet*, 2005. **14**(22): p. 3347-59.
 286. Pan, L., et al., *Functional equivalence of Brn3 POU-domain transcription factors in mouse retinal neurogenesis*. *Development*, 2005. **132**(4): p. 703-12.
 287. Fujimura, N., et al., *Spatial and temporal regulation of Wnt/beta-catenin signaling is essential for development of the retinal pigment epithelium*. *Dev Biol*, 2009. **334**(1): p. 31-45.
 288. Kim, J.Y., et al., *Yap is essential for retinal progenitor cell cycle progression and RPE cell fate acquisition in the developing mouse eye*. *Dev Biol*, 2016. **419**(2): p. 336-347.
 289. West-Mays, J.A., et al., *AP-2alpha transcription factor is required for early morphogenesis of the lens vesicle*. *Dev Biol*, 1999. **206**(1): p. 46-62.
 290. Zhu, Y., et al., *Brahma regulates the Hippo pathway activity through forming complex with Yki-Sd and regulating the transcription of Crumbs*. *Cell Signal*, 2015. **27**(3): p. 606-13.
 291. Chang, L., et al., *The SWI/SNF complex is a mechanoregulated inhibitor of YAP and TAZ*. *Nature*, 2018. **563**(7730): p. 265-269.
 292. Laurette, P., et al., *Transcription factor MITF and remodeler BRG1 define chromatin organisation at regulatory elements in melanoma cells*. *Elife*, 2015. **4**.
 293. Ved, N., et al., *Tamoxifen administration in pregnant mice can be deleterious to both mother and embryo*. *Lab Anim*, 2019. **53**(6): p. 630-633.
 294. Lizen, B., et al., *Perinatal induction of Cre recombination with tamoxifen*. *Transgenic Res*, 2015. **24**(6): p. 1065-77.
 295. Zhang, Z., et al., *Autism-Associated Chromatin Regulator Brg1/SmadA4 Is Required for Synapse Development and Myocyte Enhancer Factor 2-Mediated Synapse Remodeling*. *Mol Cell Biol*, 2016. **36**(1): p. 70-83.
 296. Kulis, M., et al., *Intragenic DNA methylation in transcriptional regulation, normal differentiation and cancer*. *Biochim Biophys Acta*, 2013. **1829**(11): p. 1161-74.
 297. Jessa, S., et al., *Stalled developmental programs at the root of pediatric brain tumors*. *Nat Genet*, 2019. **51**(12): p. 1702-1713.

11 Appendix

11.1 Supplementary Figures



Supplementary Figure 1 *hGFAP-cre::Brg1^{fl/wt}* mice do not show morphological alterations in the brain. A heterozygous *Brg1* loss in *hGFAP* expressing cells does not disrupt normal brain development. H&E stains display representative images of sagittal (A) and frontal (B) brain sections of *hGFAP-cre::Brg1^{fl/wt}* animals which were sacrificed after half a year. Scale bars correspond to 1000 μm .



Supplementary Figure 2: Reelin expressing cells in neocortical layer I are not altered due to *hGFAP* mediated *Brg1* loss. H&E stains of cerebral cortices illustrate the severely thinned neocortex in *hGFAP-cre::Brg1^{fl/fl}* mice compared to controls (A-C, E). The location and abundance of Reelin expressing Cajal-Retzius cells is unchanged in *Brg1* deprived cortices (D, F). All controls include *hGFAP*, *Brg1^{fl/wt}* and *Brg1^{fl/fl}* mice. Scale bars correspond to 100 μm (A, B) and 20 μm (C-F).

11.2 Supplementary Tables

Supplementary Table 1 List of DEGs after tamoxifen exposure at E7.5. DEGs with a log2 fold change of $\geq \pm 0.6$ and a FDR <0.1 are listed, including (if available) Gene Symbol, Uniprot ID and Ensembl ID.

GeneSymbol	Uniprot ID	Ensembl ID	log2 Fold Change	FDR
Sla	Q60898	ENSMUSG00000022372	-1.631	8.72E-18
Fos	P01101	ENSMUSG00000021250	-1.516	2.60E-13
Lmo7		ENSMUSG00000033060	-1.345	1.71E-10
		ENSMUSG00000092341	-1.325	4.12E-105
		ENSMUSG00000106099	-1.214	5.62E-18
		ENSMUSG00000109321	-1.175	1.09E-09
		ENSMUSG00000102411	-1.154	2.49E-09
		ENSMUSG00000105572	-1.139	6.09E-08
Rasgrf1		ENSMUSG00000032356	-1.120	4.82E-07
Neb		ENSMUSG00000026950	-1.113	4.31E-08
Gria2		ENSMUSG00000033981	-1.112	3.96E-57
		ENSMUSG00000110411	-1.076	8.56E-07
		ENSMUSG00000109394	-1.042	2.89E-09
		ENSMUSG00000109438	-1.017	1.33E-06
Gramd1b		ENSMUSG00000040111	-1.004	2.03E-15
		ENSMUSG00000106717	-0.989	2.67E-06
Atxn1	P54254	ENSMUSG00000046876	-0.977	8.13E-11
Grk3	Q3UYH7	ENSMUSG00000042249	-0.976	1.43E-08
Gipr	Q0P543	ENSMUSG00000030406	-0.970	4.22E-06
		ENSMUSG00000109005	-0.966	2.66E-05
Ryr1		ENSMUSG00000030592	-0.960	5.38E-07
Kcnn3	P58391	ENSMUSG00000000794	-0.958	5.15E-10
Cacna1e		ENSMUSG00000004110	-0.946	4.60E-27
Gm1043		ENSMUSG00000117286	-0.943	2.85E-05
Fosb	P13346	ENSMUSG00000003545	-0.942	4.74E-05
Elmod1	Q3V1U8	ENSMUSG00000041986	-0.941	4.70E-11
		ENSMUSG00000045813	-0.935	1.81E-06
		ENSMUSG00000021268	-0.913	7.39E-41
Jun	P05627	ENSMUSG00000052684	-0.904	1.15E-18
Hivep3	A2A884	ENSMUSG00000028634	-0.901	1.71E-11
Cacna1d	Q99246	ENSMUSG00000015968	-0.890	1.89E-09
Nin	Q61043	ENSMUSG00000021068	-0.878	3.28E-21
Kcnq3	Q8K3F6	ENSMUSG00000056258	-0.870	1.11E-16
Arhgef1		ENSMUSG00000040940	-0.865	1.64E-14
Dlgap1	Q9D415	ENSMUSG00000003279	-0.861	5.07E-06
Pfkip	Q9WUA3	ENSMUSG00000021196	-0.860	9.22E-15
Hivep2	Q3UHF7	ENSMUSG00000015501	-0.849	2.30E-04
Clstn2	Q9ER65	ENSMUSG00000032452	-0.846	1.52E-07
		ENSMUSG00000105804	-0.842	3.34E-04

1700109H08Rik		ENSMUSG00000008307	-0.842	3.07E-04
Stxbp2	Q64324	ENSMUSG00000004626	-0.837	6.95E-06
Leng8		ENSMUSG00000035545	-0.837	5.01E-38
Cssp1		ENSMUSG00000056763	-0.836	1.05E-14
Carmil3		ENSMUSG00000022211	-0.834	1.37E-17
		ENSMUSG00000104597	-0.827	7.37E-12
Adamts18	Q4VC17	ENSMUSG00000053399	-0.826	2.04E-05
Kcnt1		ENSMUSG00000058740	-0.825	3.40E-04
Tmem132b		ENSMUSG00000070498	-0.823	8.26E-09
Ctnnbp2		ENSMUSG00000000416	-0.818	4.45E-12
Adamts3		ENSMUSG00000043635	-0.817	5.98E-06
		ENSMUSG00000102602	-0.814	3.93E-05
Dlg2		ENSMUSG00000052572	-0.806	1.17E-10
Zbtb20		ENSMUSG00000022708	-0.799	1.51E-33
Arpp21	Q9DCB4	ENSMUSG00000032503	-0.795	4.15E-05
Stard9	Q80TF6	ENSMUSG00000033705	-0.790	1.12E-07
		ENSMUSG00000107756	-0.790	2.05E-04
St3gal1	P54751	ENSMUSG00000013846	-0.777	2.14E-06
Dhtkd1	A2ATU0	ENSMUSG00000025815	-0.776	3.07E-04
		ENSMUSG00000109536	-0.776	7.49E-04
		ENSMUSG00000116305	-0.775	7.39E-05
Kcnn2		ENSMUSG00000054477	-0.774	1.34E-03
		ENSMUSG00000102562	-0.772	1.13E-03
Inf2		ENSMUSG00000037679	-0.768	7.24E-04
Mef2c	Q8CFN5	ENSMUSG00000005583	-0.765	1.55E-08
Rgs6		ENSMUSG00000021219	-0.761	1.81E-04
		ENSMUSG00000117011	-0.760	6.62E-05
Cnih3		ENSMUSG00000026514	-0.760	1.30E-03
		ENSMUSG00000103039	-0.759	2.26E-03
Itpr1	P11881	ENSMUSG00000030102	-0.756	7.09E-06
Ryr3	A2AGL3	ENSMUSG00000057378	-0.756	8.74E-05
Ppp1r15a		ENSMUSG00000040435	-0.755	3.43E-04
		ENSMUSG00000096780	-0.754	1.04E-03
Zc3h11a	Q6NZF1	ENSMUSG00000102976	-0.754	1.21E-04
Lrrc7		ENSMUSG00000028176	-0.753	3.25E-07
Scn8a		ENSMUSG00000023033	-0.743	4.60E-11
		ENSMUSG00000103651	-0.741	2.00E-03
		ENSMUSG00000097156	-0.741	4.80E-20
		ENSMUSG00000116908	-0.739	3.19E-03
		ENSMUSG00000087022	-0.733	1.68E-03
Pcdhgc5		ENSMUSG00000102543	-0.732	3.60E-03
Tnc	Q80YX1	ENSMUSG00000028364	-0.731	9.78E-07
Camk4		ENSMUSG00000038128	-0.729	2.95E-03
Prkca		ENSMUSG00000050965	-0.728	4.03E-07

Shtn1	Q8K2Q9	ENSMUSG00000041362	-0.727	7.59E-13
Prkce	P16054	ENSMUSG00000045038	-0.725	1.73E-10
		ENSMUSG00000100826	-0.725	6.97E-09
Mpped1	Q91ZG2	ENSMUSG00000041708	-0.716	6.12E-04
Med13l		ENSMUSG00000018076	-0.716	1.61E-17
Gria1		ENSMUSG00000020524	-0.715	4.19E-11
		ENSMUSG00000111390	-0.713	4.96E-03
Fam135b	Q9DAI6	ENSMUSG00000036800	-0.711	3.18E-03
Clip4		ENSMUSG00000024059	-0.705	6.79E-04
		ENSMUSG00000102302	-0.703	5.39E-03
Sbsn		ENSMUSG00000046056	-0.703	5.81E-03
Htr3a		ENSMUSG00000032269	-0.701	5.80E-03
		ENSMUSG00000092981	-0.701	4.19E-03
Gad1	P48318	ENSMUSG00000070880	-0.694	1.23E-09
		ENSMUSG00000094868	-0.694	1.68E-03
Ndrgr1	Q62433	ENSMUSG00000005125	-0.690	2.34E-03
Caln1		ENSMUSG00000060371	-0.689	6.38E-03
Dgkh		ENSMUSG00000034731	-0.683	1.38E-04
Nxph3	Q91VX5	ENSMUSG00000046719	-0.683	2.83E-03
Necab3	Q9D6J4	ENSMUSG00000027489	-0.678	7.11E-03
Nsun7	Q14AW5	ENSMUSG00000029206	-0.676	8.36E-03
Kcnq4	Q9JK97	ENSMUSG00000028631	-0.676	8.71E-03
Map4k2		ENSMUSG00000024948	-0.675	3.45E-05
Ninl	Q6ZQ12	ENSMUSG00000068115	-0.675	2.09E-04
		ENSMUSG00000109539	-0.674	9.16E-03
Nos1		ENSMUSG00000029361	-0.673	1.14E-03
Opcml		ENSMUSG00000062257	-0.672	4.12E-04
Sh3rf3	Q8C120	ENSMUSG00000037990	-0.671	1.04E-05
Porcn	Q9JJJ7	ENSMUSG00000031169	-0.671	1.24E-05
Safb2		ENSMUSG00000042625	-0.669	6.11E-09
		ENSMUSG00000114624	-0.667	7.88E-03
Lca5		ENSMUSG00000032258	-0.665	3.20E-05
Camkv	Q3UHL1	ENSMUSG00000032936	-0.664	2.85E-03
Rexo5		ENSMUSG00000030924	-0.663	1.03E-02
March4	Q80TE3	ENSMUSG00000039372	-0.663	1.78E-04
Gas7		ENSMUSG00000033066	-0.663	3.41E-05
Hemk1	Q921L7	ENSMUSG00000032579	-0.662	5.13E-03
Arl4d	Q99PE9	ENSMUSG00000034936	-0.662	1.19E-03
1810032O08Rik		ENSMUSG00000020812	-0.662	1.08E-02
Pou2f1		ENSMUSG00000026565	-0.662	1.32E-09
		ENSMUSG00000105985	-0.661	5.15E-03
		ENSMUSG00000106944	-0.660	1.01E-02
		ENSMUSG00000109198	-0.660	7.81E-03
Mfsd8	Q8BH31	ENSMUSG00000025759	-0.660	2.09E-03

Gm20219		ENSMUSG00000110218	-0.659	7.94E-03
		ENSMUSG00000097311	-0.657	7.93E-03
Tbc1d8	Q9Z1A9	ENSMUSG00000003134	-0.657	4.59E-03
Ank1	Q02357	ENSMUSG00000031543	-0.656	7.08E-04
		ENSMUSG00000103831	-0.655	1.21E-02
Gsap		ENSMUSG00000039934	-0.652	7.74E-03
		ENSMUSG00000103697	-0.651	3.00E-03
Slc6a1	P31648	ENSMUSG00000030310	-0.650	7.61E-15
Clmp	Q8R373	ENSMUSG00000032024	-0.648	1.34E-10
		ENSMUSG00000097767	-0.646	1.26E-43
		ENSMUSG00000087042	-0.645	1.33E-02
Lhx6	Q9R1R0	ENSMUSG00000026890	-0.642	3.82E-05
Herc3		ENSMUSG00000029804	-0.639	9.01E-06
Ppfia4		ENSMUSG00000026458	-0.635	6.56E-03
Uggt2		ENSMUSG00000042104	-0.634	1.53E-04
		ENSMUSG00000110631	-0.633	1.24E-05
Lypd6	Q8BPP5	ENSMUSG00000050447	-0.633	1.90E-03
Zzef1		ENSMUSG00000055670	-0.632	1.08E-10
Ndufs5	Q99LY9	ENSMUSG00000028648	-0.631	2.42E-03
Flrt1	Q6RKD8	ENSMUSG00000047787	-0.631	3.70E-04
Aim2	Q91VJ1	ENSMUSG00000037860	-0.629	8.37E-03
		ENSMUSG00000095123	-0.629	1.64E-02
Rlbp1	Q9Z275	ENSMUSG00000039194	-0.626	2.91E-04
Serinc5	Q8BHJ6	ENSMUSG00000021703	-0.625	5.13E-06
		ENSMUSG00000105382	-0.624	1.37E-02
Lrnf5	Q8BXA0	ENSMUSG00000035653	-0.623	6.64E-04
Ccdc80	Q8R2G6	ENSMUSG00000022665	-0.623	1.87E-02
Atf7		ENSMUSG00000099083	-0.622	1.42E-05
Csmd2		ENSMUSG00000028804	-0.620	5.56E-07
Pcnx		ENSMUSG00000021140	-0.620	1.42E-10
Slc6a17	Q8BJI1	ENSMUSG00000027894	-0.620	4.22E-06
Cux2	P70298	ENSMUSG00000042589	-0.620	2.01E-06
		ENSMUSG00000029878	-0.617	1.73E-02
Unc80		ENSMUSG00000055567	-0.614	1.32E-02
Nrg3	O35181	ENSMUSG00000041014	-0.613	9.08E-03
Zfp280c	Q6P3Y5	ENSMUSG00000036916	-0.613	9.54E-07
Grin2b		ENSMUSG00000030209	-0.611	4.45E-12
Pclaf	Q9CQX4	ENSMUSG00000040204	-0.610	4.11E-04
Ubp1	Q811S7	ENSMUSG00000009741	-0.609	1.41E-14
Kcnh7	Q9ER47	ENSMUSG00000059742	-0.608	3.60E-07
Adamts10		ENSMUSG00000024299	-0.607	3.64E-06
		ENSMUSG00000103509	-0.606	1.35E-02
		ENSMUSG00000089726	-0.606	1.33E-02
Unc5d	Q8K1S2	ENSMUSG00000063626	-0.605	2.71E-04

		ENSMUSG00000107021	-0.601	2.35E-02
Thsd7a		ENSMUSG00000032625	0.603	1.64E-06
Grm3	Q9QYS2	ENSMUSG00000003974	0.606	2.27E-02
Gata3	P23772	ENSMUSG00000015619	0.607	1.57E-02
Igfbp7		ENSMUSG00000036256	0.607	3.84E-04
Gjd2	O54851	ENSMUSG00000068615	0.607	1.63E-02
Nid2	O88322	ENSMUSG00000021806	0.609	2.16E-02
Nuak2	Q8BZN4	ENSMUSG00000009772	0.612	9.21E-04
Zic2		ENSMUSG00000061524	0.613	1.93E-05
Tmem132c		ENSMUSG00000034324	0.616	4.61E-03
Axin2	O88566	ENSMUSG00000000142	0.619	1.93E-05
Nt5c		ENSMUSG00000020736	0.621	3.17E-03
Senp8	Q9D2Z4	ENSMUSG00000051705	0.627	1.75E-02
Abcc9	P70170	ENSMUSG00000030249	0.627	4.59E-04
Zfp37	P17141	ENSMUSG00000028389	0.631	1.46E-03
Ccnd1	P25322	ENSMUSG00000070348	0.631	2.44E-05
Col18a1	P39061	ENSMUSG00000001435	0.632	1.09E-03
Itgb3bp	Q9CQ82	ENSMUSG00000028549	0.633	9.28E-03
Lmx1a	Q9JKU8	ENSMUSG00000026686	0.633	1.51E-02
Tstd3	Q9D0B5	ENSMUSG00000028251	0.634	1.33E-02
Col6a2	Q02788	ENSMUSG00000020241	0.635	2.22E-03
Pou6f2		ENSMUSG00000009734	0.635	1.38E-02
Lef1	P27782	ENSMUSG00000027985	0.635	9.21E-05
Ntng1	Q8R4G0	ENSMUSG00000059857	0.640	1.09E-03
Hbb-bt		ENSMUSG00000073940	0.642	3.60E-03
Hdhd3	Q9CYW4	ENSMUSG00000038422	0.643	2.47E-03
Prokr2		ENSMUSG00000050558	0.643	1.99E-03
Rfx4	Q7TNK1	ENSMUSG00000020037	0.644	1.09E-03
Smad3	Q8BUN5	ENSMUSG00000032402	0.646	6.02E-05
Itm2a	Q61500	ENSMUSG00000031239	0.646	1.18E-02
Neurog2		ENSMUSG00000027967	0.647	7.96E-06
Hmox1	P14901	ENSMUSG00000005413	0.648	1.10E-02
Zic3		ENSMUSG00000067860	0.649	6.12E-05
Sulf1	Q8K007	ENSMUSG00000016918	0.653	4.05E-03
Rspo1		ENSMUSG00000028871	0.653	2.77E-03
Dcn	P28654	ENSMUSG00000019929	0.655	1.60E-03
Chrdl1	Q920C1	ENSMUSG00000031283	0.656	1.20E-02
Wls	Q6DID7	ENSMUSG00000028173	0.656	2.20E-03
Hsd11b2	P51661	ENSMUSG00000031891	0.659	1.12E-02
Nek7	Q9ES74	ENSMUSG00000026393	0.661	1.15E-03
Ebf3	O08791	ENSMUSG00000010476	0.661	1.91E-03
Gli1	P47806	ENSMUSG00000025407	0.664	6.84E-03
Rgs5	O08850	ENSMUSG00000026678	0.668	9.88E-03
Tpbp	Q9Z0L0	ENSMUSG00000035274	0.669	2.29E-03

Uncx	O08934	ENSMUSG00000029546	0.669	8.56E-03
Slc1a2	P43006	ENSMUSG00000005089	0.672	1.25E-11
Kirrel2	Q7TSU7	ENSMUSG00000036915	0.674	7.23E-03
Olig3	Q6PFG8	ENSMUSG00000045591	0.688	2.05E-03
Gper1	Q8BMP4	ENSMUSG00000053647	0.689	2.47E-03
Dlk1		ENSMUSG00000040856	0.690	2.50E-05
Fam173a	Q501J2	ENSMUSG00000057411	0.699	5.32E-03
Irs4	Q9Z0Y7	ENSMUSG00000054667	0.701	5.97E-03
Sim1		ENSMUSG00000019913	0.701	4.59E-03
Fezf1	Q0VDQ9	ENSMUSG00000029697	0.703	5.41E-03
Pnoc	Q64387	ENSMUSG00000045731	0.705	4.62E-03
Epas1	P97481	ENSMUSG00000024140	0.707	6.67E-04
Foxa1	P35582	ENSMUSG00000035451	0.709	5.24E-03
Gata2	O09100	ENSMUSG00000015053	0.710	5.11E-03
Samd5		ENSMUSG00000060487	0.715	5.84E-04
Pcp4l1	Q6W8Q3	ENSMUSG00000038370	0.716	1.46E-03
Ebf2	O08792	ENSMUSG00000022053	0.717	7.83E-05
Fst		ENSMUSG00000021765	0.732	3.41E-03
Gsx1	P31315	ENSMUSG00000053129	0.752	2.52E-03
Igfbp5	Q07079	ENSMUSG00000026185	0.758	1.05E-09
Pax5	Q02650	ENSMUSG00000014030	0.762	1.72E-03
Has3	O08650	ENSMUSG00000031910	0.770	4.32E-04
Hyal2		ENSMUSG00000010047	0.772	1.13E-06
Vav3	Q9R0C8	ENSMUSG00000033721	0.774	1.05E-04
Esrrb		ENSMUSG00000021255	0.775	1.75E-03
Ascl1	Q02067	ENSMUSG00000020052	0.778	2.67E-09
Lhx1	P63006	ENSMUSG00000018698	0.780	1.22E-04
Gpc3	Q8CFZ4	ENSMUSG00000055653	0.786	1.34E-03
Tmem163	Q8C996	ENSMUSG00000026347	0.786	8.74E-05
Postn	Q62009	ENSMUSG00000027750	0.791	9.41E-05
Tfap2a		ENSMUSG00000021359	0.803	9.76E-04
Crabp2	P22935	ENSMUSG00000004885	0.803	5.57E-04
Lhx5	P61375	ENSMUSG00000029595	0.812	1.34E-04
Sparc		ENSMUSG00000018593	0.814	9.39E-08
Alad	P10518	ENSMUSG00000028393	0.841	5.71E-06
Chrna4		ENSMUSG00000027577	0.862	4.92E-06
Nhlh2	Q64221	ENSMUSG00000048540	0.864	4.25E-13
Arl4a	P61213	ENSMUSG00000047446	0.900	5.64E-08
Gsta4		ENSMUSG00000032348	0.906	7.27E-05
Tfap2b	Q61313	ENSMUSG00000025927	0.911	2.74E-06
Tcf7l2		ENSMUSG00000024985	0.914	1.95E-07
Otx2		ENSMUSG00000021848	0.929	5.64E-08
Cdkn1c	P49919	ENSMUSG00000037664	0.930	1.31E-16
Fndc3c1	Q6DFV6	ENSMUSG00000033737	0.931	5.18E-05

Irx3	P81067	ENSMUSG00000031734	0.941	2.01E-05
Nkx2-2		ENSMUSG00000027434	0.951	4.20E-05
Barhl2	Q8VIB5	ENSMUSG00000034384	0.967	6.44E-07
Col4a2	P08122	ENSMUSG00000031503	0.977	2.36E-06
Pax3		ENSMUSG00000004872	0.980	1.39E-05
Fgf15	O35622	ENSMUSG00000031073	0.989	3.23E-08
Fzd10	Q8BKG4	ENSMUSG00000081683	0.995	7.55E-06
Pitx2	P97474	ENSMUSG00000028023	1.004	1.15E-05
Irx5		ENSMUSG00000031737	1.005	1.04E-05
		ENSMUSG00000113263	1.010	7.03E-07
Lhx9	Q9WUH2	ENSMUSG00000019230	1.018	5.19E-20
Syt13	Q9EQT6	ENSMUSG00000027220	1.046	1.41E-14
Irx2	P81066	ENSMUSG00000001504	1.047	4.27E-08
Foxb1	Q64732	ENSMUSG00000059246	1.068	5.38E-07
Col4a1	P02463	ENSMUSG00000031502	1.095	3.23E-08
Mab2111	O70299	ENSMUSG00000056947	1.100	4.45E-12
Shox2		ENSMUSG00000027833	1.124	5.71E-16
Ric3		ENSMUSG00000048330	1.126	1.71E-07
Hbb-bs		ENSMUSG00000052305	1.150	1.53E-07
Dbx1	P52950	ENSMUSG00000030507	1.161	7.40E-08
Gbx2	P48031	ENSMUSG00000034486	1.214	1.46E-09
Pou4f1	P17208	ENSMUSG00000048349	1.224	7.94E-11
		ENSMUSG00000094344	1.294	1.79E-09
Col1a2		ENSMUSG00000029661	1.371	1.43E-10
Col1a1	P11087	ENSMUSG00000001506	1.389	2.17E-11
Tal2	Q62282	ENSMUSG00000028417	1.453	1.79E-14
Col3a1	P08121	ENSMUSG00000026043	1.668	4.82E-16
		ENSMUSG00000100801	1.948	3.09E-41

Supplementary Table 2 List of DEGs after tamoxifen exposure at E9.5. DEGs with a log2 fold change of $\geq \pm 0.6$ and a FDR < 0.1 are listed, including (if available) Gene Symbol, Uniprot ID and Ensembl ID.

GeneSymbol	Uniprot ID	Ensembl ID	log2 Fold Change	FDR
Lmo1	Q924W9	ENSMUSG00000036111	-1.651	2.58E-33
Wdfy1	E9Q4P1	ENSMUSG00000073643	-1.404	3.96E-35
Aph1b	Q8C7N7	ENSMUSG00000032375	-0.885	9.11E-15
Ndn	P25233	ENSMUSG00000033585	-0.746	4.06E-18
Arl4d	Q99PE9	ENSMUSG00000034936	-0.742	1.07E-05
Pnoc	Q64387	ENSMUSG00000045731	-0.736	5.14E-05
Cyb561	Q60720	ENSMUSG00000019590	-0.679	6.10E-04
Asic4		ENSMUSG00000033007	-0.674	1.70E-06
Arrdc3		ENSMUSG00000074794	-0.662	9.87E-10
Caln1		ENSMUSG00000060371	-0.649	1.49E-03

Sox14	Q04892	ENSMUSG00000053747	-0.642	4.29E-04
Pax7	P47239	ENSMUSG00000028736	-0.636	5.11E-04
Gprin3	Q8BWS5	ENSMUSG00000045441	-0.634	2.19E-03
Aldh1a3	Q9JHW9	ENSMUSG00000015134	-0.633	2.37E-03
Kcnq4	Q9JK97	ENSMUSG00000028631	-0.631	2.02E-03
Adarb2	Q9JI20	ENSMUSG00000052551	-0.627	2.64E-07
Chrna3		ENSMUSG00000032303	-0.624	1.85E-03
Sptbn4		ENSMUSG00000011751	-0.610	9.86E-04
Emx1	Q04742	ENSMUSG00000033726	0.605	1.06E-05
Rspo3		ENSMUSG00000019880	0.610	2.70E-04
Plekhg1		ENSMUSG00000040624	0.614	8.96E-04
Itm2a	Q61500	ENSMUSG00000031239	0.614	3.02E-03
Dct	P29812	ENSMUSG00000022129	0.621	2.46E-03
Tgif1	P70284	ENSMUSG00000047407	0.622	1.46E-03
Lmx1a	Q9JKU8	ENSMUSG00000026686	0.626	1.90E-03
Erf		ENSMUSG00000040857	0.628	1.20E-04
Lsr	Q99KG5	ENSMUSG00000001247	0.634	2.23E-03
Adamts1	P97857	ENSMUSG00000022893	0.638	8.20E-04
Vwf		ENSMUSG00000001930	0.640	7.90E-05
Ppp1r10	Q80W00	ENSMUSG00000039220	0.641	2.60E-13
Stra6		ENSMUSG00000032327	0.642	1.84E-03
Nes	Q6P5H2	ENSMUSG00000004891	0.643	5.55E-10
Ramp2	Q9WUP0	ENSMUSG00000001240	0.643	5.60E-04
Col5a1	O88207	ENSMUSG00000026837	0.646	1.25E-04
Lhfp12	Q8BGA2	ENSMUSG00000045312	0.648	6.56E-04
Jhy	E9Q793	ENSMUSG00000032023	0.651	7.02E-05
Ttr	P07309	ENSMUSG00000061808	0.659	5.98E-08
Rspo1		ENSMUSG00000028871	0.663	6.92E-04
Lama4	P97927	ENSMUSG00000019846	0.668	1.04E-03
Lamc3		ENSMUSG00000026840	0.678	6.89E-05
Fn1		ENSMUSG00000026193	0.681	1.18E-08
Ltbp1		ENSMUSG00000001870	0.683	9.53E-06
Adgra2		ENSMUSG00000031486	0.687	2.72E-04
Ahnak		ENSMUSG00000069833	0.692	2.65E-04
Cavin1	O54724	ENSMUSG00000004044	0.692	5.69E-05
Bmp7	P23359	ENSMUSG00000008999	0.695	5.90E-04
Mmp9		ENSMUSG00000017737	0.697	2.04E-04
Robo4		ENSMUSG00000032125	0.698	2.08E-06
Dmrt3	Q80WT2	ENSMUSG00000042372	0.703	4.29E-04
Adgre5		ENSMUSG00000002885	0.703	5.06E-06
Col1a2		ENSMUSG00000029661	0.703	1.74E-06
Hba-x	P06467	ENSMUSG00000055609	0.705	5.80E-06
Tcf711		ENSMUSG00000055799	0.705	8.92E-06
Elk3	P41971	ENSMUSG00000008398	0.707	2.33E-04

Serpinh1	P19324	ENSMUSG00000070436	0.708	1.35E-08
Efcab7		ENSMUSG00000073791	0.710	4.25E-04
Clybl	Q8R4N0	ENSMUSG00000025545	0.713	3.35E-04
Alad	P10518	ENSMUSG00000028393	0.717	1.70E-06
Itga1	Q3V3R4	ENSMUSG00000042284	0.718	3.30E-04
Rspo2	Q8BFU0	ENSMUSG00000051920	0.734	1.91E-04
Slc38a5		ENSMUSG00000031170	0.734	1.67E-06
Lum	P51885	ENSMUSG00000036446	0.737	1.74E-06
Slc2a1	P17809	ENSMUSG00000028645	0.738	5.70E-06
Wwtr1	Q9EPK5	ENSMUSG00000027803	0.739	4.84E-07
Spata6	Q3U6K5	ENSMUSG00000034401	0.742	1.86E-04
Gja1	P23242	ENSMUSG00000050953	0.748	5.28E-08
Mcam		ENSMUSG00000032135	0.750	5.14E-05
Sparc		ENSMUSG00000018593	0.759	1.55E-07
Col6a3		ENSMUSG00000048126	0.763	5.46E-05
Tie1		ENSMUSG00000033191	0.765	3.58E-06
Tgfbr2	Q62312	ENSMUSG00000032440	0.770	2.92E-06
Hspg2		ENSMUSG00000028763	0.770	2.82E-08
Esam	Q925F2	ENSMUSG00000001946	0.773	1.54E-05
Dcn	P28654	ENSMUSG00000019929	0.779	4.82E-06
Wnt8b		ENSMUSG00000036961	0.793	4.02E-05
Col1a1	P11087	ENSMUSG00000001506	0.800	3.86E-07
Trp73	Q9JJP2	ENSMUSG00000029026	0.803	5.48E-08
Stab1		ENSMUSG00000042286	0.809	7.75E-06
Car12		ENSMUSG00000032373	0.812	5.80E-06
Lcp1		ENSMUSG00000021998	0.815	9.12E-06
Aplnr	Q9WV08	ENSMUSG00000044338	0.816	1.91E-06
Apod	P51910	ENSMUSG00000022548	0.824	2.80E-06
Nos3		ENSMUSG00000028978	0.825	1.63E-07
Col4a1	P02463	ENSMUSG00000031502	0.829	3.16E-06
Anxa2	P07356	ENSMUSG00000032231	0.829	1.09E-05
Dock6		ENSMUSG00000032198	0.832	3.76E-06
Aqp1	Q02013	ENSMUSG00000004655	0.836	1.23E-06
Vtn	P29788	ENSMUSG00000017344	0.838	2.39E-06
Aebp1	Q640N1	ENSMUSG00000020473	0.844	2.04E-06
Slco1c1		ENSMUSG00000030235	0.866	2.81E-08
Cav1	P49817	ENSMUSG00000007655	0.867	1.74E-06
Epas1	P97481	ENSMUSG00000024140	0.867	1.03E-06
		ENSMUSG00000000031	0.870	1.38E-09
		ENSMUSG00000053117	0.877	2.83E-06
		ENSMUSG00000081824	0.903	2.99E-08
Cldn5	O54942	ENSMUSG00000041378	0.907	5.98E-08
Col3a1	P08121	ENSMUSG00000026043	0.907	5.95E-09
Uaca		ENSMUSG00000034485	0.909	1.01E-08

Eng		ENSMUSG00000026814	0.925	1.21E-07
Col6a2	Q02788	ENSMUSG00000020241	0.929	7.06E-08
Cd34	Q64314	ENSMUSG00000016494	0.942	2.09E-08
Rgs5	O08850	ENSMUSG00000026678	0.979	7.01E-08
Tnfrsf19	Q9JLL3	ENSMUSG00000060548	0.994	3.27E-18
Clic6		ENSMUSG00000022949	0.996	5.95E-09
Col18a1	P39061	ENSMUSG00000001435	1.025	1.04E-10
Pecam1	Q08481	ENSMUSG00000020717	1.027	5.95E-09
Adgrf5	G5E8Q8	ENSMUSG00000056492	1.035	1.28E-09
Bgn	P28653	ENSMUSG00000031375	1.038	2.20E-09
Cd93	O89103	ENSMUSG00000027435	1.060	1.07E-09
Nid2	O88322	ENSMUSG00000021806	1.093	9.12E-10
Capn11	Q6J756	ENSMUSG00000058626	1.385	3.08E-13
Cdh5	P55284	ENSMUSG00000031871	1.484	1.61E-19
		ENSMUSG00000094344	1.541	6.45E-20
Ric3		ENSMUSG00000048330	2.038	3.51E-146
		ENSMUSG00000100801	6.060	3.66E-89

12 List of all figures and tables

List of all figures

Figure 1 Overview of postnatal cerebellar development.	3
Figure 2 Schematic overview of the embryonic eye development.	4
Figure 3 Histopathology of a Brg1 deficient AT/RT.	6
Figure 4 Survival of AT/RT patients is reduced in case of a <i>BRG1</i> mutation.	7
Figure 5 Characteristics of AT/RT subgroups.	8
Figure 6 Structure of Brg1.	11
Figure 7 Postnatal development is impaired in <i>hGFAP-cre::Brg1^{fl/fl}</i> mice.	30
Figure 8 <i>hGFAP</i> dependent Brg1 loss results in a hypoplastic cerebellum without proper foliation and lamination.	33
Figure 9 Brg1 is important for late stages of CGNPs migration <i>in vitro</i> .	35
Figure 10 The SVZ is highly affected by the loss of Brg1 and loses stem cell capacities.	36
Figure 11 The cerebral cortex is severely thinner upon Brg1 loss.	37
Figure 12 Cortical layers II-IV are thinner and pyramidal neurons have an altered morphology in <i>hGFAP-cre::Brg1^{fl/fl}</i> mice at P7.	38
Figure 13 The hippocampus is highly underdeveloped in <i>hGFAP-cre::Brg1^{fl/fl}</i> mice.	40
Figure 14 Postnatal knockout of Brg1 in <i>Math1</i> expressing cells increases the proliferation of cells in the EGL.	42
Figure 15 A postnatal Brg1 loss in GNPCs does not hinder normal brain development.	43
Figure 16 Experimental design to investigate time point specific roles of Brg1 in <i>Sox2</i> expressing NSCs.	45
Figure 17 Loss of Brg1 in <i>Sox2</i> expressing NSCs causes architectural alterations in the brain.	47
Figure 18 Regions of altered morphology are predominantly formed by Brg1 competent cells.	49
Figure 19 Experimental setup of fate-mapping experiments.	50
Figure 20 Brg1 deficiency decreases cell numbers <i>in vivo</i> und prevents neurosphere formation <i>in vitro</i> .	52
Figure 21 Loss of Brg1 results in distinct changes in gene expression.	54
Figure 22 Downregulated GO terms are related to neuronal function.	55
Figure 23 ECM related GO terms are upregulated upon loss of Brg1.	56
Figure 24 Brg1 is likely indispensable for normal eye development at E7.5 in <i>Sox2</i> expressing NSCs.	57

Figure 25 IHC analysis reveals similarities of the basal lesion in Brg1 deprived embryos and physiological retina.	59
---	----

List of all tables

Table 1 List of all chemicals, reagents and solutions	16
Table 2 List of all primers used for genotyping	18
Table 3 Table of primary antibodies	18
Table 4 List of all secondary antibodies used in this study	19
Table 5 List of all kit systems used in this study	20
Table 6 Formula for PCR mastermixes	21
Table 7 Overview of the PCR programs used for genotyping	21
Table 8 Programs used for automated tissue dehydration	24
Table 9 Deparaffinization procedure for IHC or IF	25
Table 10 <i>hGFAP-cre::Brg1^{fl/fl}</i> mice are born with the expected Mendelian ratio.	29
Table 11 Overview of born mice after embryonal tamoxifen exposure	60
Table 12 List of abbreviations	76

List of all supplementary figures

Supplementary Figure 1 <i>hGFAP-cre::Brg1^{fl/wt}</i> mice do not show morphological alterations in the brain	i
Supplementary Figure 2: Reelin expressing cells in neocortical layer I are not altered due to <i>hGFAP</i> mediated Brg1 loss	i

List of all supplementary tables

Supplementary Table 1 List of DEGs after tamoxifen exposure at E7.5	ii
Supplementary Table 2 List of DEGs after tamoxifen exposure at E9.5.	viii

13 Danksagung

Zunächst möchte ich mich bei meinem Doktorvater, Prof. Dr. Ulrich Schüller, für die anregenden Diskussionen und das ständige Fordern und Fördern bedanken. Ohne Deine Betreuung wäre diese Doktorarbeit nicht möglich gewesen. Des Weiteren möchte ich meinen Dank meinen beiden zusätzlichen Mitgliedern des Thesis Komitees, Prof. Dr. Matthias Kneussel und Prof. Dr. Martin Horstmann, aussprechen, die mich während der drei Jahre mit wissenschaftlichem Input unterstützt haben.

Ich möchte mich bei allen Mitarbeitern des Tierstalls des HPIs (Oliver, Ulla, Beate, Ines, Anke, Sandra, Jasmin, Alex, Kristian) dafür bedanken, das sie stets für das Wohl meiner Mäuschen gesorgt haben und mir mit Rat und Tat zur Seite standen. Zusätzlich möchte ich auch Arne, Jana und Daniela aus dem HPI für ihre technische Unterstützung bei den Fate-mapping Experimenten und den Transkriptomanalysen danken. In diesem Zuge möchte ich auch Michael meinen großen Dank aussprechen, da er mir bei allen bioinformatischen Fragestellungen geduldig weitergeholfen hat und mir alle (vermutlich für ihn sehr trivialen) Fragen stets beantwortet hat. Ein großer Dank gebührt auch allen Mitarbeiterinnen der Neuropathologie (vor allem Tasja und Kristin) sowie Gundula aus dem HPI. Danke, dass ihr die vielen Serienschritte für mich angefertigt habt. Ohne Euch säße ich vermutlich noch die nächsten Jahre am Mikrotom.

Vielen Dank auch an alle Mitglieder des Kinderkrebs Zentrums. Vor allem der Mittagessen Crew möchte ich für eine endlose Anzahl an schönen Pausen danken. Den Müller Mietzen (vor allem Lena) möchte ich besonders dafür danken, dass wir auch außerhalb des Labors viel Spaß hatten, entweder bei einer Runde Doppelkopf oder bei einigen Alsterrunden.

Zuletzt möchte ich mich bei allen aktuellen und ehemaligen Mitgliedern der AG Schüller bedanken. Danke an Pia, Anne, Jacky und Nick für die technische Unterstützung, Judith für die Beantwortung methodischer Fragen und Malte, vor allem für das Spritzen von Mäusen in der Anfangszeit, als ich nach 10 Bissen aufgegeben hatte. Vielen Dank an Till, der stets eine Flasche Weißwein im Kühlschrank hat und an Caro und Catena, die zwar noch nicht allzu lange dabei sind, aber sofort komplett dazu gehört haben. Melanie möchte ich ganz besonders dafür danken, dass sie wirklich immer mit Rat und Tat ausgeholfen hat und auch für die schönen Erlebnisse außerhalb des Labors. So werde ich die Busfahrt vom Elbstrand nach Hause nie vergessen. Zu guter Letzt gilt mein großer Dank auch Margarethe, nicht nur für die technische Unterstützung im Labor, sondern vor allem dafür, dass Du immer offene Ohren und Arme hast.

Zu allerletzt möchte ich mich auch bei Mama, Papa, Frederike und Nielsi für das Zuhören und Ablenken, wenn es grad nicht so lief, bedanken.

14 Curriculum Vitae

Der Lebenslauf wurde aus datenschutzrechtlichen Gründen entfernt.

15 List of publications

Schoof M, Hellwig M, Harrison L, Holdhof D, Lauffer MC, Niesen J, Viridi S, Indenbirken D, Schüller U. 2020. The basic helix-loop-helix transcription factor TCF4 impacts brain architecture as well as neuronal morphology and differentiation. *The European journal of neuroscience*. In press.

Schoof M, Launspach M, Holdhof D, Nguyen L, Engel V, Filser S, Peters F, Immenschuh J, Hellwig M, Niesen J, Mall V, Ertl-Wagner B, Hagel C, Spohn M, Lutz B, Sedlacik J, Indenbirken D, Merk DJ, Schüller U. 2019. The transcriptional coactivator and histone acetyltransferase CBP regulates neural precursor cell development and migration. *Acta Neuropathologica communications*. 7(1):199.

Holdhof D, Schoof M, Hellwig M, Holdhof NH, Niesen J, Schüller U. 2019. hGFAP-Positive Stem Cells Depend on Brg1 for Proper Formation of Cerebral and Cerebellar Structures. *Cerebral cortex (New York, N.Y. : 1991)*.

Miarka L, Hauser C, Helm O, Holdhof D, Beckinger S, Egberts J, Gundlach J, Lenk L, Rahn S, Mikulits W, Trauzold A, Sebens S. 2019. The Hepatic Microenvironment and TRAIL-R2 Impact Outgrowth of Liver Metastases in Pancreatic Cancer after Surgical Resection. *Cancers*. 11(6).

Hellwig M, Lauffer MC, Bockmayr M, Spohn M, Merk DJ, Harrison L, Ahlfeld J, Kitowski A, Neumann JE, Ohli J, Holdhof D, Niesen J, Schoof M, Kool M, Kraus C, Zweier C, Holmberg D, Schüller U. 2019. TCF4 (E2-2) harbors tumor suppressive functions in SHH medulloblastoma. *Acta Neuropathologica*. 137(4):657–673.

16 Eidesstattliche Versicherung

Ich versichere ausdrücklich, dass ich die Arbeit selbständig und ohne fremde Hilfe verfasst, andere als die von mir angegebenen Quellen und Hilfsmittel nicht benutzt und die aus den benutzten Werken wörtlich oder inhaltlich entnommenen Stellen einzeln nach Ausgabe (Auflage und Jahr des Erscheinens), Band und Seite des benutzten Werkes kenntlich gemacht habe.

Ferner versichere ich, dass ich die Dissertation bisher nicht einem Fachvertreter an einer anderen Hochschule zur Überprüfung vorgelegt oder mich anderweitig um Zulassung zur Promotion beworben habe.

Ich erkläre mich einverstanden, dass meine Dissertation vom Dekanat der Medizinischen Fakultät mit einer gängigen Software zur Erkennung von Plagiaten überprüft werden kann.

Unterschrift: